A Study on Equilibrium Form of Tensegrity and Development of Contact Analysis for Its Folding Behavior

Muhammad Nizam bin Zakaria
(Z. M. Nizam)

Department of Science and Advanced Technology
Graduate School of Science and Engineering
Saga University
JAPAN

March 2014

A Study on Equilibrium Form of Tensegrity and Development of Contact Analysis for Its Folding Behavior

by

Muhammad Nizam bin Zakaria
(Z. M. Nizam)

A dissertation submitted in partial fulfillment of the requirements for the degree of Doctor of Engineering in Civil Engineering

Department of Science and Advanced Technology
Graduate School of Science and Engineering
Saga University
JAPAN

March 2014

Copyright © 2014 by Z. M. Nizam. All rights reserved.

Examination Committee

_____

Professor Obiya Hiroyuki
(Chairman)

_____

Professor Ijima Katsushi

_____

Professor Ishibashi Kouji

_____

Professor ItouYukihiro

_____

Professor Emeritus Goto Shigeo

Department of Science and Advanced Technology
Saga University, JAPAN

Preface

The author wishes to acknowledge many people who had a hand in the creation of this dissertation. The work presented in this dissertation was carried out at the Department of Science and Advanced Technology, Graduate School of Science and Technology, Saga University, Japan. First and foremost, I would like to extend my sincere appreciation and gratitude to my respected supervisor, Professor Obiya Hiroyuki, for his continuous encouragement and support throughout my study. I feel really blessed and immeasurably grateful for the unlimited guidance, feedback and suggestion throughout this study. I also would like to express my sincere gratitude to Professor Ijima Katsushi, Professor Ishibashi Kouji, Professor Itou Yukihiro and Professor Emeritus Goto Shigeo for their support as well as providing me valuable comments and suggestions while serving as members of the examination committee. A thank goes to colleagues and former colleagues of Obiya and Ijima laboratory; the Faculty of Civil and Environmental Engineering, University Tun Hussein Onn Malaysia; and acquaintances that were involved directly or indirectly towards the completion of this dissertation. Financial support from the Department of Higher Education Malaysia and University Tun Hussein Onn Malaysia is also gratefully acknowledged.

The table of contents

Chapter			Title	Page
			Title page	i
			Preface	iii
			Table of contents	iv
			List of figures	viii
			List of tables	xi
1	:		**Introduction**	1
	1.1	:	Background –Concept of tensegrity–	1
	1.2	:	Scope and aims	3
	1.3	:	Outline of thesis	6
			References	9
2	:		**Fundamental concept of tangent stiffness method**	12
	2.1	:	Introduction	12
	2.2	:	The general formulation of TSM	13
	2.3	:	The derivation of tangent geometric stiffness	14
	2.4	:	The iterational process of TSM	17
	2.5	:	Discussion	20
			List of symbols	22
3	:		**The advantage of tangent stiffness method**	23
	3.1	:	Introduction	23
	3.2	:	Application of TSM in plane frame structure	24
		3.2.1	: Tangent geometric stiffness	24
		3.2.2	: Definition for element behavior	26
		3.2.3	: Estimation of difference between curve and string length	28
		3.2.4	: The tangent element force equation for curve element	31
		3.2.5	: The Newton–Raphson numerical method for determining the axial force	33

The table of contents

Chapter		Title	Page
	3.3	: General formulation for geometrically nonlinear analysis in FEM	34
		3.3.1 : Nonlinear stiffness equation	34
		3.3.2 : The iterational process for FEM	36
	3.4	: Robustness aspect in large deformational plane frame analyses	38
	3.5	: Numerical example	39
	3.6	: Discussion	41
		References	42
		List of symbols	43
4	:	**Static form-finding procedure for tensegrity structures and evaluation of equilibrium solutions**	45
	4.1	: Introduction	45
	4.2	: Fundamental concept of force density method	47
		4.2.1 : Connectivity matrix	49
		4.2.2 : Singular matrix and rank deficiency	50
	4.3	: Form-Finding by TSM	55
		4.3.1 : The development of measure-potential element with virtual stiffness	55
		4.3.2 : Element potential function	55
		4.3.3 : Axial line element	56
		4.3.4 : Truss element with real stiffness for struts	56
	4.4	: Comparison of FDM and measure-potential element with virtual stiffness	59
	4.5	: Path finding method	60
	4.6	: Bifurcation path pursuing procedure	61
	4.7	: Numerical example	62
		4.7.1 : The shape determination of tensegrity tower under gravitational influence	62
		4.7.2 : Equilibrium path finding of tensegrity tower	66

The table of contents

Chapter		Title	Page
	4.7.3	: Equilibrium solution under gravitational influence	67
	4.7.4	: Self-equilibrium shapes for pure tensegrity	72
	4.7.5	: Double storey tensegrity tower with a single control node	73
	4.8	: Discussion	81
		References	84
		List of symbols	86
5	:	**Frictionless contact analysis comprising axial force element and frame element with large displacement**	88
	5.1	: Introduction	88
	5.2	: The derivation of tangent stiffness equation for three dimensional contact case comprising axial force elements	90
	5.3	: Numerical example	92
	5.3.1	: Contact between two axial force elements	92
	5.3.2	: Multiple contact analysis	95
	5.4	: Contact of a plane frame element	100
	5.5	: Definition of contact element behavior for contact problem	105
	5.6	: The application of Timoshenko beam in node–element contact analysis	108
	5.7	: The arbitrary point load on a simply supported beam	109
	5.8	: Numerical example	111
	5.8.1	: Frictionless contact analysis of a cantilever beam	111
	5.8.2	: Accuracy comparison of FEM to TSM	115
	5.8.3	: Contact of two cantilever beams	117
	5.9	: Discussion	119
		References	121
		List of symbols	122
6	:	**Conclusion**	124
	6.1	The superiority of TSM	124

6.2 An efficient approach for form-finding analysis 125
6.3 The improvement for strong geometrically nonlinear contact analysis 126
6.4 Conclusion 127

Acknowledgement 129

List of figures

Figure	Title	Page
1.1	Snelson's Needle Tower	2
1.2	Outline of chapter structure of the dissertation	7
2.1	The increment of each digital quantities and energy	15
2.2	Iterational process of TSM	18
2.3	Flow chart of an algorithm using TSM	20
3.1	Element edge force and coordinate system of a plane frame beam	24
3.2	Nodal forces on element edges	24
3.3	Element force and element deformation quantity	27
3.4	Equilibrium state of an infinitesimal linear element in a beam element	27
3.5	Difference of length between curve and string length	28
3.6	The deformation of infinitesimal segment *dx*	29
3.7	Element deformation diagram according to FEM	35
3.8	Analysis model	39
3.9	Analysis Result	40
3.10	The comparison of convergence behavior between TSM and FEM	40
4.1	The flow of tensegrity structure analysis	46
4.2	Simplex tensegrity	48
4.3	Vector of a single node	50
4.4	Illustration of vectors by cases	51
4.5	Circulating vector	52
4.6	Vector converging at one point	52
4.7	Five storey tensegrity tower	62
4.8	The relation of incidence rate and total potential energy for equilibrium solutions	63
4.9	Deformation diagram of tensegrity tower under gravitational influence	65
4.10	The initial configuration for a double storey tensegrity tower	66
4.11	Equilibrium shape for the double storey tensegrity tower	69

List of figures

Figure	Title	Page
4.12	The equilibrium path that contains solution (A), (B), (E), (I) and (J)	69
4.13	The equilibrium path that contains solution (G), (H), (K) and (L)	70
4.14	The equilibrium path that contains solution (C) and (D)	70
4.15	The equilibrium path that contains solution (M) and (N)	71
4.16	The equilibrium path that contains solution (F), (F’) and (F”)	71
4.17	The total equilibrium paths for double storey tensegrity tower under gravitational influence	72
4.18	Equilibrium paths and self-equilibrium solutions for double storey pure tensegrity tower	73
4.19	Initial configuration, connectivity and equilibrium shape of double storey tensegrity tower	74
4.20	Main paths of the tensegrity tower	74
4.21	Equilibrium solutions obtained in the main path	75
4.22	Bifurcation points obtained from the main path	76
4.23	Bypass that connects ①-a and ①’-a	77
4.24	Equilibrium solutions obtained from bypass ①–a to ①’-a	77
4.25	The bifurcation paths from bifurcation point ①-b and ①’-b	78
4.26	The bypass that connects point ② to ②’	78
4.27	The bypass that connects point ③-a to ④’-a and ④’-a to ③’-a	79
4.28	The bypass that connects point ③-b to ④’-b, point ④-b and equilibrium solutions obtained from the paths	80
4.29	The total paths for the double storey tensegrity tower with a single control node	81
5.1	Equilibrium condition of a contact element	90
5.2	Analysis model	93
5.3	The convergence of unbalanced force and the deformation diagrams	95
5.4	Initial configuration of wire mesh	96
5.5	Compulsory displacement on each nodes	96

List of figures

Figure	Title	Page
5.6	Deformation diagrams of the wire mesh	100
5.7	Element edge forces and contact force	101
5.8	Nodal forces for contact node and both element edges	101
5.9	Element length, and length between contact node and both edges	102
5.10	Deformation of the plane frame beam	105
5.11	Deformation of a plane frame beam by the contact force	106
5.12	Beam deformation combined by the principle of super position	106
5.13	Forces working on a contacted plane frame beam	107
5.14	The BMD and SFD of a simply supported beam	109
5.15	Cantilever beam model	112
5.16	Beam deformation diagrams	113
5.17	Comparison of “critical area” by three different element force equations	114
5.18	Deformation behavior of the cantilever beam	115
5.19	The comparison of beam deformation by TSM and FEM	116
5.20	Cantilever beam deformation due to the compulsory displacement of the contact node	117
5.21	Control node displacement quantity and beam deformation diagrams	118

List of tables

Table	Title	Page
3.1	Taylor expansion of deflection angle coefficient	31
4.1	Comparison of axial force element by both methods	59

Chapter 1
Introduction

1.1 Background –Concept of tensegrity–

The field of structural engineering originated as early as the day the pyramids were built, which was followed by the construction of several ancient masterpieces such as the Great Wall of China; this field has been progressing in recent times, through the use of modern technology to construct engineering masterpieces such as the Tokyo Sky tree. In the nineteenth and twentieth centuries, architectural design was mostly developed by artisans such as Leonardo da Vinci and, Antoni Gaudi without the use of any computational method, but the integrity of such architectural structures is intact even today. Consider examples of the well-known architectural structures created by Gaudi (1852 – 1926), such as the Sagrada Familia, Casa Calvert and Park Guell. These structures are based on geometrical forms such as a hyperbolic paraboloid, hyperboloid, helicoid, and cone, which reflect forms visible in nature. Such inspirations from nature have been converted into new architectural art forms that are simple, practical and aesthetic.

Figure 1.1: Snelson's Needle Tower [1]

“Tensegrity” is a style of modern architectural design that was developed in the mid-21st century. It is based on a unique mechanical concept that “self-equilibrium” of a structure can be achieved even without a stable support condition under non-gravity. Furthermore, it does not require a sufficient number of members to satisfy Maxwell’s condition for the stability of truss structures. Although tensegrity is not a perfect reflection of Gaudi’s artwork, it is a much simpler modern design. It was first imagined in the 1920s by Karl Loganson, who displayed a proto-tensegrity system called “Gleichgewichtkonstruktion.” In the early 1940s, David Emmerich was inspired by Loganson’s work and began to study several kinds of tensile prisms and more complex tensegrity systems. Following this, in the late 1940s, R.B. Fuller initiated innovations in several concepts of tensegrity which led to research on and application of tensegrity structures. Then, inspired by Fuller, K. Snelson─a contemporary sculptor and photographer─created a structure composed of flexible and rigid members based on the tensegrity concept, which in turn led to the creation of Snelson’s “Needle Tower” (Fig. 1.1). An understanding of this structure, composed of aluminum cylinders and stainless steel cables, is considered to be crucial for studies on tensegrity structures.

Recently, tensegrity structures have attracted attention as a research topic in several fields of study, such as architectural, medical [2], mechanical, robotic [3] and civil engineering. Numerous studies on tensegrity have been conducted extensively, pertaining to aspects such as morphology, form-finding, and foldable behavior. In particular, considerable progress is expected in the application of tensegrity to a solar panel with the aim of harvesting energy in space. Tensegrity offers advantages of making a structure light weight and flexible in space, which is free from gravitational influence. However, many factors regarding tensegrity remain unknown, because of its

strong geometrical nonlinearity. This thesis attempts to make a breakthrough for the mechanism of tensegrity, by using the tangent stiffness method [4] which is a valuable tool for geometrically nonlinear analysis.

1.2 Scope and aims

A tensegrity structure, also known as “tensional integrity” was developed mathematically by Emmerich and Fuller in the 1940s'. During that period, it was initially called “structures tendues et autotendants” in French (translating to “tensile and self-stressed structures”). The main characteristic of this structure is internal self-equilibrium under the condition that the no external forces act on it. The structure is formed by groups of isolated strut components to sustain the compression forces and continuous pre-stressed cable lines to resist the tensional forces [5]. Tensegrity is applicable on Earth and also has high potential in space. A small weight, flexibility and eco-friendliness of structures are the key characteristics in modern construction and the architecture industry; a tensegrity structure possesses all these characteristics in addition to being inexpensive and durable. Although analytical studies on tensegrity have been conducted for decades, several factors pertaining to tensegrity remain unknown and are yet to be studied, although new discoveries have been made and reported sporadically.

In a general structural design process, morphologies are determined by form-finding analysis and a subsequent stress-deformation analysis using elements with real stiffness to examine its behavior. However, since a tensegrity structure is classified as one of the most extreme soft structures, large deformation should be prospected and consideration of a strong geometrical nonlinearity should be prioritized. Therefore, the author has previously applied the tangent stiffness method (TSM), which is effective in the analysis of such cases of extremely strong nonlinearity [6], including the form-finding of tensegrity [7]. In this method, a simple yet precise definition of elements can be achieved without any additional parameters for accelerating convergence or any complex derivations for expressing element’s shape.

Several methods have been developed for the form-finding of tensegrity structures. A commonly employed method for calculating the equilibrium form of pre-stressed and self-stressed reticulated structures is the force density method, which was proposed by Linkwitz and Sheck in the 1970s [8][9][10]. This method is based on the concept of defining the force-length ratios for each element, called “force densities,”

as constant [11][12]. This method was initially idealized to perform form-finding analysis for tensile structures, and it is also applicable to tensegrity structures through determination of a feasible force densities. In other words, force density method requires a special numerical process, which is indisputably nonlinear, to calculate a feasible force density. Therefore, recent studies have focused on rational acquisition of a feasible set of force densities, because this may govern the accuracy of the equilibrium shape. For example, Zhang and Ohsaki [13] demonstrated an approach to determine the feasible force densities using eigenvalue analysis, and Tibert [8] and Zhang et al. [14] examined the application of dynamic relaxation. Moreover, a study done by Micheletti and Williams [15] presented an algorithm by a second-order stress test. However, in the case a model has complex connectivity or a low-symmetry configuration, the calculation process also becomes complex and the solution becomes rather unreliable.

Ijima and Obiya [16] and Obiya et al. [17] proposed measure-potential elements with virtual stiffness and applied them to the form-finding problem for form-finding of cable nets and membrane-pneumatic structures. The proposed elements have “measure potential,” defined in function of an element's area or length. In other words, the elements have virtual stiffness that is defined freely by users. For example, if the potential of a triangular element is proportionate to its area, the element will behave as a soap film element. Furthermore, common geometric stiffness can be used in both of the following cases—form-finding analysis using virtual elements and the large-deformation analysis using actual elements. Therefore, the application of measure-potential elements to the TSM improves its performance considerably, and accuracy depends simply on the performance of the geometrical nonlinear analysis. Obiya et al. [18] showed that the measure-potential elements are also effective in the form-finding of tensegrity structures, on the basis of the definition that the axial force is proportional to the power (more than the square power) of the element length.

In general, a tensegrity structure has many equilibrium solutions corresponding to each connectivity that satisfies the tensegrity rule. Therefore, in the form-finding process, it is difficult to determine a smart, desirable and useful shape by just one set of iterations. For example, a tensegrity tower that has a stable support condition may have many solutions when subjected to an arbitrary load. Examination of equilibrium paths (which indicated by continuously plotting the fluctuation of nodal force and the displacement of the control node on the load–displacement curve) during the form-finding of a tensegrity tower provides information that can be grouped according

to and classified within each independent path. The graphical plot of these paths—obtained by form-finding on the load–displacement curve—shows analogy with elastic buckling. When load control or displacement control is applied to the computation and the path is plotted, multiple equilibrium shapes with different morphologies can be obtained where the nodal force of the control node is zero.

In the present study, each equilibrium path is considered to be classified as a main path or a bifurcation path. The equilibrium path is classified as a bifurcation path when the symmetricity of the structural configuration degenerates, i.e., when the tensegrity tower undergoes lateral buckling. The existence of multiple bifurcation paths may depend on the difference of the total number of negative eigenvalues in the tangent stiffness matrix [19]. The TSM facilitates switching from a main path to a bifurcation path through the use of eigenvectors and many paths obtained by the method will contribute to the development of a more effective form-finding method.

In addition, this study, by characterizing each self-equilibrium morphology of the tensegrity structure, may share the concept of the group theory, proposed by Kawaguchi and Kawata [20]. They characterized (grouped) structural morphologies according to the symmetry characteristic of a shape, and sub grouped other shapes that lose the degree of symmetries. However, in the present study, the forms are characterized on an equilibrium path, which is a more rational approach for evaluating structural morphologies.

An important problem to be considered in the design of tensegrity structures is "contact." Because a deployed tensegrity structure exhibits an extremely large deformation, the contact problem between elements (struts and cables) should be taken into account in its design. Further, owing to the high possibilities of strut–strut contact, cable–cable contact and strut–cable contact, contact analysis should be considered for simulating the compacting sequence numerically. Furthermore, the deformation of a tensegrity structure may even be highly complex; therefore a more than usually complicated shape function maybe required in a typical finite element method (FEM) to solve the contact problem. Previous studies on contact phenomena involving large displacements can be classified into the following four categories; contact between surfaces [21][22][23], contact between a node and a surface [24], contact between a node and an element [25][26], and contact between elements [9]. The present study, however, proposes the use of a simple yet effective approach that uses the TSM for studying the basic phenomenon of node–element contact. Some numerical examples based on element–element contact and node–element contact are demonstrated as a preliminary

assumption for the contact problem of tensegrity structures.

In case of node–element contact, it is difficult to achieve equilibrium with convergence when the contact node approaches the element edge. The sliding of the contact point toward the element edges relatively leads to the divergence of the unbalanced force. To solve this problem, in this study, a Timoshenko beam was employed as a countermeasure, including for slender beams. Although employment of the Timoshenko beam theory, the "critical area," i.e., the area where the unbalanced force hardly converges, can be made significantly smaller than those in the case of the Euler–Bernoulli beam theory.

This thesis also presents a simple algorithm for "passing through" using the inner and outer vector products, in the case that a contact point passes an edge of an element. This algorithm is shown to give stable convergence results, including in an area extremely close to the tip of the element. The findings of this study are expected to facilitate further studies on node–element contact because its definitions and analytical results are precise, reliable, simple, and highly robust.

1.3 Outline of thesis

Chapter 2 presents the fundamental concept of the TSM. The TSM includes a unique iterational process, which consists of a compatibility equation, element stiffness equation, and equilibrium equation. A particularly significant concept of TSM is the strictness of compatibility between "nodal displacement" and "element edge deformation." Therefore, the iterational process steadily leads to convergence, and it is mathematically as effective as the Newton–Raphson method. In chapter 2, the derivation of the tangent geometric stiffness based on the expansion of the "principle of stationary total potential energy" is presented.

Chapter 3 provides a precise explanation of derivation of a plane frame beam by the TSM for a geometrically nonlinear analysis. The relation between load and displacement is demonstrated schematically through derivation of equations for the tangent geometric stiffness and an element stiffness matrix. This is followed by the derivation of FEM that is based on the relation between nonlinear strain and displacement. Further, a numerical example is presented for comparing the accuracies of the TSM and FEM methods under the same initial conditions and the same element configuration. The comparison results inductively show the superiority of the TSM.

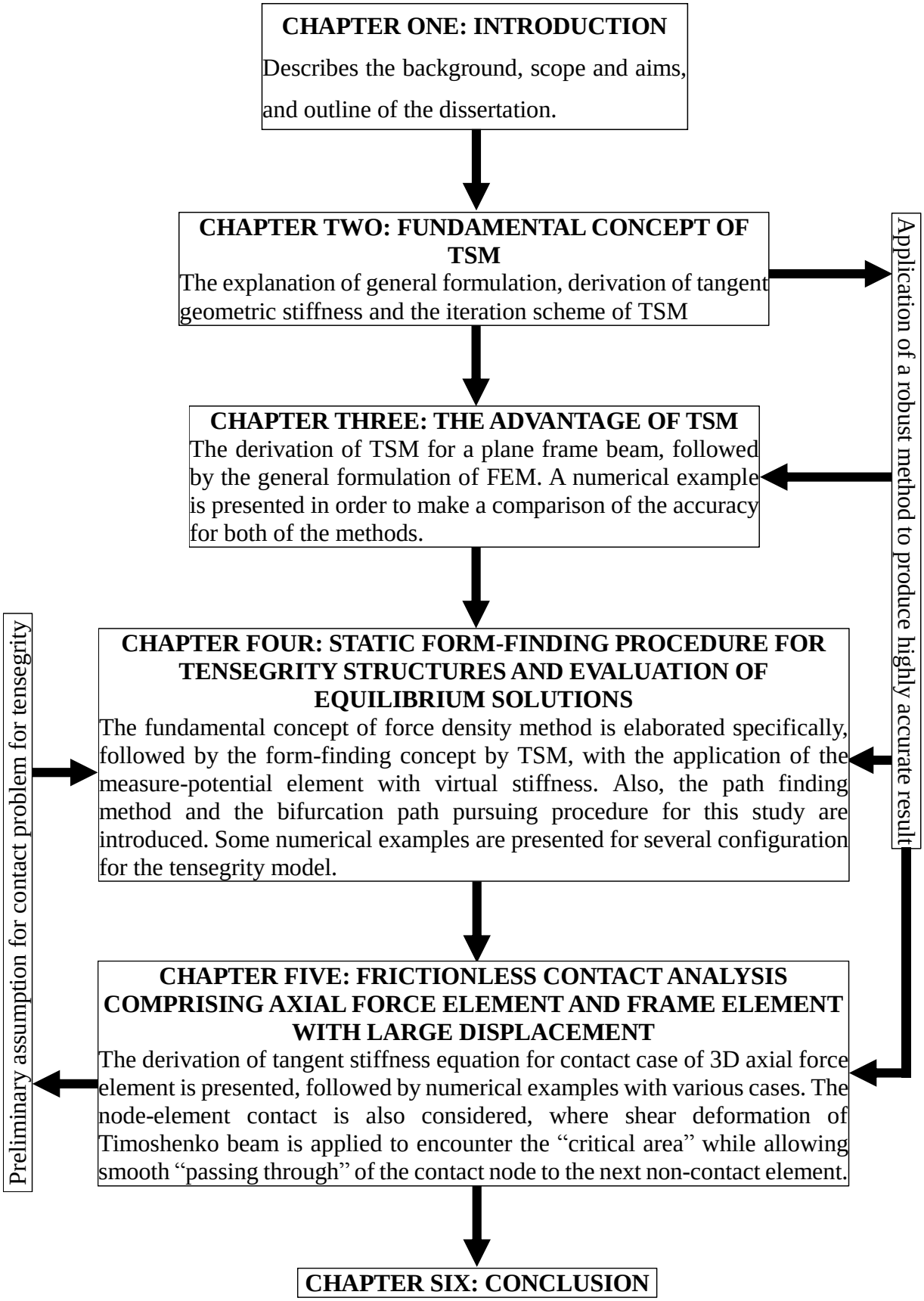

Figure 1.2: Outline of chapter structure of the dissertation

Chapter 4 presents derivation of the fundamental concept of form-finding by the force density method using a simplex tensegrity model to obtain the force density for each element. This is followed by a description of the concept of form-finding using a measure-potential element with a virtual stiffness, proposed previously by the author. In this chapter, a form-finding method for a tensegrity structure is introduced, and an equilibrium path-finding analysis is demonstrated through several examples. The analysis determines the bifurcation points by using eigenvalue analyses to obtain all paths that may exist in a single configuration of a tensegrity tower. Furthermore, a suitable number of eigenvectors are applied to switch the path direction from the main path to the bifurcation path. The solutions on the path can be classified according to the number of negative eigenvalues in the tangent stiffness matrix. Therefore, determination of all equilibrium paths provides a large amount of valuable information about the nature of self-reliant solutions of tensegrity.

Chapter 5 presents two cases for the contact problem that may occur during the process of deploying or folding a tensegrity structure. One case assumes contact between two cable elements, and the other case assumes contact between a node and a beam element. In the case of contact between cable elements, one element has the opportunity to come into contact with several other elements, when a tensegrity structure is folded. In this study, compatibility and geometric stiffness are shown under a non-friction condition. The algorithm introduced in section 1.2 can derive element edge forces explicitly non-concern with the displacement of contact node, because of strict compatibility. Numerical examples are presented, which show that the element can have many intermediate sliding nodes and that net structures with many sliding nodes can be simulated easily.

As mentioned above, this chapter also addresses contact between a node and an element of a plane frame beam. A frictionless contact element with three nodes—both of its ends and a contact node—is developed in order to apply the TSM. Here, it is shown that the contact element created by the Timoshenko beam theory has much smaller “critical area” than does an element created by Euler–Bernoulli beam theory. Two numerical examples are provided to validate the performance of the developed elements, and then, a comparison with a contact case by FEM is also presented and discussed.

Finally, chapter 6 summarizes all the findings obtained in this study. This chapter also discusses the superiority of the TSM in handling geometrically nonlinear cases.

References

[1] Needle Tower (2011): http://en.wikipedia.org/wiki/Needle_Tower

[2] **D. E. Ingber, J. D. Iamieson,** (1985): Cells as tensegrity structures: Architectural regulation of histodifferentiation by physical forces transduced over basement membrane. *Orlando Academic Press*, pp. 13–32.

[3] **F. Saijo, S. Mizuho, S. Hirai,** (2008): Analysis of deformable crawling robot with tensegrity structure. *The 9th SICE System Integration Division Annual Conference*, vol. 15 no. 8, pp. 1173–1174.

[4] **H. Obiya,** (1998): A study on accuracy and versatile of the tangent stiffness method by separation of element stiffness from geometrical stiffness (In Japanese). *Saga University, Japan*.

[5] **K. Linkwitz, H. J. Sheck,** (1971): Einige Bemerkungen zur Berechnung von vorgespannten Seilnetzkonstruktionen (In German). *Ingenieur-Archiv*, vol. 40, pp. 145–158.

[6] **H. Obiya, S. Goto, K. Ijima, K. Koga,** (1995): Equilibrium analysis of plane structures by the tangent stiffness method. *International Colloquium Stability of Steel Structures*, vol. 2, pp. 305–312.

[7] **H. Obiya, Z. M. Nizam, K. Ijima, N. Kawasaki, A. Matsuo,** (2012): A study on squilibrium shape of tensegrity structures with virtual stiffness through some numerical experiments. *Journal of Applied Mechanics JSCE*, vol. 15, pp. 45–56.

[8] **G. Tibert,** (2002): Deployable tensegrity structures for space applications. *Royal Thesis, Institute of Technology, Sweden*.

[9] **C. Sultan, R. Skelton,** (2003): Deployment of tensegrity structures. *International Journal of Solids and Structures*, vol. 40, pp. 4637–4657.

[10] **H. J. Schek,** (1974): The force density method for form finding and computation of general networks. *Computer Methods in Applied Mechanics and Engineering*, vol. 3, pp. 115–134.

[11] **N. Vassart, R. Motro,** (1999): Multiparameter form finding method: application to tensegrity systems. *International Journal of Space Structures*, vol. 14. no. 2, pp. 147–154.

[12] **R. Motro,** (1996): Structural morphology of tensegrity systems. *International Journal of Space Structures*, vol. 11. Nos. 1–2, pp. 233–240.

[13] **J. Y. Zhang, M. Ohsaki,** (2006): Adaptive force density method for form-finding method of tensegrity structures. *International Journal of Solid Structures*, vol. 43, pp.

5658–5673.

[14] **J. Y. Zhang, B. Maurin, R. Motro,** (2006): Form-finding of non-regular tensegrity systems. *Journal of Structural Engineering, ASCE*, vol. 132 no 9, pp. 1435–1440.

[15] **A. Micheletti, W. O. Williams,** (2006): A marching procedure for form-finding for tensegrity structures. *Journal of Mechanics of Materials and Structures*, pp. 101–126.

[16] **K. Ijima, H. Obiya,** (1997): Form finding of single layer structure by measure potential function of element. *International Colloquium on Structural Morphology – Towards the New Millenium*, vol. 4, pp. 249–256.

[17] **H. Obiya, K. Ijima, S. Goto, G. Aramaki, N. Kawasaki,** (2002): Shape analyses of inflation surface by the simultaneous control (In Japanese). *Transactions of JSCES*, vol. 4, pp. 37–44.

[18] **H. Obiya, K. Ijima, N. Kawasaki, N. Matsunaga, A. Matsuo,** (2010): Form finding of tensegrity structures with rigid bodies and axial line element (In Japanese). *Journal of Applied Mechanics, JSCE*, vol. 9, pp. 291–303.

[19] **S. Okazawa, F. Fujii, T. Usami,** (1997): An eigenvalue-control to trace the equilibrium path to compute an elastoplastic bifurcation point. *Journal of Structural Engineering*, vol. 43A, pp. 311–320.

[20] **K. Kawaguchi, T. Kawata,** (2008): Group theory approach of a tensegrity model with mechanisms. *Journal of Structural and Construction Engineering, Architectural Institute of Japan*, vol. 73. no. 631, pp. 1561–1568.

[21] **M. H. Aliabadi, D. Martin,** (2000): Boundary element hyper-singular formulation for elastoplastic contact problems. *International Journal for Numerical Methods in Engineering*, vol. 48, pp. 995–1014.

[22] **G. Rebel, K. C. Park, C. A. Felippa,** (2002): A contact formulation based on localized Lagrange multipliers: Formulation and application to two-dimensional problems. *International Journal for Numerical Methods in Engineering*, vol. 54, pp. 263–297.

[23] **Y. Ayyad, M. Barboteu, J. R. Fernandez,** (2009): A frictionless viscoelastodynamic contact problem with energy consistent properties: Numerical analysis and computational aspects. *Computer Methods in Applied Mechanics and Engineering*, vol. 198, pp. 669–679.

[24] **A. Klarbring,** (2002): Stability and critical points in large displacement frictionless contact problems. *J.A.C. Martins and M. Raous (Eds.) Friction and*

Instabilities, Springer, no. 457, pp. 39–64.

[25] **X. Chen, K. Nakamura, M. Mori, T. Hisada,** (1998): Finite element analysis for large deformation frictional contact problems with finite sliding. *JSME International Journal*, vol. 64, pp. 50–57.

[26] **T. Tsutsui, H. Obiya, K. Ijima,** (2009): An Algorithm for contact problem with large deformation of plane frame structures. *Advances in Computational Engineering & Science*.

Chapter 2
Fundamental Concept of Tangent Stiffness Method

2.1 Introduction

In accordance with the progress and advancement of the scientific and industrial revolution, design codes today, such as British Standard (BS), Eurocode, Japanese Industrial Standard (JIS) or American National Standard Institute (ANSI) are developed to ensure the integrity and sustainability of the modern structures. Accordingly, there are also plenty of commercial software products with specific analytical approaches that provide structural analyses and designs to meet the requirements of those design codes, such as the Abacus, NASTRAN, ANSYS etc., which allow the realization of large scale structures. The software contributes to rapid construction process, allowing limitless capabilities and speed in the designing process. Most of the above mentioned software apply the finite element method (FEM) as an analytical tool and is widely used all over the world. However, as discussed in chapter 1, the application of tangent stiffness method (TSM) to a geometrically nonlinear analysis can also satisfy all the requirements of the computational precision and efficiency, because of its concept of “equilibrium of forces”. In addition, TSM is also applicable for many types of elements such as shell, plate, cable etc.

In this chapter, the formulation of the tangent stiffness equation including tangent geometric stiffness is derived specifically; and the chapter also describes the mechanism of the iterational process which makes the unbalanced force converge. The tangent stiffness equation could be easily derived by the differentiation of equilibrium equation that connects nodal force vector in global coordinate system and element force vector in local coordinate system. Here, the element stiffness is independent from the tangent geometric stiffness, and any approximation of element behavior (described in the element force equation) is not included in the tangent geometric stiffness to even deal with complex cases.

By applying the principle of stationary potential energy, it is possible to express a symmetrical form of tangent geometric matrix. Thus, the derivation of any complicated nonlinear element stiffness equation is not necessary in TSM. Furthermore, the obtained solution does strictly adjust to the element behavior that is prescribed in the element force equation. Strict compatibility equation and equilibrium equation are used for iterational process to converge the unbalanced forces. The converged solution obtained from the iterational process in this method is mathematically adequate to the Newton-Raphson method. By comparing TSM to the general application of FEM to geometrically nonlinear analysis, it shows a very high efficiency in the performance of convergence behavior.

2.2 The general formulation of TSM

In an element within a finite element structure, the element force vector **S** and element deformation vector **s** form the element force equation, which is defined as in Eq. 2-1.

$$\mathbf{S} = \mathbf{ks} \qquad 2\text{-}1$$

(**k**= Stiffness Matrix)

Due to the mechanical fluctuation, the differentiation of Eq. 2-1 could be expressed as,

$$\delta\mathbf{S} = \boldsymbol{\kappa}\delta\mathbf{s} \qquad 2\text{-}2$$

The tangent element force equation is applied in the case of nonlinearity caused by the element deformation as shown in Eq. 2-2. In addition, when the element behavior is defined as linear, then element stiffness is defined as $\mathbf{k} = \boldsymbol{\kappa}$. Here, if the local coordinate system of a single element represents the nodal force vector in a primary equilibrium condition as **D**, the equilibrium matrix as **J**, the equilibrium equation could be expressed as;

$$\mathbf{JS} = \mathbf{D} \qquad 2\text{-}3$$

After differentiation,

$$\mathbf{J}\delta\mathbf{S} + \delta\mathbf{J}\mathbf{S} = \delta\mathbf{D} \qquad 2\text{-}4$$

the $\delta\mathbf{S}$ and $\delta\mathbf{J}$ are possible to be expressed strictly, and the linear function of nodal displacement vector, $\delta\mathbf{u}$ in the local coordinate system Eq. 2-4, could be expressed as the following equation.

$$(\mathbf{K}_O + \mathbf{K}_G)\delta\mathbf{d} = \mathbf{K}_T\delta\mathbf{d} = \delta\mathbf{D} \qquad 2\text{-}5$$

Eq. 2-5 shows the tangent stiffness equation for TSM. Here $\mathbf{K}_O$ represents the element stiffness matrix, obtained by converting $\boldsymbol{\kappa}$ from Eq. 2-2 into a local coordinate system in the compatibility equation which is calculated in every iteration step. $\mathbf{K}_G$ is the tangent geometric stiffness with nonlinear characteristics from compatibility equation which links nodal displacement vector and element deformation vector. It is also essential to develop an equation that strictly connects the geometrically nonlinear characteristics and rigid body displacements. In TSM, strict tangent stiffness equation can be obtained by a concise induction process without calculating nonlinear stiffness equation. For this, the complexity of the induction process in Lagrangian style FEM is relatively more complicated compared to the method mentioned above.

2.3 The derivation of tangent geometric stiffness

Referring to Eq. 2-3 and Eq. 2-4, the tangent geometric stiffness $\mathbf{K}_G$, could be expressed as Eq. 2-6.

$$\mathbf{K}_G = \frac{\partial(\delta\mathbf{JS})}{\partial\delta\mathbf{d}} \qquad 2\text{-}6$$

Here, it is possible to express the tangent geometric stiffness matrix based on the expansion of the principle of stationary potential energy by inducing the element force vector obtained from the prior equilibrium condition. Fig. 2.1 shows a relationship between digitalized mechanical quantities vs. energy consisting of nodal displacement, element deformation, element force and nodal force in TSM. In the first quadrant, the stiffness equation is formed from the relation of nodal displacement and nodal force, and as for the second quadrant to the rest circulated orderly is the equilibrium equation, element force equation and compatibility equation, with each mechanical quantity respectively. In addition, in Fig. 2.1, the inner rectangles consist of the known quantities of the preceding equilibrium condition. The outer rectangle consists of fluctuations for each quantities in equilibrium condition at post-deformation when the

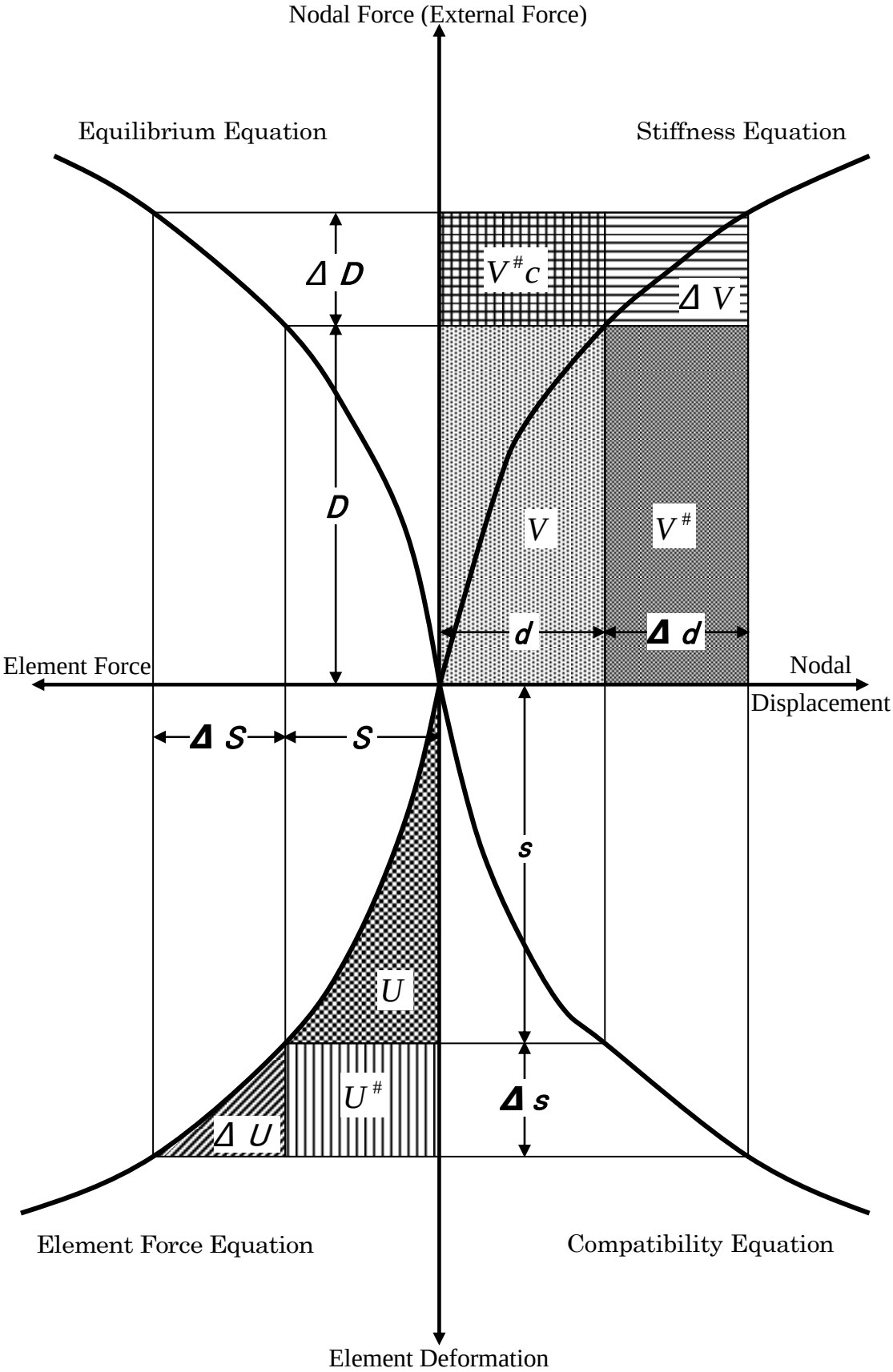

Figure 2.1: The increment of each digital quantities and energy

external load varies throughout the incremental process. Here, if the strain energy is defined as V and the loss potential due to the external force is U, then the total potential energy Π in prior equilibrium condition could be expressed as Eq. 2-7.

$$\Pi = U - V \qquad 2\text{-}7$$

The total potential energy in post deformation Π' could be expressed in Eq. 2-8.

$$\Pi' = U' - V' = \Pi + \Delta U + U^{\#} - (\Delta V + V^{\#} + V_c^{\#}) \qquad 2\text{-}8$$

According to the equilibrium condition in pre and post deformation, the total potential energy for both conditions is shown in Eq. 2-9 and Eq. 2-10.

$$\frac{\partial \Pi}{\partial \Delta \mathbf{d}} = \mathbf{0} \qquad 2\text{-}9 \qquad\qquad \frac{\partial \Pi'}{\partial \Delta \mathbf{d}} = \mathbf{0} \qquad 2\text{-}10$$

Note that in Fig. 2.1, the conjugation of node displacement $\Delta\mathbf{d}$, does not affect $V_c^{\#}$, and could be expressed in of Eq. 2-11.

$$\frac{\partial V_c^{\#}}{\partial \Delta \mathbf{d}} = 0 \qquad 2\text{-}11$$

For the remaining variables of strain energy $V^{\#}$, ΔV, and external force $U^{\#}$, ΔU, the possible impression of each mechanical components to the node displacement fluctuation are shown in Eq. 2-12 to Eq. 2-15.

$$\frac{\partial V^{\#}}{\partial \Delta \mathbf{d}} = \mathbf{D} \qquad 2\text{-}12 \qquad\qquad \frac{\partial \Delta V}{\partial \Delta \mathbf{d}} = \Delta \mathbf{D} \qquad 2\text{-}13 \qquad\qquad \frac{\partial U^{\#}}{\partial \Delta \mathbf{d}} = \frac{\partial \Delta \mathbf{s}^{\mathrm{T}}}{\partial \Delta \mathbf{d}} \mathbf{S} \qquad 2\text{-}14$$

$$\frac{\partial \Delta U}{\partial \Delta \mathbf{d}} = \frac{\partial}{\partial \Delta \mathbf{d}} \int_0^{\Delta \mathbf{s}} \Delta \mathbf{S} \mathrm{d} \Delta \mathbf{s} = \frac{\partial \Delta \mathbf{s}^{\mathrm{T}}}{\partial \Delta \mathbf{d}} \frac{\partial}{\partial \Delta \mathbf{s}^{\mathrm{T}}} \int_0^{\Delta \mathbf{s}} \Delta \mathbf{S}\, \mathbf{d} \Delta \mathbf{s} = \frac{\partial \Delta \mathbf{s}^{\mathrm{T}}}{\partial \Delta \mathbf{d}} \Delta \mathbf{S} \qquad 2\text{-}15$$

Eventually, Eq. 2-10 could be rewritten as Eq. 2-16.

$$\frac{\partial \Delta \mathbf{s}^{\mathrm{T}}}{\partial \Delta \mathbf{d}} (\mathbf{S} + \Delta \mathbf{S}) = \mathbf{D} + \Delta \mathbf{D} \qquad 2\text{-}16$$

Therefore, from the comparison of Eq. 2-16 and Eq. 2-3, it could be concluded that the conjunction of the equilibrium matrix;

$$\mathbf{J} + \Delta \mathbf{J} = \frac{\partial \Delta \mathbf{s}^{\mathrm{T}}}{\partial \Delta \mathbf{d}} \qquad 2\text{-}17$$

could be shown as Eq. 2-17. Referring to Eq. 2-4, the tangent geometric stiffness could be expressed as Eq. 2-18.

$$\mathbf{K_G} = \frac{\partial (\delta \mathbf{JS})^{\mathrm{T}}}{\partial \delta \mathbf{d}} = \left. \frac{\partial (\Delta \mathbf{JS})^{\mathrm{T}}}{\partial \Delta \mathbf{d}} \right|_{\Delta \mathbf{d} \to 0} = \left. \frac{\partial}{\partial \Delta \mathbf{d}} \left(\frac{\partial \Delta \mathbf{s}^{\mathrm{T}} \mathbf{S}}{\partial \Delta \mathbf{d}} \right) \right|_{\Delta \mathbf{d} \to 0} \qquad 2\text{-}18$$

Now, let the increment of the element deformation vector Δs, is expanded as a quadratic function form of $\Delta\mathbf{d}$, the quantity of work that has been done by element

force **S** and the fluctuation Δ**s**, so the tangent geometric stiffness $\mathbf{K_G}$ could possibly be expressed by the second order differential of Δ**d**, based on the geometrical and dynamic quantity achieved from the primary equilibrium condition. In conclusion, the tangent geometric matrix for an element with *i* row and *j* column (matrix expression) is shown in Eq. 2-19.

$$\mathbf{K}_{\mathbf{G}_{\mathbf{ij}}} = \left.\frac{\partial^2\left(\sum \Delta\mathbf{s}_{\mathbf{k}}\mathbf{S}_{\mathbf{k}}\right)}{\partial\Delta\mathbf{d}_i\partial\Delta\mathbf{d}_j}\right|_{\Delta\mathbf{d}_1,\Delta\mathbf{d}_2,\cdots,\Delta\mathbf{d}_n\to 0} \qquad 2\text{-}19$$

2.4 The iterational process of TSM

The analytical procedure of TSM can be described as the followings. The iterational process proceeds until convergence of the unbalanced force to a strict equilibrium position. The common procedure steps are:

Primary displacement	:	$\Delta\mathbf{d}_0$
Primary load	:	$\mathbf{D}_0$
Load increment	:	$\Delta\mathbf{D}$
Displacement for step of iteration (*r*)	:	$\Delta\mathbf{d}_r$
Element deformation vector	:	$\Delta\mathbf{s}_r$
Element force vector	:	$\mathbf{S}_r$
Element edge force–nodal force transformation matrix	:	$\mathbf{J}_r$
Tangent stiffness matrix	:	$\mathbf{K}_{\mathbf{T}r}$

Fig. 2.2 shows a convergence diagram for TSM. The calculation flow is executed clockwise. The first quadrant represents the relation of load and displacement. In TSM, the nonlinear stiffness equation is not involved in the calculation process and it is marked as a dotted line on the graph. The fourth quadrant represents the compatibility equation that expresses relation between nodal displacements Δ**d** in global coordinate system and element deformation vector Δ**s** in the local coordinate system. The third quadrant represents element force equation; where element behavior is prescribed in order to obtain element force vector **S** from element deformation vector. The second quadrant represents equilibrium equation, which is obtained from element force vector and the coordinate transformation for the current displacement. This is necessary to calculate in order to obtain the nodal force vector.

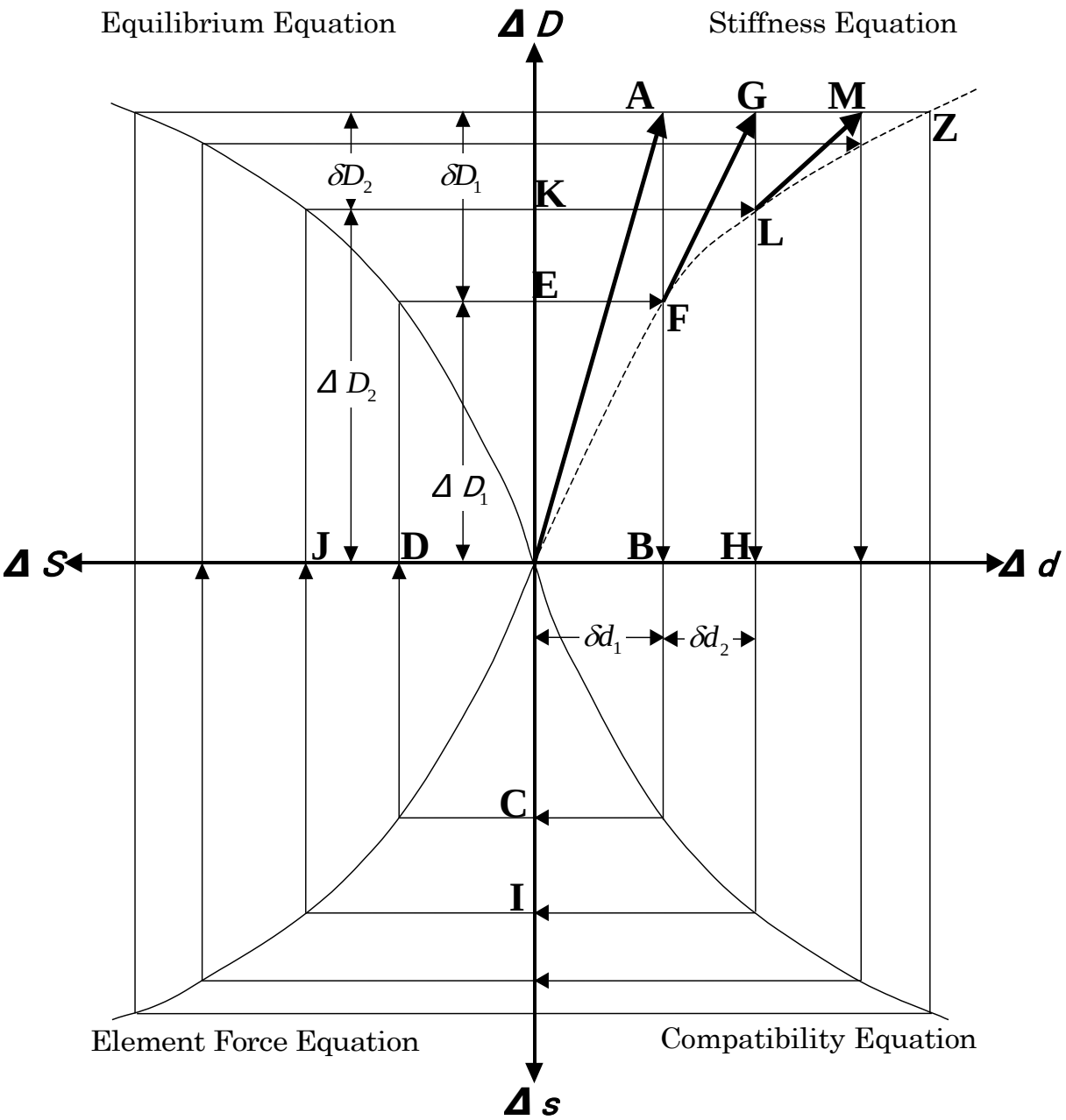

Figure 2.2: Iterational process of TSM

In Fig. 2.2, the iterational process in TSM begins from the given equilibrium state, which starts from the point of origin **O**, and the following steps describe the iteration process until converged solution is obtained.

i) $\boldsymbol{\delta}\mathbf{d}_1$ is obtained by solving tangent stiffness equation at point of origin **O**, for given value of load increment $\Delta\mathbf{D}$. (**O**→**A**→**B**)

ii) Calculation of $\Delta\mathbf{d}_1$ by adding $\boldsymbol{\delta}\mathbf{d}_1$ to the displacement $\Delta\mathbf{d}_0$ in the primary state.

iii) From the displacement $\Delta\mathbf{d}_1$, strict compatibility equation is used to obtain the element deformation vector $\Delta\mathbf{s}$. (**B**→**C**)

iv) From the element force equation $\mathbf{S}_1$, equilibrium equation is reapplied to obtain $\Delta\mathbf{D}_1$, the equilibrium state **F** could be achieved. (**C→D→E→F**)

v) Unbalanced force $\boldsymbol{\delta}\mathbf{D}_1$ is calculated by the iterational process, achieved from the difference between load condition $\Delta\mathbf{D}$ along with displacement condition $\Delta\mathbf{d}_1$, and the load vector $\Delta\mathbf{D}_1$.

vi) In this stage, **F** is reset as a primary state, the solution, $\boldsymbol{\delta}\mathbf{d}_2$ that is correspondent to the unbalanced force $\boldsymbol{\delta}\mathbf{D}_1$ is obtained by the tangent stiffness equation. (**F→G→H**)

vii) New displacement condition $\Delta\mathbf{d}_2$ is calculated by the achieved solution $\boldsymbol{\delta}\mathbf{d}_2$.

viii) The calculation for the next equilibrium state **L** is performed similar to the previous steps **H→I→J→K**.

ix) From here, the steps are repeated gradually until the equilibrium state in the first quadrant enable **s** to reach **Z**, and obtain the converged solution.

The iterational process in TSM can be expressed as

$$\boldsymbol{\Delta}\mathbf{d}_{r+1} = \boldsymbol{\Delta}\mathbf{d}_r + \mathbf{K}_{\mathrm{T}r}^{-1} \cdot \left(\mathbf{D}_0 + \boldsymbol{\Delta}\mathbf{D} - \mathbf{J}_r\mathbf{S}_r\right) \qquad \text{2-20}$$

Thus, based on Eq. 2-20, it is not necessary to formulate or apply any approximation concept in order to achieve converged solution in the calculation performed by TSM. The results from the iterational process which was explained previously, is presented by the dotted line in the first quadrant shown of Fig. 2.2 which exhibits nonlinear stiffness equation which was solved strictly while passing through the rest of the quadrants clock wisely.

In addition, Fig. 2.3 is the flow chart for a geometrically nonlinear analysis program based on the TSM. Here, the expression for each coefficient applied in the tangent stiffness matrix shows that the composition of a logical algorithm is possible without involving any complicated procedure such as shape function, dynamic relaxation, numerical integration etc. to calculate the unbalanced force. Furthermore, TSM can be easily adapted for a three-dimensional frame structure analysis which requires the consideration of rotational displacements. And in TSM, the rotation of nodes and element elongation are independent to each other which makes it possible to apply rotational composition technique by using coordinate transformation matrix.

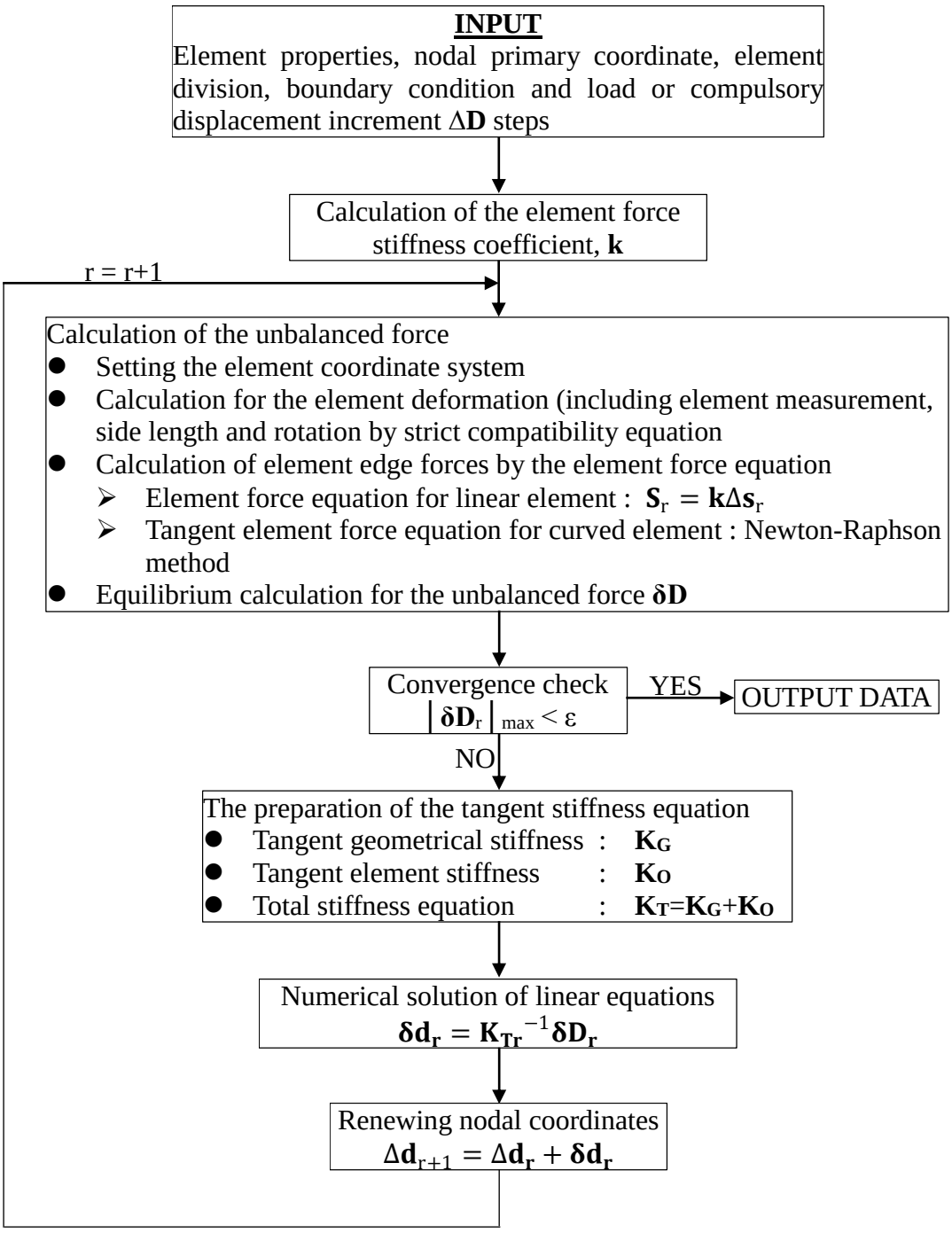

Figure 2.3: Flow chart of an algorithm using TSM

2.5 Discussion

The fundamental concept of the TSM is based on the equilibrium of forces and strictness of compatibility. As shown in Eq. 2-3 and Eq. 2-4, the derivation of the tangent stiffness equation is to calculate micro increments of nodal force by differentiation of the equilibrium condition. It is clearly shown in Eq. 2-5 that the

tangent geometric stiffness and the element stiffness are treated separately and are independent to each other. Therefore, the geometrical nonlinearity, which is caused by element's rigid body displacement, can be evaluated strictly. This makes it possible for us to select and define element behavior freely by composing element force equations. Even virtual stiffness elements can be used as well as truss, beam, membrane and plate elements, and the tangent geometric stiffness has common configuration in all cases of element definition.

Furthermore, the linear tangent stiffness matrix can be calculated explicitly and strictly in every iteration step. Therefore, the iterational process in TSM realizes rapid convergence of the unbalanced forces calculated from a strict compatibility equations. It is concluded that TSM has a very efficient geometrically nonlinear algorithm for general purposes.

List of symbols

Symbol		Description
$\mathbf{S}$	:	Element edge force vector
$\mathbf{k}$	:	Stiffness matrix for an element
$\mathbf{s}$	:	Element deformation vector
$\boldsymbol{\kappa}$	:	Tangent stiffness matrix for an element
$\mathbf{J}$	:	Element edge force–nodal force transformation matrix
$\mathbf{D}$	:	Nodal force vector
$\mathbf{K}_{\mathbf{O}}$	:	Element stiffness matrix
$\mathbf{K}_{\mathbf{G}}$	:	Tangent geometric stiffness matrix
$\mathbf{d}$	:	Nodal displacement vector
Π	:	Total potential energy
U	:	Strain energy
V	:	Loss potential due to external force

Chapter 3
The Advantage of Tangent Stiffness Method

3.1 Introduction

Tangent stiffness method (TSM) is a method that is able to treat many kinds of nonlinear cases. TSM is different from the finite element method (FEM), in that it does not have to apply any complicated nonlinear equations. The equilibrium of forces is the main concept in TSM, where every converged solution satisfies the perfect equilibrium condition. Furthermore, the high quality and accuracy of the solutions generated by TSM with strict convergence makes the calculation more reliable and realistic than other kinds of geometrically nonlinear analyzing methods. In addition, TSM could be easily applied to a wide range of elements such as truss, frame, membrane, cable elements, etc. and also could be easily configured as the method uses the displacement approach, which is a basic knowledge in the structural analysis field.

On the other hand, FEM formulates the geometric stiffness from the compatible relation between strain and nodal displacements. The fundamental concept of FEM is to discretize continuum problems which will simulate the behavior of a deformed body by the connecting nodes while obeying the equations whether it is linear, curve or parabolic, depending on the chosen shapes (which is also known as shape function). The shape function is a mathematical equation applied to interpolate all the information carried by the nodes, and depending on the shape functions, it has a bigger difference in the degree of interpolation which presumably affects the precision of the solution.

3.2 Application of TSM in plane frame structure

3.2.1 Tangent geometric stiffness

It is possible to obtain tangent geometric stiffness for plane frame structure by substituting the expansion of compatibility equation into Eq. 2-19. In this chapter, the derivation by a simple induction process which requires the differential of equilibrium equation will be shown.

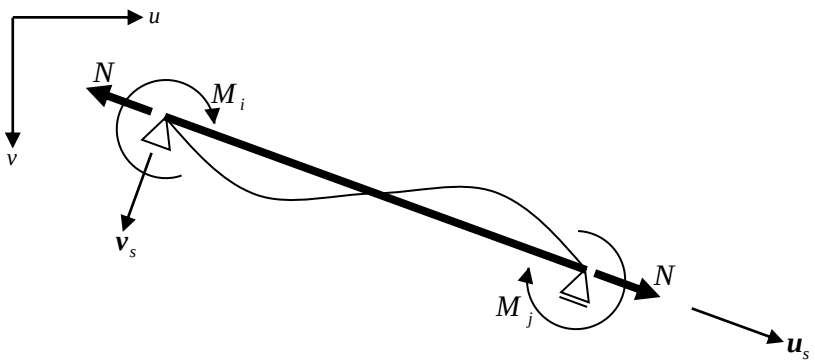

Figure 3.1: Element edge force and coordinate system of a plane frame beam

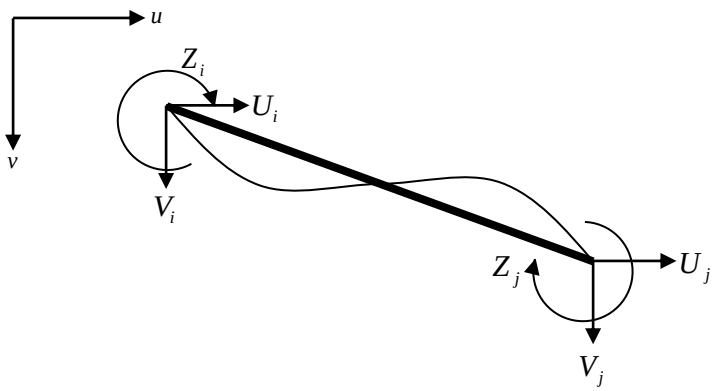

Figure 3.2: Nodal forces on element edges

Fig. 3.1 represents a single element of a plane frame beam, which the support

conditions are statically determinate. The element edge force vector for this combination of element edge forces, corresponding to the support conditions is shown in the next equation.

$$\mathbf{S} = [N \quad M_i \quad M_j]^{\mathrm{T}} \tag{3-1}$$

Further, node i is a pin fixed node, and node j is a roller node which is movable in the element axial direction. The direction from node i to node j is set as primary axial direction, and a beam coordinate system is applied for the element coordinate system. In addition, Fig. 3.2 shows the nodal forces on the element edges. When replacing global coordinate system to the element coordinate system, the expression of nodal force on the element edges could be shown as the following equation.

$$\mathbf{D} = [U_i \quad V_i \quad Z_i \quad U_j \quad V_j \quad Z_j]^{\mathrm{T}} \tag{3-2}$$

Therefore, if the cosine vectors is $\{\alpha \quad \beta\}$ and the element length is l, the equilibrium equation between element force vector and nodal force vector can be expressed as,

$$\begin{bmatrix} U_i \\ V_i \\ Z_i \\ U_j \\ V_j \\ Z_j \end{bmatrix} = \begin{bmatrix} -\alpha & -\frac{\beta}{l} & -\frac{\beta}{l} \\ -\beta & \frac{\alpha}{l} & \frac{\alpha}{l} \\ 0 & 1 & 0 \\ \alpha & \frac{\beta}{l} & \frac{\beta}{l} \\ \beta & -\frac{\alpha}{l} & -\frac{\alpha}{l} \\ 0 & 0 & 1 \end{bmatrix} \begin{bmatrix} N \\ M_i \\ M_j \end{bmatrix} \tag{3-3}$$

Here, if the node coordinates for both edges are expressed as $u_{ij}=u_j-u_i$, $v_{ij}=v_j-v_i$, the differentiation for each matrix element of the equilibrium matrix in Eq. 3-3 are shown as follows.

$$\delta l = \alpha \delta u_{ij} + \beta \delta v_{ij} \tag{3-4}$$

$$\delta \alpha = \frac{1}{l}\left(\beta^2 \delta u_{ij} + \alpha\beta \delta v_{ij}\right) \tag{3-5}$$

$$\delta \beta = \frac{1}{l}\left(-\alpha\beta \delta u_{ij} + \alpha^2 \delta v_{ij}\right) \tag{3-6}$$

$$\delta\left(\frac{\alpha}{l}\right) = \frac{1}{l^2}\left((\beta^2 - \alpha^2)\delta u_{ij} - 2\alpha\beta \delta v_{ij}\right) \tag{3-7}$$

$$\delta\left(\frac{\beta}{l}\right) = \frac{1}{l^2}\left(-2\alpha\beta \delta u_{ij} - (\beta^2 - \alpha^2)\delta v_{ij}\right) \tag{3-8}$$

If the element edge forces in Eq. 3-3 are constant, the tangent geometric stiffness matrix $\mathbf{K_G}$ could be obtained in the similar procedure as shown in Eq. 3-1 by differentiating the

equilibrium equation (see Eq. 3-3).

$$\mathbf{k_G} = \frac{N}{l}\begin{bmatrix} \beta^2 & -\alpha\beta & 0 \\ -\alpha\beta & \alpha^2 & 0 \\ 0 & 0 & 0 \end{bmatrix} + \frac{Q}{l}\begin{bmatrix} 2\alpha\beta & \beta^2-\alpha^2 & 0 \\ \beta^2-\alpha^2 & -2\alpha\beta & 0 \\ 0 & 0 & 0 \end{bmatrix} \qquad 3\text{-}9$$

$$Q = \frac{M_i + M_j}{l} \qquad 3\text{-}10$$

$$\mathbf{K_G} = \begin{bmatrix} k_G & -k_G \\ -k_G & k_G \end{bmatrix} \qquad 3\text{-}11$$

In addition, if the rotation component in Eq. 3-9 is neglected, then the equation is similar to the geometric stiffness of a plane truss element.

3.2.2 Definition for element behavior

Fig. 3.3 shows a non-stressed state for a linear plane frame beam element with a stable support condition and the deformation diagram of the beam when axial force N and edge moments M_i, M_j are applied on both edges. Here, the extensional stiffness is EA, bending stiffness EI, and non-stressed length is l_o. In Fig. 3.4, when considering infinitesimal element of the beam in an equilibrium state, the equilibrium condition of bending moment on the right edge is;

$$\frac{dM}{du_s} + N\frac{d\underline{v}}{du_s} - Q = 0 \qquad 3\text{-}12$$

If there is no existence of intermediate force, the differentiation of Eq. 3-12 makes the shear force Q becomes zero and shown in Eq. 3-13.

$$\frac{d^2M}{{du_s}^2} + N\frac{d^2\underline{v}}{{du_s}^2} = 0 \qquad 3\text{-}13$$

Here, by substituting $M = -EI(d^2v_s/{du_s}^2)$ to Eq. 3-13, then the equation represents the beam deflection as shown in Eq. 3-14.

$$\frac{d^4\underline{v}}{{du_s}^4} + N\frac{d^2\underline{v}}{{du_s}^2} = 0 \qquad 3\text{-}14$$

Using Eq. 3-15 to Eq. 3-18 as the boundary condition,

$$\underline{v}(0) = 0 \qquad 3\text{-}15 \qquad\qquad \underline{v}(l) = 0 \qquad 3\text{-}16$$

$$\left.\frac{d\underline{v}}{du_s}\right|_{x=0} = \theta_i \qquad 3\text{-}17 \qquad\qquad \left.\frac{d\underline{v}}{du_s}\right|_{x=l} = \theta_j \qquad 3\text{-}18$$

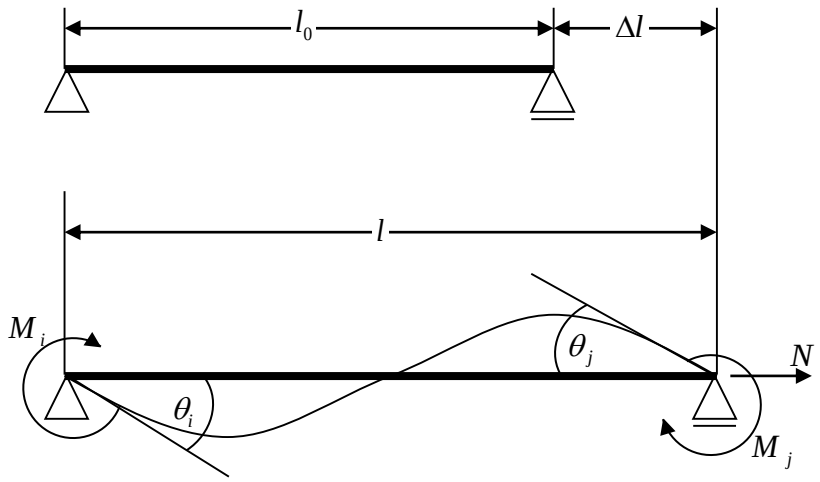

Figure 3.3: Element force and element deformation quantity

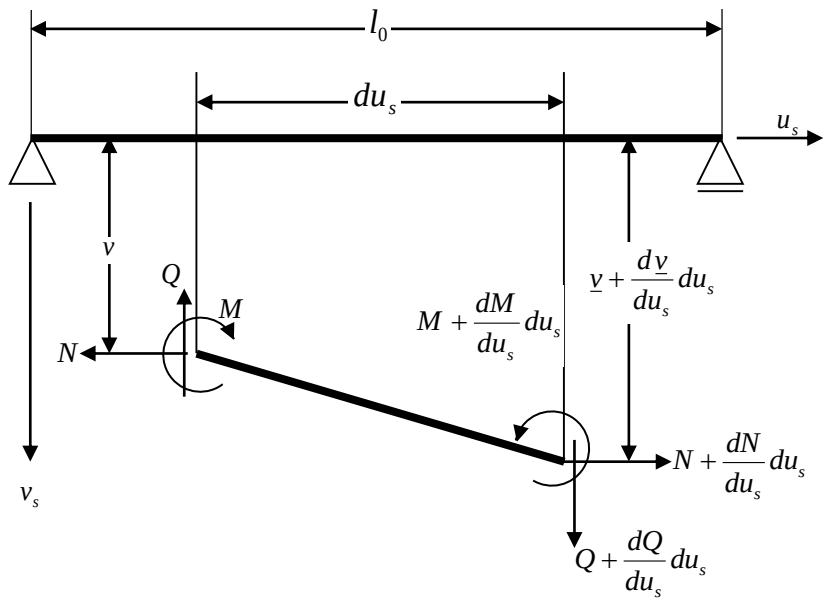

Figure 3.4: Equilibrium state of an infinitesimal linear element in a beam element

$$\left.\frac{d\underline{v}}{du_s}\right|_{x=0} = \theta_i \qquad 3\text{-}19 \qquad\qquad \left.\frac{d\underline{v}}{du_s}\right|_{x=l} = \theta_j \qquad 3\text{-}20$$

$$\begin{bmatrix} M_i \\ M_j \end{bmatrix} = \xi \begin{bmatrix} a & b \\ b & a \end{bmatrix} \begin{bmatrix} \theta_i \\ \theta_j \end{bmatrix} \qquad 3\text{-}21$$

$$\xi = \frac{EI}{l_0} \qquad 3\text{-}22$$

The result could be simplified in a matrix form as shown in Eq. 3-21, which exhibits the relation of edge moments and deflection angles for both edges. In addition, the coefficient for deflection angle *a* or *b*, are defined by the tensile or compressional force of the axial direction *N*.

$N > 0$

$$a = \frac{\omega^2 \cosh\omega - \omega \sinh\omega}{\omega \sinh\omega + 2(1 - \cosh\omega)} \quad 3\text{-}23 \qquad b = \frac{\omega \sinh\omega - \omega^2}{\omega \sinh\omega + 2(1 - \cosh\omega)} \quad 3\text{-}24$$

$N < 0$

$$a = \frac{\omega^2 \cos\omega - \omega \sin\omega}{\omega \sin\omega - 2(1 - \cos\omega)} \quad 3\text{-}25 \qquad b = \frac{\omega \sin\omega - \omega^2}{\omega \sin\omega - 2(1 - \cos\omega)} \quad 3\text{-}26$$

$$\omega = l_0 \sqrt{\frac{N}{EI}} \quad 3\text{-}27$$

3.2.3 Estimation of difference between curve and string length

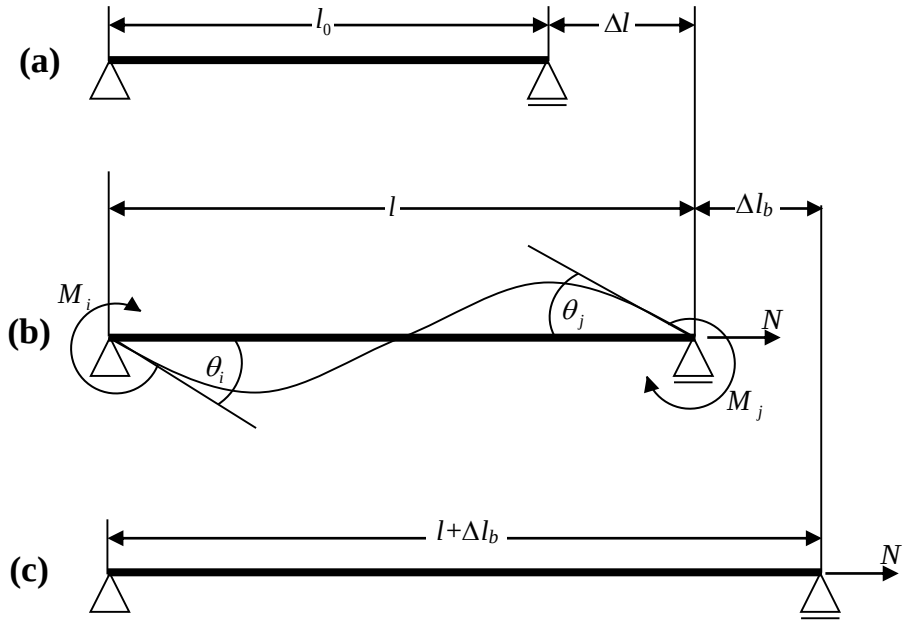

Figure 3.5: Difference of length between curve and string length

Fig. 3.5, (a) represents the non-stressed length of the beam, (b) the deformation when both axial force N and edge moments M_i and M_j are subjected simultaneously and (c) represents the deformation when axial force N is subjected on the beam. Here, when considering case (b), the elongation Δl is no longer proportionate and could be shown as the following equation.

$$N = F_0(\Delta l + \Delta l_b) \quad 3\text{-}28$$

However, referring to the effect of edge moments M_i and M_j as shown in Eq.3-21, the coefficient of deflection angle a and b as written in Eq. 3-23 and Eq. 3-24, the expression as a matrix form for Eq. 3-21 can be written as;

$$\mathbf{M} = \mathbf{G\theta} \quad 3\text{-}29$$

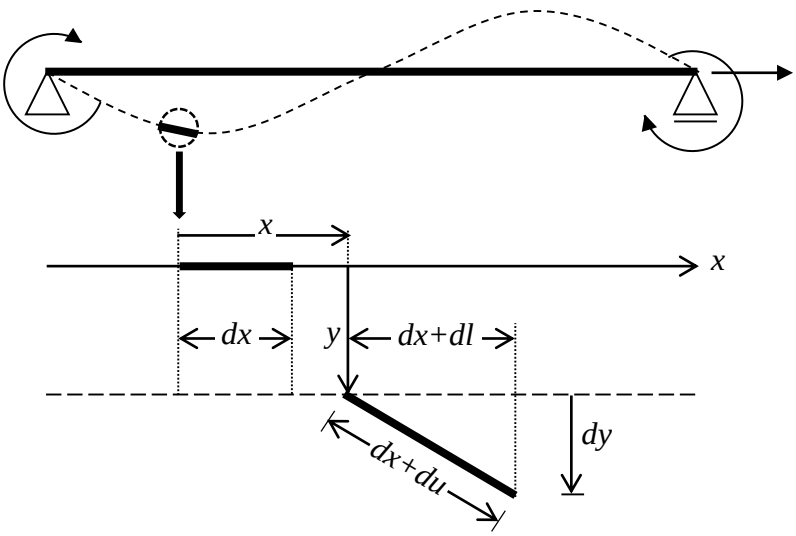

Figure 3.6: The deformation of infinitesimal segment *dx*

where **G** is the deflection angle stiffness vector. Here, the Δl_b (the difference between curve and string length), as stated in Eq. 3-28 will be derived precisely. As shown in Fig. 3.6, if the infinitesimal length *dx* of the non-stressed length and the length at post-deformation is *dx*+*du*, the relation between *dl* and *du* could be simply expressed as a Pythagoras relation shown in Eq. 3.30.

$$(dx + dl)^2 + dy^2 = (dx + du)^2$$

$$\frac{dl}{dx} + \frac{1}{2}\frac{dl^2}{dx^2} + \frac{1}{2}\frac{dy^2}{dx^2} = \frac{du}{dx} + \frac{1}{2}\frac{du^2}{dx^2} \qquad 3\text{-}30$$

The axial strain could be shown as;

$$\varepsilon = \frac{du}{dx} = \frac{dl}{dx} + \frac{1}{2}\left(\frac{dy}{dx}\right)^2 + \frac{1}{2}\left(\frac{dl^2 - du^2}{dx^2}\right) \qquad 3\text{-}31$$

By excluding the square component (extremely small) in Eq. 3-31, the equation could be rewritten as;

$$\varepsilon = \frac{du}{dx} = \frac{dl}{dx} + \frac{1}{2}\left(\frac{dy}{dx}\right)^2 \qquad 3\text{-}32$$

Eq. 3-32 represents the infinitesimal strain within a finite strain. Since the axial force could be expressed by the integration of the axial strain;

$$N = \frac{du}{dx} = \frac{\mathrm{EA}}{l_0}\int_0^{l_0} \varepsilon dx = F_0\left\{\Delta l + \frac{1}{2}\int_0^{l_0}\left(\frac{dy}{dx}\right)^2 dx\right\} \qquad 3\text{-}33$$

In addition, the difference Δl_b when edge moments are subjected on the beam (Fig. 3.8(b));

$$\Delta l_b = \frac{1}{2}\int_0^{l_0}\left(\frac{dy}{dx}\right)^2 dx \qquad 3\text{-}34$$

The Δl_b could be shown as Eq. 3-34. As shown in Fig. 3.5 (a), the case when the beam is subjected solely to axial force N, and the case when edge moments M_i and M_j are applied on both edges, Δl_b in Fig. 3.5 (c) shows the decrement of length. The strain energy produced from the difference could be shown as,

$$U = \frac{1}{2}\boldsymbol{\theta}^{\mathrm{T}}\mathbf{M} = \frac{1}{2}\boldsymbol{\theta}^{\mathrm{T}}\mathbf{G}\boldsymbol{\theta} \qquad 3\text{-}35$$

However, in this case, the axial force remains constant. With the application of the Castigliano's theory, Δl_b could be expressed as Eq. 3-36.

$$\Delta l_b = \frac{\partial \bar{U}}{\partial N} = \frac{1}{2}\boldsymbol{\theta}^{\mathrm{T}}\frac{d\mathbf{G}}{dN}\boldsymbol{\theta} \qquad 3\text{-}36$$

Using Eq. 3-36, Eq.3-33 could be rewritten as;

$$N = F_0\left(\Delta l + \frac{1}{2}\boldsymbol{\theta}^{\mathrm{T}}\frac{d\mathbf{G}}{dN}\boldsymbol{\theta}\right) \qquad 3\text{-}37$$

The deflection angle coefficient a and b are differentiated to the axial force, N and are shown in Eq. 3-38 and Eq. 3-39. The differentiation result could be simplified into a matrix form as shown in Eq. 3-40.

$$\frac{da}{dN} = \frac{l_0}{2k}\frac{a-b^2}{\omega^2} \qquad 3\text{-}38 \qquad\qquad \frac{db}{dN} = \frac{l_0}{2k}\frac{a+2b-ab}{\omega^2} \qquad 3\text{-}39$$

$$\frac{d\mathbf{G}}{dN} = \begin{bmatrix} \acute{a}k & \acute{b}k \\ \acute{b}k & \acute{a}k \end{bmatrix} = \frac{l_0}{2}\begin{bmatrix} p & \bar{p} \\ \bar{p} & p \end{bmatrix} \qquad 3\text{-}40$$

Here, Eq. 3-37 could be expressed as;

$$N = F_0\left[\Delta l + \frac{l_0}{4}\left\{p\left({\theta_i}^2 + {\theta_j}^2\right) - 2\bar{p}\theta_i\theta_j\right\}\right] \qquad 3\text{-}41$$

When the axial force $|N|<1$, the deflection angle coefficient a and b could be obtained by the Taylor expansion (Table 3.1) to obtain the p and $\bar{p}$ as shown in Eq. 3-42 and Eq. 3-43.

$$p = \frac{1}{15}\sum_{i=1}^{\infty}(-1)^{i-1}\, i \cdot a_i \left(\frac{N{l_0}^2}{30\mathrm{EI}}\right)^{i-1} \qquad 3\text{-}42$$

$$\bar{p} = \frac{1}{15}\sum_{i=1}^{\infty}(-1)^{i-1}\, i \cdot b_i \left(\frac{N l_0}{30\mathrm{EI}}\right)^{i-1} \qquad 3\text{-}43$$

According to Table 3.1, for the initial expansion when i=1, the deflection angle coefficient a=4 and b=2 which shows no influence of axial force and Eq. 3-40 is the element force equation based on infinitesimal displacement theory.

Table 3.1: Taylor expansion of deflection angle coefficient

i	1	2	3	4	5	6	7	8
a_i	4	$\frac{11}{7}$	1	$\frac{1527}{14}$	$\frac{14617}{28028}$	$\frac{153221}{392392}$	$\frac{280767}{952952}$	$\frac{17419904067}{78073451456}$
b_i	1	$\frac{13}{14}$	$\frac{11}{14}$	$\frac{2721}{4312}$	$\frac{27641}{56056}$	$\frac{298183}{784784}$	$\frac{554091}{1905904}$	$\frac{34613373741}{156146902912}$

3.2.4 The tangent element force equation for curve element

For the curve element case, the difference of element length Δl and Δl_b caused by the effect of axial force is considered and by this, the element deformation originated from the geometrical nonlinearity will be derived. Both of the axial force N in Eq. 3-41 and the deflection angle coefficient a and b in Eq. 3-21 are nonlinear equations. Here, the fluctuation of both Eq. 3-41 and Eq. 3-21 will represent the tangent element force equation. Initially, since the component of Δl_b is contained in Eq. 3-41, which shows a function of axial force N and deflection angle θ, the fluctuation could be expressed as;

$$\begin{aligned}\delta N &= F_0\left\{\delta l + \frac{\partial \Delta l_b}{\partial \theta_i}\delta\theta_i + \frac{\partial \Delta l_b}{\partial \theta_j}\delta\theta_j + \frac{\partial \Delta l_b}{\partial N}\delta N\right\} \\ &= F\left\{\delta l + \frac{1}{2}\boldsymbol{\theta}^{\mathrm{T}}\frac{d\mathbf{G}}{dN}\delta\boldsymbol{\theta} + \frac{1}{2}\boldsymbol{\theta}^{\mathrm{T}}\frac{d\mathbf{G}}{dN}\boldsymbol{\theta} + \frac{1}{2}\boldsymbol{\theta}^{\mathrm{T}}\frac{d^2\mathbf{G}}{dN^2}\delta N\right\}\end{aligned} \qquad 3\text{-}44$$

For the deflection angle component, it could be expressed as Eq. 3-45.

$$\frac{\partial \Delta l_b}{\partial \theta_i}\delta\theta_i + \frac{\partial \Delta l_b}{\partial \theta_j}\delta\theta_j = \frac{l_0}{2}\left(p\theta_i - \bar{p}\theta_j\right)\delta\theta_i + \frac{l_0}{2}\left(p\theta_j - \bar{p}\theta_i\right)\delta\theta_j = \mathbf{u}^{\mathrm{T}}\delta\boldsymbol{\theta} \qquad 3\text{-}45$$

Here,

$$\mathbf{u} = \begin{bmatrix} u_1 \\ u_2 \end{bmatrix} = \frac{l_0}{2}\begin{bmatrix} p\theta_i & -\bar{p}\theta_j \\ -\bar{p}\theta_j & p\theta_i \end{bmatrix} \qquad 3\text{-}46$$

In order to obtain $\partial \Delta l_b / \partial N$, the deflection angle coefficient a and b should be differentiate by the second derivative order.

$$\frac{d^2 a}{dN^2} = \frac{{l_0}^2}{4{\omega_0}^2 k^2}\{-a - 3b^2 + 2ab(b-1)\} \qquad 3\text{-}47$$

$$\frac{d^2 b}{dN^2} = \frac{{l_0}^2}{4{\omega_0}^2 k^2}[\{(a+b)^2 - a\}(b-1) - 2ab^2] \qquad 3\text{-}48$$

The $d^2\mathbf{G}/dN^2$ component in Eq. 3-44 could be expressed as;

$$\frac{d^2\mathbf{G}}{dN^2} = \begin{bmatrix} \ddot{a}k & \ddot{b}k \\ \ddot{b}k & \ddot{a}k \end{bmatrix} = -\frac{{l_0}^2}{2k}\begin{bmatrix} q & -\bar{q} \\ -\bar{q} & q \end{bmatrix} \qquad 3\text{-}49$$

Here, the q and $\bar{q}$ are the deflection angle coefficients and are shown as Eq. 3-50 and Eq. 3-51.

$$q = \frac{a + 3b^2 + 2ab(b-1)}{2{\omega_0}^2} \qquad 3\text{-}50 \qquad \bar{q} = \frac{\{(a+b)^2 - a\}(b-1) - 2ab^2}{2{\omega_0}^2} \qquad 3\text{-}51$$

The Taylor expansions for the deflection angle coefficients q and $\bar{q}$ are;

$$q = \frac{1}{255}\sum_{i=1}^{\infty}(-1)^{i-1}\frac{i(i+1)}{2}\cdot a_{i+1}\left(\frac{N{l_0}^2}{30\mathrm{EI}}\right)^{i-1} \qquad 3\text{-}52$$

$$\bar{q} = \frac{1}{255}\sum_{i=1}^{\infty}(-1)^{i-1}\frac{i(i+1)}{2}\cdot b_{i+1}\left(\frac{N{l_0}^2}{30\mathrm{EI}}\right)^{i-1} \qquad 3\text{-}53$$

By using the equations derived, Eq. 3-44 could be rewritten as Eq. 3-54.

$$\delta N = F_0\{\delta l + \mathbf{u}^{\mathrm{T}}\delta\boldsymbol{\theta} + \bar{W}\delta N\} \qquad 3\text{-}54$$

Here, the $\bar{W}$ is

$$\bar{W} = -\frac{1}{2}\boldsymbol{\theta}^{\mathrm{T}}\frac{d^2\mathbf{G}}{dN^2}\delta N = \frac{{l_0}^2}{4k^2}\left\{q\left({\theta_i}^2 + {\theta_j}^2\right) - 2\bar{q}\theta_i\theta_j\right\} \qquad 3\text{-}55$$

In Eq. 3-54, both sides of the equation represent the fluctuation of axial force δN, while showing a linear expression of the tangent stiffness equation. It could also be rewritten as;

$$\delta N = \frac{F_0}{1 + F_0\bar{W}}(\delta l + \mathbf{u}^{\mathrm{T}}\delta\boldsymbol{\theta}) = [F \quad Fu_1 \quad Fu_2]\begin{bmatrix} \delta l \\ \delta\theta_i \\ \delta\theta_j \end{bmatrix} \qquad 3\text{-}56$$

By differentiating Eq. 3-29, the general equation for tangent element force equation can be expressed as;

$$\begin{aligned} \delta\mathbf{M} &= \mathbf{G}\delta\boldsymbol{\theta} + \delta\mathbf{G}\boldsymbol{\theta} \\ &= \mathbf{G}\delta\boldsymbol{\theta} + \frac{\mathrm{d}\mathbf{G}}{dN}\boldsymbol{\theta}\delta N \end{aligned} \qquad 3\text{-}57$$

Further, by substituting Eq. 3-38, Eq. 3-39, Eq. 3-46 and Eq. 3-56 into the $\mathrm{d}\mathbf{G}/dN \cdot \boldsymbol{\theta}\delta N$ component of Eq. 3-57, it could be expressed as Eq. 3-58.

$$\frac{\mathrm{d}\mathbf{G}}{dN}\theta\delta N = \frac{l_0}{2}\begin{bmatrix} p & -\bar{p} \\ -\bar{p} & p \end{bmatrix}\begin{bmatrix} \theta_i \\ \theta_j \end{bmatrix}[F \quad Fu_1 \quad Fu_2]\begin{bmatrix} \delta l \\ \delta\theta_i \\ \delta\theta_j \end{bmatrix} \qquad 3\text{-}58$$

$$= \begin{bmatrix} u_1 \\ u_2 \end{bmatrix} [F \quad Fu_1 \quad Fu_2] \begin{bmatrix} \delta l \\ \delta\theta_i \\ \delta\theta_j \end{bmatrix} = \begin{bmatrix} F & {Fu_1}^2 & Fu_1u_2 \\ Fu_2 & Fu_1u_2 & {Fu_2}^2 \end{bmatrix} \begin{bmatrix} \delta l \\ \delta\theta_i \\ \delta\theta_j \end{bmatrix}$$

Furthermore, by compiling Eq. 3-54 into Eq. 3-57, the tangent element force equation could be expressed as Eq. 3-59.

$$\begin{bmatrix} \delta N \\ \delta M_i \\ \delta M_j \end{bmatrix} = \begin{bmatrix} F & Fu_1 & Fu_2 \\ Fu_1 & {Fu_1}^2 + ak & Fu_1u_2 + bk \\ Fu_2 & Fu_1u_2 + bk & {Fu_2}^2 + ak \end{bmatrix} \begin{bmatrix} \delta l \\ \delta\theta_i \\ \delta\theta_j \end{bmatrix} \qquad 3\text{-}59$$

In the algorithm, Eq. 3-59 is linked with equilibrium condition matrix and compatibility matrix to form the element stiffness matrix and by adding geometric stiffness matrix, the tangent stiffness matrix is formed. Here, by super positioning all of these equation, it is solved numerically by the simultaneous linear equation.

3.2.5 The Newton–Raphson numerical method for determining the axial force

In order to converge the unbalanced force using the iterational process by TSM, the process starts with determining the element deformation $\mathbf{s} = [\Delta l \quad \theta_i \quad \theta_j]^{\mathrm{T}}$ from a strict compatibility equation using the current nodal position, and the element force equation in Eq. 3-1 is applied to produce the solution. However, the axial force N, expressed in Eq. 3-41 is a nonlinear function which involves Δl_b and it is required to expand the equation in order to determine to precise value of N. Here, if a value of N is given,

$$\psi(N) = N - F_0(\Delta l + l_b) \qquad 3\text{-}60$$

According to the difference equation, the $\psi(N)\rightarrow 0$ is calculated and renewed using the Newton–Raphson iterative method. According to Eq. 3-59, the initial value of N when Δl_b=0, the deflection angle coefficient p and $\bar{p}$ would simulate N as a linear function could be applied. However, Eq. 3-41 will be a linear equation and if the value in the second term of Taylor expansion is applied to the deflection angle coefficients;

$$p_2 = \frac{4}{15} - \frac{11{l_0}^2}{1575\mathrm{EI}} N \qquad 3\text{-}61 \qquad\qquad \bar{p}_2 = \frac{1}{15} - \frac{13{l_0}^2}{3150\mathrm{EI}} N \qquad 3\text{-}62$$

By substituting Eq. 3-61 and Eq. 3-62 into Eq. 3-59, the calculation by iterational process could be executed with low convergence step, and the initial value for N could be expressed as Eq. 3-63.

$$N_0 = F_0\left[\Delta l + \frac{l_0}{4}\{p(\theta_i{}^2 + \theta_j{}^2) - 2\bar{p}\theta_i\theta_j\}\right]$$

$$= F_0\left[\Delta l + \frac{l_0}{30}(2\theta_i{}^2 + 2\theta_j{}^2 - \theta_i\theta_j) - \frac{l_0{}^3}{6300\mathrm{EI}}\{11(\theta_i{}^2 + \theta_j{}^2) - 13\theta_i\theta_j\}N\right] \quad 3\text{-}63$$

$$N_0 = F_0(\Delta l + G_1 - G_2 N)$$

By the simplification of Eq. 3-63,

$$N_0 = F_0\frac{\Delta l + G_1}{1 - F_0 G_2} \quad 3\text{-}64$$

Eq. 3-64 is applied to obtain the initial value. By the differentiation of Eq. 3-60, referring to Eq. 3-44 and Eq. 3-54, the iteration scheme in the Newton–Raphson method could be expressed as

$$\frac{d\psi}{dN} = \frac{d}{dN}(N - F_0\Delta l_b) = 1 - F_0\frac{d\Delta l_b}{dN} = 1 + F_0\bar{W} \quad 3\text{-}65$$

$$\bar{W} = \frac{l_0{}^2}{4k}\{q(\theta_i{}^2 + \theta_j{}^2) - 2\bar{q}\theta_i\theta_j\} \quad 3\text{-}66$$

Here, the $\bar{W}$ is applied as a replacement for the differential function. Using Eq. 3-67, the axial force N is converged with the application of the iteration scheme.

$$\frac{d\psi}{dN}(N_i + N_{i+1}) = \psi_i$$

$$N_{i+1} = N_i - \frac{\psi_i}{1 + F_0\bar{W}} \quad 3\text{-}67$$

3.3 General formulation for geometrically nonlinear analysis in FEM[2]

3.3.1 Nonlinear stiffness equation

In a plane frame structure, the cross sectional area of each member is assumed to be constant, which makes the relation between stress and strain within the cross section becomes a linear function. It also could be expressed as a common Hooke law shown in Eq. 3-68.

$$\sigma = \mathrm{E}\varepsilon \quad 3\text{-}68$$

Similar to the case of plane rigid frame, the total strain is assumed from the sum of the axial strain ε_x, and flexural strain ε_m. The approximation of axial strain ε_x and the curvature φ is shown in Eq. 3-69 and Eq. 3-70. While the flexural strain ε_m is given in

Eq. 3-71.

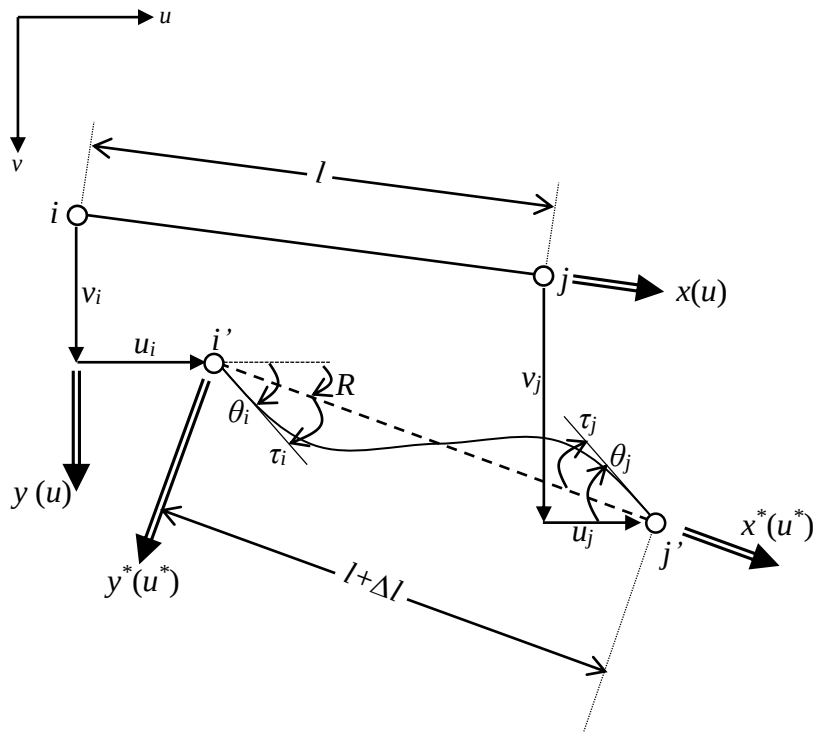

Figure 3.7: Element deformation diagram according to FEM

$$\varepsilon_x = \frac{du}{dx} + \frac{1}{2}\left(\frac{dv}{dy}\right)^2 \qquad 3\text{-}69$$

$$\varphi = -\frac{d^2v}{dx^2} \qquad 3\text{-}70$$

$$\varepsilon_m = -y\frac{d^2v}{dx^2} \qquad 3\text{-}71$$

The strain energy U for the element could be defined as;

$$U = \int_v \frac{1}{2}\mathrm{E}\varepsilon^2\mathrm{V}$$
$$= \frac{\mathrm{EA}}{2}\int_0^l \left\{\left(\frac{du}{dx}\right)^2 + \left(\frac{du}{dx}\right)\left(\frac{dv}{dx}\right)^2 + \frac{1}{4}\left(\frac{dv}{dx}\right)^4 + \frac{\mathrm{I}}{\mathrm{A}}\left(\frac{d^2v}{dx^2}\right)\right\}dx \qquad 3\text{-}72$$

Here, if the horizontal displacement is u and the lateral displacement is v, then the element displacement could be represented as Eq. 3-73 and Eq. 3-74. These are the shape functions for plane frame elements, which are applied in FEM.

$$u = \left(1 - \frac{x}{l}\right)u_i + \left(\frac{x}{l}\right)u_j \qquad 3\text{-}73$$

$$v = \left(2 - 3\frac{x^2}{l^2} + 2\frac{x^3}{l^3}\right)v_i + \left(3\frac{x^2}{l^2} - 2\frac{x^3}{l^3}\right)v_j + \left(x - 2\frac{x^2}{l} + \frac{x^3}{l^2}\right)\theta_i + \left(-\frac{x^2}{l} + \frac{x^3}{l^2}\right)\theta_j \qquad 3\text{-}74$$

The strain energy U in a non-stressed state could be described (Fig 3.7) as a function of element edge displacement $\mathbf{d} = (u_i \quad v_i \quad \theta_i \quad u_j \quad v_j \quad \theta_j)$ in the element coordinate system. Based on the induction of total potential energy, the relation of element edge force **f**, element edge displacement **d** and the stiffness matrix **k** could be shown as;

$$\mathbf{f} = \mathbf{k}(\mathbf{d}) \cdot \mathbf{d} = \{\mathbf{k_0} + \mathbf{k_1}(\mathbf{d}) + \mathbf{k_2}(\mathbf{d})\}\mathbf{d} \qquad 3\text{-}75$$

Here, $\mathbf{k_0}$ represents the stiffness matrix according to infinitesimal displacement theory, $\mathbf{k_1}$ and $\mathbf{k_2}$ are the nonlinear terms for both of the first and second order of the displacement term **d**. In addition, according to Eq. 3-75, the relation between the increment of both element edge force $\Delta\mathbf{f}$ and element edge displacement $\Delta\mathbf{d}$ could be defined as Eq. 3-76.

$$\Delta\mathbf{f} = \Delta\mathbf{k}(\mathbf{d}) \cdot \Delta\mathbf{d} = \{\mathbf{k_0} + 2\mathbf{k_1}(\mathbf{d}) + 3\mathbf{k_2}(\mathbf{d})\}\Delta\mathbf{d} \qquad 3\text{-}76$$

3.3.2 The iterational process for FEM

There are several hypothetic approximations when inducting Eq. 3-75, which exhibits the importance of avoiding the violation of those assumptions when performing a numerical analysis and the consideration of a proper calculation technique is considered to be crucial. Eq. 3-73 and Eq. 3-74 is an approximation of the displacement function which is based on infinitesimal displacement theory and the equation for the curvature contains the assumption which is $(dv/dx)^2 \leq 1$. Furthermore, the element edge displacement which is displayed in element coordinate system in post deformation state eliminates the rigid body displacement.

This shows that the rotation angle of each node does not represent the nodal rotation θ, but represents the tangential rotation angle τ. Hereby, although the element rotation is in large quantity, the tangential rotation angle remains infinitesimal, which matches the approximation in Eq. 3-70. When obtaining element edge force using the iterational process, and by applying Eq. 3-75, the post deformation equation is shown in Eq. 3-77. Further, the local coordinate system or the nodal force vector **D** could be converted and shown in Eq. 3-78.

$$\mathbf{f}^* = \mathbf{k}(\mathbf{d}^*) \cdot \mathbf{d}^* \qquad 3\text{-}77$$

$$\begin{aligned} \mathbf{D} &= \mathbf{C}(\mathbf{X}) \cdot \mathbf{k}(\mathbf{d}^*) \cdot \mathbf{d}^* \\ &= \mathbf{C}(\mathbf{X}) \cdot \mathbf{k}(\mathbf{d}^*) \cdot \mathbf{C}(\mathbf{X})^{\mathrm{T}} \cdot \mathbf{d} \end{aligned} \qquad 3\text{-}78$$

Here, **C(X)** is the coordinate's transformation matrix, obtained from the local

coordinate system which is converted to the element coordinate system in post deformation, and **X** is the nodal coordinate in post deformation achieved from the local coordinate system. Furthermore, if the element edge displacement in post deformation could be assumed as $\mathbf{d}^* = \begin{pmatrix} u_i^* & v_i^* & \theta_i^* & u_j^* & v_j^* & \theta_j^* \end{pmatrix}$, then the matrix elements are defined as Eq. 3-79 to Eq. 3-84.

$$u_j^* - u_i^* = \Delta l \qquad 3\text{-}79$$

$$v_j^* = v_i^* = 0 \qquad 3\text{-}80$$

$$\theta_i^* = \left.\frac{dv^*}{dx^*}\right|_{\boldsymbol{i}} = \tan\tau_i = \frac{(l + u_j - u_i)\cdot T_i - (v_j - v_i)}{(l + u_j - u_i) + (v_j - v_i)\cdot T_i} \qquad 3\text{-}81$$

$$\theta_j^* = \left.\frac{dv^*}{dx^*}\right|_{\boldsymbol{j}} = \tan\tau_j = \frac{(l + u_j - u_i)\cdot T_j - (v_j - v_i)}{(l + u_j - u_i) + (v_j - v_i)\cdot T_j} \qquad 3\text{-}82$$

$$T_i = \tan\theta_i = \left.\frac{dv}{dx}\right|_i \qquad 3\text{-}83 \qquad\qquad T_j = \tan\theta_j = \left.\frac{dv}{dx}\right|_j \qquad 3\text{-}84$$

In addition, equations that are related to the stiffness matrix **k(d*)**, which are from Eq. 3-77 to Eq. 3-82 are shown in the following equation.

$$\mathbf{k_o} = \begin{bmatrix} A_0 & 0 & 0 & -A_0 & 0 & 0 \\ & B_0 & C_0 & 0 & -B_0 & -C_0 \\ & & D_0 & 0 & -C_0 & E_0 \\ & & & A_0 & 0 & 0 \\ & \textit{symmetry} & & & B_0 & C_0 \\ & & & & & D_0 \end{bmatrix} \qquad 3\text{-}85$$

$$A_0 = \frac{\mathrm{EA}}{l} \qquad B_0 = \frac{12\mathrm{EI}}{l^3} \qquad C_0 = \frac{6\mathrm{EI}}{l^2}$$

$$D_0 = \frac{4\mathrm{EI}}{l} \qquad E_0 = \frac{2\mathrm{EI}}{l}$$

For the nonlinear first order of displacement term $\mathbf{k_1}$,

$$\mathbf{k_1} = \begin{bmatrix} 0 & A_1 & B_1 & 0 & -A_1 & C_1 \\ & D_1 & E_1 & -A_1 & -D_1 & E_1 \\ & & F_1 & -B_1 & -E_1 & G_1 \\ & & & 0 & A_1 & -C_1 \\ & \textit{symmetry} & & & D_1 & -E_1 \\ & & & & & F_1 \end{bmatrix} \qquad 3\text{-}86$$

$$A_1 = -\frac{\mathrm{EA}}{20l}\left(\theta_i^* + \theta_j^*\right) \qquad B_1 = -\frac{\mathrm{EA}}{60}\left(4\theta_i^* - \theta_j^*\right) \qquad C_1 = -\frac{\mathrm{EA}}{60}\left(-\theta_i^* + 4\theta_j^*\right)$$

$$D_1 = \frac{3}{5l}N^* \qquad E_1 = \frac{1}{20}N^* \qquad F_1 = \frac{l}{15}N^*$$

$$G_1 = \frac{l}{60}N^* \qquad N^* = \frac{\mathrm{EA}}{l}\left(u_j^* - u_i^*\right) = \mathrm{EA}\frac{\Delta l}{l}$$

And for the second order of the displacement term $\mathbf{k_2}$, it could be shown as the followings.

$$\mathbf{k_2} = \begin{bmatrix} 0 & 0 & 0 & 0 & 0 & 0 \\ & A_2 & B_2 & 0 & -A_2 & C_2 \\ & & E_2 & 0 & -B_2 & D_2 \\ & & & 0 & 0 & 0 \\ & \textit{symmetry} & & & A_2 & -C_2 \\ & & & & & F_2 \end{bmatrix} \qquad \text{3-87}$$

$$A_2 = \frac{3\mathrm{EA}}{70l}\left\{(\theta_i^*)^2 + \left(\theta_j^*\right)^2\right\} \qquad B_2 = -\frac{\mathrm{EA}}{280l}\left\{(\theta_i^*)^2 - 2\theta_i^*\theta_j^* - \left(\theta_j^*\right)^2\right\}$$

$$C_2 = -\frac{\mathrm{EA}}{280l}\left\{(\theta_i^*)^2 + 2\theta_i^*\theta_j^* + \left(\theta_j^*\right)^2\right\} \qquad D_2 = -\frac{\mathrm{EA}l}{840}\left\{3(\theta_i^*)^2 + 3\left(\theta_j^*\right)^2 - 4\theta_i^*\theta_j^*\right\}$$

$$E_2 = -\frac{\mathrm{EA}l}{420}\left\{12(\theta_i^*)^2 + \left(\theta_j^*\right)^2 - 3\theta_i^*\theta_j^*\right\} \qquad A_2 = -\frac{\mathrm{EA}}{20l}\left\{(\theta_i^*)^2 + 12\left(\theta_j^*\right)^2 - 3\theta_i^*\theta_j^*\right\}$$

3.4 Robustness aspect in large deformational plane frame analyses

With the aforementioned elaborations, it is appropriate to conclude that the idealization of the tangent stiffness method is much simpler and could solve any geometrically nonlinear problem, either for infinitesimal or extremely large deformation cases. In this section, the author made a comparison between TSM and FEM using a commonly used Euler–Bernoulli beam theory. Depending on the adoption of the kinematic parameters in the stiffness equation for both methods, the results of convergence steps differ, although with the same geometrical properties as of the plane frame model is being applied.

When a tremendous amount of load is subjected on a simply supported beam in a single incremental step, the amount of displacement will be in extremely large quantity, corresponding to the subjected load. In a geometrically nonlinear analysis, if the element definition is precise, the unbalanced force will tend to be easily converged. Therefore,

by the idealization of an element using displacement method in TSM, it is expected to obtain a better solution. In this subsection, the author will provide a numerical example using a plane frame beam model.

3.5 Numerical Example

In this analysis, a simply supported plane beam model is being used, and an extremely large amount of moment force is applied at the roller support until the beam deforms and buckled into a double layer circular shape. The theory can simulate a nonlinear behavior of plane frame beam with huge load in a single load incremental step. In general sense of FEM, the load is divided into small incremental steps and subjected gradually. However, the author applied an extremely large loading amount until the beam coordinate deforms in an extremely large scale. Here, a comparison of unbalanced force convergence behavior by both TSM and FEM have been done, the comparison scheme is shown in Fig. 3.9.

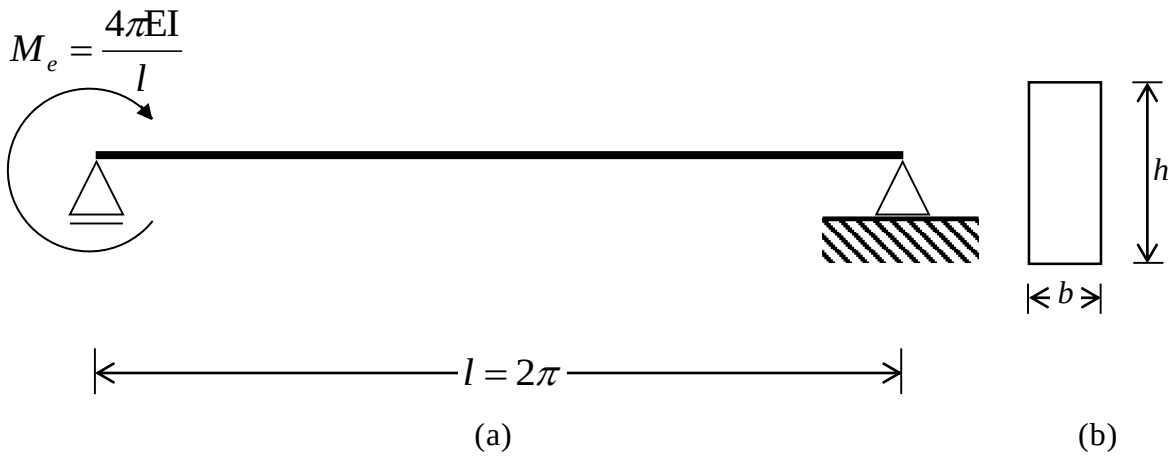

Figure 3.8: Analysis model

The magnitude of the moment load is M_e=4πEI/l on the roller node, and is applied in a single incremental step. Referring to Fig. 3.8, a simply supported plane frame beam is used for the analysis. For the analysis condition, the beam model is divided into 12 divisions, the span is 2π[m], the beam cross section is b=0.2[m] and h=0.5[m] and the Young Modulus is E=2.1x10^8[kN/m^2]. Here, the comparison of accuracy has been done by using the tangent element force equation in Eq. 3-59 for TSM, while for FEM, Eq. 3-73 and Eq. 3-74 are applied.

Method	Beam deformation	Convergence step
TSM		42
FEM		535

Figure 3.9: Analysis result

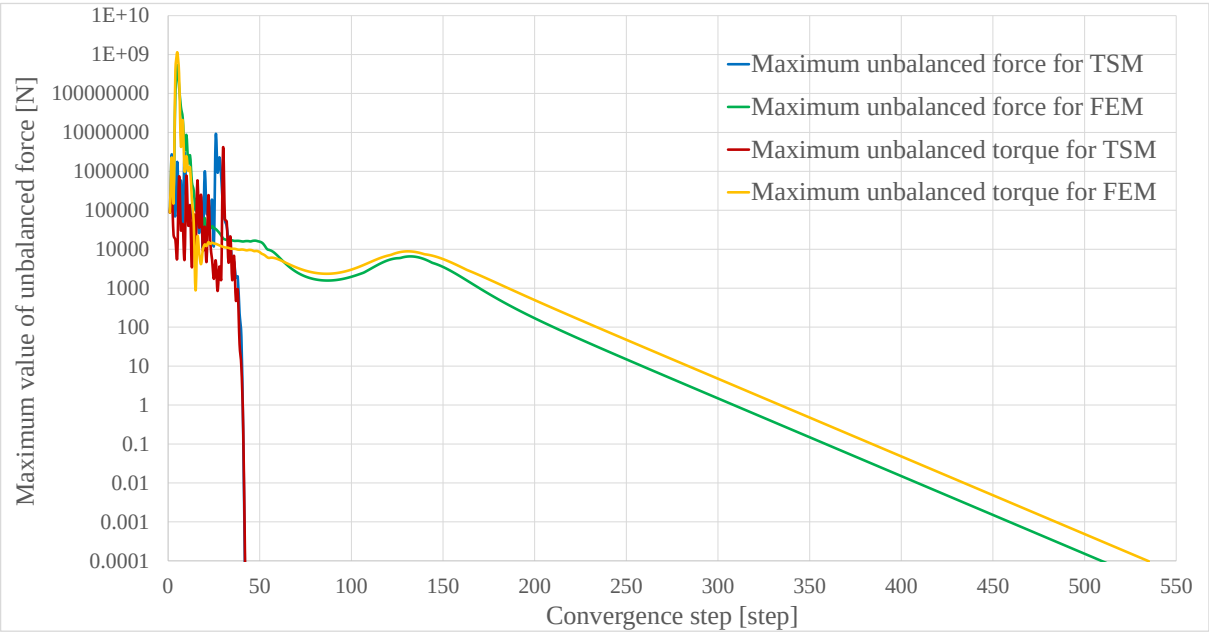

Figure 3.10: The comparison of convergence behavior between TSM and FEM

From the result of the analysis, as shown in Fig 3.9, the beam deformation by TSM shows that all nodes are perfectly aligned and redundant to each other. In addition, a curve element has been applied for TSM, which allows it to exhibit a perfectly redundant circular shape. This is because TSM considers a strict compatible condition for the element. While for FEM, the deformational shape shows a dispersed and unaligned shape. This is due to the approximation of nodal displacement by the shape function which was substituted in the nonlinear axial strain equation in Eq. 3-69. The problem is due to the derivation of stiffness equation from the compatibility equation which treats

the axial strain within the element in the global coordinate system.

The convergence behavior for both methods could be seen in Fig. 3.10. Here, the unbalanced force was converged in 42 convergence steps in TSM. TSM shows a rapid convergence behavior, while for FEM, the convergence behavior is very slow until the unbalanced force is totally converged. The total convergence step is 535 steps, which also exhibits a low accuracy of the method. This is due to the basic characteristic of FEM which does not consider strict tangent stiffness equation as shown in Eq. 3-76, and simultaneously does not evaluate the compatibility equation properly, as stated in Eq. 3-78.

In addition, the application of the tangent element force equation simulates a very strict and accurate solution, compared to the FEM. Depending on the degree of accuracy which is required, the normal tangent geometrical stiffness equation in Eq. 3-9 to Eq. 3-11 is also sufficient enough to produce a highly accurate result and significant comparison could always be made smoothly.

3.6 Discussion

In this chapter, by executing the analysis of a plane beam model using TSM, an accurate solution has been achieved, even for the case of an extremely large loading which makes the structure in the numerical example (section **3.5**) deforms with an enormous amount of nodal displacement. Here, by the derivation of tangent geometric stiffness in subsection **3.2.1**, the definition of element behavior whether a linear or a curve element in subsection **3.2.4**, and the definition of the highly accurate tangent element force equation, it is clear that TSM complies with the theoretical assumption of snap-through phenomena.

In TSM, the tangent geometric stiffness and the tangent element stiffness are defined and handled separately. In addition, delicate or complex derivations as shown in section **3.3** is not necessary, but simultaneously producing a better result. Consequently, it becomes evident that this method could be applied to any geometrically nonlinear cases [1]. Furthermore, as shown in the numerical example, it is also clear that a common FEM analysis could not comply, or even impossible to deal with extremely large deformation or extremely large loading condition, and therefore it should be revised in order to generate accurate solutions that are equivalent with the results obtained by TSM.

References

[1] **H, Obiya, S. Goto, K. Ijima, K. Koga,** (1995): Equilibrium analysis of plane frame structures by the tangent stiffness method. *International Colloquium European Session, Stability of Steel Structures*, vol. 2, pp. 305–312.

[2] **Y. Maeda, M. Hayashi, M. Nakamura,** (1974): An acceleration approach for large deformation structural analysis by incremental method. *Journal of JSCE*, vol. 223, pp. 1–9.

List of symbols

Symbol		Description
$\mathbf{S}$	:	Element edge force vector
$\mathbf{D}$	:	Nodal force vector
$\mathbf{k_G}$	:	Tangent geometric stiffness matrix
$\mathbf{M}$	:	Edge moment vector
$\mathbf{G}$	:	Deflection angle stiffness vector
$\boldsymbol{\theta}$	:	Deflection angle vector
$\mathbf{u}$	:	Axial force function vector
$\mathbf{d}$	:	Element edge displacement vector
$\mathbf{f}$	:	Element edge force vector (in FEM)
$\mathbf{k_0}$	:	Element stiffness matrix (in FEM)
$\mathbf{k_1}$	:	1st order of nonlinear term in displacement vector (in FEM)
$\mathbf{k_2}$	:	2nd order of nonlinear term in displacement vector (in FEM)
$\mathbf{C}$	:	Coordinate's transformation matrix (in FEM)
$\mathbf{X}$	:	Nodal coordinate in post deformation (in FEM)
N	:	Axial force
M_i	:	Edge moment on *i* edge
M_j	:	Edge moment on *j* edge
U_i	:	Horizontal component on *i* edge
V_i	:	Vertical component on *i* edge
Z_i	:	Rotation component on *i* edge
U_j	:	Horizontal component on *j* edge
V_j	:	Vertical component on *j* edge
Z_j	:	Rotation component on *j* edge
l	:	Element length
α	:	Cosine vector component in horizontal direction
β	:	Cosine vector component in vertical direction
u_{ij}	:	Horizontal component between *i* and *j* edge
v_{ij}	:	Vertical component between *i* and *j* edge
Q	:	Shear force
k_G	:	The matrix element of tangent geometric stiffness matrix
u_s	:	Horizontal displacement in global coordinate system (in FEM)
v_s	:	Vertical displacement in global coordinate system (in FEM)

List of symbols

Symbol		Description
θi	:	Deflection angle on *i* edge
θj	:	Deflection angle on *j* edge
l_0	:	Non-stressed length of an element
ξ	:	Bending stiffness coefficient
ω	:	Characteristic equation
Δl_b	:	String length
F_0	:	Axial force coefficient
ε	:	Element strain
u	:	Horizontal coordinate
v	:	Vertical coordinate
U	:	Strain energy
$\bar{W}$	:	Component of the fluctuation of axial force
F	:	Fluctuation of element force
ψ	:	The substitution of initial value of the axial force
σ	:	Element stress
ε_x	:	Axial strain
ε_m	:	Flexural strain
x	:	Horizontal component in global coordinate system
y	:	Vertical component in global coordinate system
τ	:	Tangential rotation angle

Chapter 4
Static Form-Finding Procedure for Tensegrity Structures and the Evaluation of Equilibrium Solutions

4.1 Introduction

Tensegrity has not only unique geometry on the rule of no connection between compression members, but also unique mechanism that the structure can be stable under the condition of less restriction than the Maxwell's law. Therefore, tensegrity has attracted the interests of many researchers and there are already various studies involving the application of this structure. The study done by Bosseus et al. [1] shows the development of dynamical models for tensegrity structure under vibration or cyclic load, and they have also examined the deformation mode (modal shape) of the tensegrity tower and compared the results using the finite element method (FEM) software. Mizuho et al. [2] have demonstrated a study about a crawling deformable robot which consists of the tensegrity structure. The crawling behavior has been done by the deformation of the structure itself. This also shows that tensegrity could have various equilibrium shapes under a single setting; even the slightest modification could change the structure morphology.

Tensegrity therefore, could produce so many equilibrium shapes and this makes it difficult to determine the feasible geometry. This is the basis for the analytical approach of tensegrity to mainly focusing on the form-finding analysis (Fig. 4.1). For example, the group theory was introduced [3] as a method to classify the morphologies based on the mechanical configuration of the tensegrity structure. In addition, there are studies that have been done based on form-finding analysis, and the force density method (FDM) has usually been applied to the form-finding process. Application of FDM to form-finding of tensegrity is to determine a "feasible set of force densities". In this respect, Vassart and Motro [4] have shown dynamic relaxation algorithm, while Ohsaki et al. [5] have examined eigenvalue analysis to obtain the feasible set of force densities.

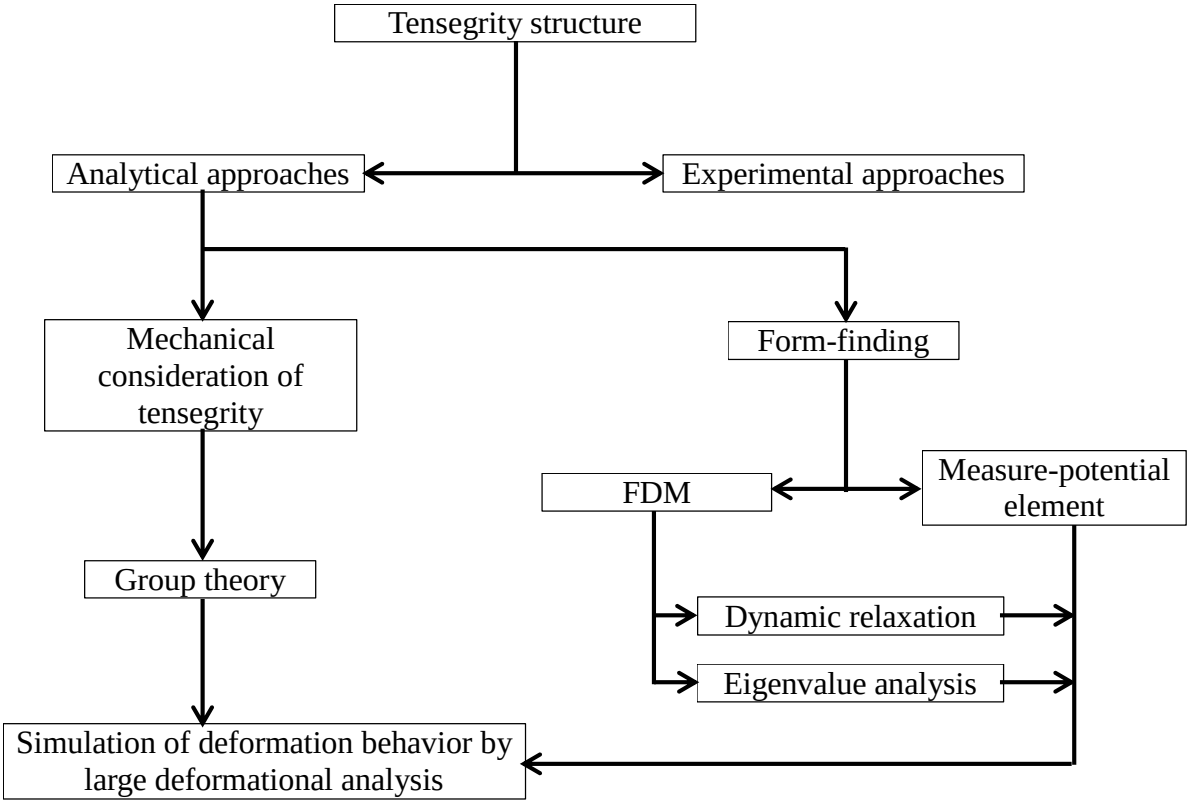

Figure 4.1: The flow of tensegrity structure analysis

In this study however, a form-finding analysis for tensegrity, and with the aid of tangent stiffness method (TSM) has been applied, which consists of measure potential element for tension members, and truss element for compression members. For the axial line elements, the potential is a proportion of (n+1)-th to the power of the element length while the axial force proportion is n-th to the power of its length; and for this, it is defined as 'n-th axial line element'. In case of n=1, the stiffness equation becomes linear and the computational process may be equal to FDM. Furthermore, when the magnitude

of n is equal or greater than 2, an iterational process is required for the form-finding process. This study also provides the investigation of paths existence; whether a main paths or secondary paths, which is also called as a bifurcation path. Using this analysis method, for each deformation mode of the structure, the negative eigenvalue of the tangent stiffness matrix would fluctuate, due to the singularity that occurs in the matrix. The negative eigenvalue usually changes at the extremum point, where the tangent of the load–displacement curve becomes zero.

When the negative eigenvalue changes except at the extremum point, singularity of the stiffness matrix occurs and this shows the existence of the bifurcation path on the curve [6]. In order to pursue the bifurcation path, an appropriate amount of eigenvector is applied and several simple technics for pursuing the path. Here, the side toppling behavior of the tensegrity tower and the decrement of symmetricity level could be observed. Every symmetrical or unsymmetrical morphologies of the tensegrity are examined and classified, by the fluctuations of negative eigenvalue and the similarity for each morphology is observed, which is simple but equivalent to the study of group of theory [4][7].

4.2 Fundamental concept of Force Density Method

The calculation procedure for FDM starts by forming branch–node matrix, where approximate value of force density vector is given for each member. Then, from the given vector, an equilibrium matrix is formed by the relation of the connectivity matrix, **C**, force density matrix, **Q**, and nodal force f_{ix} as shown in Eq. 4-1.

$$[\mathbf{C}]_i^T[\mathbf{Q}][\mathbf{C}]\{\mathbf{x}\} = \{f_{ix}\} \qquad 4\text{-}1$$

Here, the rank deficiency of the force density matrix is checked, to obtain the rank of the matrix. In FDM, the rank deficiency of the force density matrix must be equivalent to 4, which in this case, the tensegrity configuration will expand in a three dimensional space. Furthermore, by using least square method, the force density vector is determined after the nonlinear calculation process, and the feasible force density vector obtained from the calculation is applied for the form-finding analysis. The fundamental assumption of FDM for a simplex tensegrity as shown in Fig. 4.2 will be elaborated further. If the force densities of each elements for the simplex tensegrity are assumed as;

q_h : tension members that form the upper and lower triangles.

q_v : tension members that connect upper and lower nodes.

q_c : compressional members that connect upper and lower nodes.

According to FDM, the ratio of q_h, q_v and q_c could be shown the following;

$$q_h : q_v : q_c = 1 : \sqrt{3} : -\sqrt{3} \qquad 4\text{-}2$$

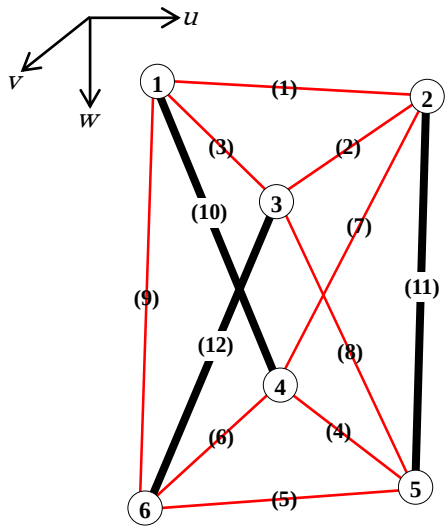

Figure 4.2: Simplex tensegrity

Based on the concept of FDM, the following equations will be derived. If the equilibrium equation is shown as;

$$\mathbf{D} = \mathbf{J} \cdot \mathbf{S} \qquad 4\text{-}3$$

In order to achieve the state of self-equilibrium where both of external and reaction forces are zero, the equation should be;

$$\mathbf{J} \cdot \mathbf{S} = \mathbf{0} \qquad 4\text{-}4$$

Here, if the equilibrium matrix J and nodal coordinate u is a linear function, according to Eq. 4-4, the self-equilibrium equation should be expressed as follow;

$$\mathbf{J} \cdot \mathbf{S} = \mathbf{Q} \cdot \mathbf{u} = \mathbf{0} \qquad 4\text{-}5$$

The nodal coordinate should obey $\mathbf{u} \neq \mathbf{0}$, as there is an existence of morphology of the structure, which means the force density matrix $\mathbf{Q} = \mathbf{0}$, into a singular matrix. As shown in Fig. 4.2, if an element (marked as 1) of the simplex tensegrity, the equilibrium equation could be expressed as;

$$\mathbf{J} \cdot \mathbf{S}_1 = \begin{bmatrix} -\alpha_1 \\ -\beta_1 \\ -\gamma_1 \\ \alpha_1 \\ \beta_1 \\ \gamma_1 \end{bmatrix} N_1 = \begin{bmatrix} -(u_2 - u_1) \\ -(v_2 - v_1) \\ -(w_2 - w_1) \\ u_2 - u_1 \\ v_2 - v_1 \\ w_2 - w_1 \end{bmatrix} \frac{N_1}{l_1} = \begin{bmatrix} q_1 & 0 & 0 & -q_1 & 0 & 0 \\ & q_1 & 0 & 0 & -q_1 & 0 \\ & & q_1 & 0 & 0 & -q_1 \\ & & & q_1 & 0 & 0 \\ & \text{Symmetry} & & & q_1 & 0 \\ & & & & & q_1 \end{bmatrix} \begin{bmatrix} u_1 \\ v_1 \\ w_1 \\ u_2 \\ v_2 \\ w_2 \end{bmatrix} \qquad 4\text{-}6$$

with, $q_1 = N_1 / l_1$ (the force density).

4.2.1 Connectivity matrix

For u, v and w directions, the equation for these directions will be the same, as shown by the following equations.

$$\begin{bmatrix} q_1 & -q_1 \\ -q_1 & q_1 \end{bmatrix} \begin{bmatrix} u_1 \\ u_2 \end{bmatrix} = \begin{bmatrix} 0 \\ 0 \end{bmatrix} \qquad 4\text{-}7$$

$$\begin{bmatrix} q_1 & -q_1 \\ -q_1 & q_1 \end{bmatrix} \begin{bmatrix} v_1 \\ v_2 \end{bmatrix} = \begin{bmatrix} 0 \\ 0 \end{bmatrix} \qquad 4\text{-}8$$

$$\begin{bmatrix} q_1 & -q_1 \\ -q_1 & q_1 \end{bmatrix} \begin{bmatrix} w_1 \\ w_2 \end{bmatrix} = \begin{bmatrix} 0 \\ 0 \end{bmatrix} \qquad 4\text{-}9$$

If all of these equations are formed together, the connectivity matrix could be expressed as;

$$\mathbf{Q} = \begin{bmatrix} Q_1 & -q_1 & -q_3 & -q_{10} & 0 & -q_9 \\ & Q_2 & -q_2 & -q_7 & -q_{11} & 0 \\ & & Q_3 & 0 & -q_8 & -q_{12} \\ & & & Q_4 & -q_4 & -q_6 \\ & \textit{Symmetry} & & & Q_5 & -q_5 \\ & & & & & Q_6 \end{bmatrix} \qquad 4\text{-}10$$

$$Q_1 = q_1 + q_3 + q_9 + q_{10} \qquad Q_2 = q_1 + q_2 + q_7 + q_{11}$$
$$Q_3 = q_2 + q_3 + q_8 + q_{12} \qquad Q_4 = q_4 + q_6 + q_7 + q_{10}$$
$$Q_5 = q_4 + q_5 + q_8 + q_{11} \qquad Q_6 = q_5 + q_6 + q_9 + q_{12}$$

Here, the solution and rank of the force density matrix, **Q** will be elaborated. Considering **u** as a column vector as shown in the following equation.

$$\mathbf{Q} \cdot \mathbf{u}^{u,v,w} = \mathbf{0} \qquad 4\text{-}11$$

As mentioned previously, with the condition of $\mathbf{u} \neq \mathbf{0}$, the matrix **Q** has to become a singular matrix. Hence, if the matrix **Q** is a n x n square matrix (rightness matrix), considering r as the rank for the matrix **Q** and r should be lower than the size, n of the matrix ($r<n$). The rank deficiency could be expressed as the following equation.

$$h = n - \mathrm{r} \geq 1 \qquad 4\text{-}12$$

Here, considering matrix **Q** as row vector,

$$\mathbf{Q} = [\mathbf{q}_1 \quad \mathbf{q}_2 \quad \mathbf{q}_3 \quad \cdots \quad \mathbf{q}_\mathrm{n}] \qquad 4\text{-}13$$

When $\mathbf{q}_1 + \mathbf{q}_2 + \mathbf{q}_3 + \cdots \mathbf{q}_\mathrm{n} = \mathbf{0}$, the theory stands up all right for not only tensegrity, but also for a frame structure which consists of axial members.

For this case, the feature of the connectivity matrix could be known as;

i) Rectangular and symmetric singular matrix.

ii) The sum of vector for the row and the column of the matrix will become a zero vector.

4.2.2 Singular matrix and rank deficiency

Consider Fig. 4.3 to exemplify the following equations within a three dimensional space, by explaining the derivation using a three dimensional vector and 3x3 matrix. In addition, this is a basic expansion concept for an *n*-th dimension for vector calculation.

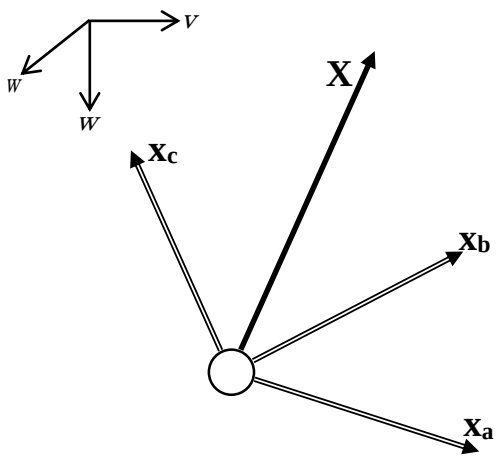

Figure 4.3: Vector of a single node

Here, in a three dimensional space, a set of three vectors are shown in the following equations;

$$\mathbf{x}_a = [x_a \quad y_a \quad z_a]^T \qquad 4\text{-}14$$

$$\mathbf{x}_b = [x_b \quad y_b \quad z_b]^T \qquad 4\text{-}15$$

$$\mathbf{x}_c = [x_c \quad y_c \quad z_c]^T \qquad 4\text{-}16$$

The common expression for a three dimensional vectors for **x** could be expressed as;

$$\mathbf{X} = l_a\mathbf{x}_a + l_b\mathbf{x}_b + l_c\mathbf{x}_c \qquad 4\text{-}17$$

Here, if vector **X** and the length **L** are expressed as;

$$\mathbf{X} = [\mathbf{x}_a \quad \mathbf{x}_b \quad \mathbf{x}_c] \qquad 4\text{-}18$$

$$\mathbf{L} = [l_a \quad l_b \quad l_c]^T \qquad 4\text{-}19$$

Then, x could be rewritten as Eq. 4-20.

$$\mathbf{x} = \mathbf{X} \cdot \mathbf{L} \qquad 4\text{-}20$$

Since l_a, l_b and l_c are independent to each other and expand randomly in a three dimensional space, there are some cases where **x** is not able to express as an axial line element, and this occurs when;

1) $\mathbf{x}_a$, $\mathbf{x}_b$ and $\mathbf{x}_c$ are together on the same plane.
2) $\mathbf{x}_a$, $\mathbf{x}_b$ or $\mathbf{x}_c$ either two of these vectors are parallel.
3) $\mathbf{x}_a$, $\mathbf{x}_b$ or $\mathbf{x}_c$ either one of these vectors is a zero vector.
4) $\mathbf{x}_a$, $\mathbf{x}_b$ and $\mathbf{x}_c$ are parallel to each other.
5) $\mathbf{x}_a$, $\mathbf{x}_b$ or $\mathbf{x}_c$ either two of these three vectors are zero vector
6) $\mathbf{x}_a$, $\mathbf{x}_b$ and $\mathbf{x}_c$ are zero vectors.

For all cases denoted above, **X** will be a singular matrix where no solution is achievable. Furthermore, for cases 1), 2) and 3), it shows a node on a plane, for 4) and 5), it shows a linear line, and for 6), it shows an origin of a point. If Eq. 4-20 could be written as

$$\begin{bmatrix} x \\ y \\ z \end{bmatrix} = \begin{bmatrix} x_a & y_a & z_a \\ x_b & y_b & z_b \\ x_c & y_c & z_c \end{bmatrix} \begin{bmatrix} l_a \\ l_b \\ l_c \end{bmatrix} \qquad 4\text{-}21$$

then, for cases 1), 2) and 3), if either one of the vector $\mathbf{x}_a$, $\mathbf{x}_b$ or $\mathbf{x}_c$ does not exist or a zero vector, the other two vectors will form a node on a plane in the three dimensional space. The rank deficiency for matrix **X** will become 2. At the same time, for cases 4) and 5) when two of the three vectors do not exist (zero vector), the rank of the matrix will become 1. In addition, for the condition of $\boldsymbol{l} \neq \mathbf{0}$and $\mathbf{x} = \mathbf{0}$, namely when l_a=l_b=l_c=0 and $\mathbf{X} \cdot \mathbf{L}$=**0**, it will be the same as for the cases 1), 4) or 6) as shown in Fig. 4.4.

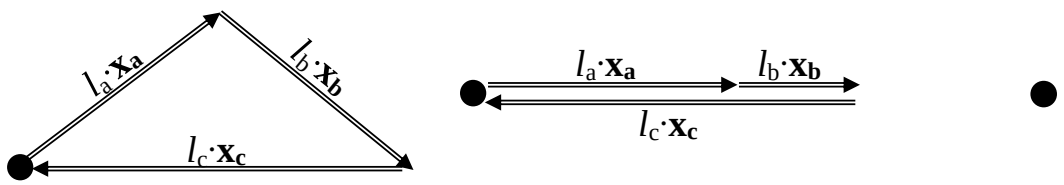

Case 1 Case 4 Case 6

Figure 4.4: Illustration of vectors by cases

In other word, if **X** is an *n* x *n* square matrix and when *l* is column vector of *n* row,

$$\mathbf{X} \cdot \mathbf{L} = \mathbf{0}, \ \ \mathbf{L} \neq \mathbf{0} \qquad 4\text{-}22$$

X will be a singular matrix, where $r < n$ (r = rank deficiency of the matrix). For case 1), when the ratio of $l_a : l_b : l_c$, is equivalent to each other, in this case, if the length of either one of the lengths is determinate, then the others will be able to be obtained. Furthermore, referring to Eq. 4-21, when defining the equilibrium matrix for tensegrity case, the force density matrix **Q** is applicable to the singular matrix **X**, which explains the feature of the connectivity matrix stated in ii). Also, when $\mathbf{x}_a + \mathbf{x}_b + \mathbf{x}_c = \mathbf{0}$, referring to Case 1), it could form the triangular shape as shown in Fig. 4.5.

In order to validate Eq. 4-17, if the condition requires the lengths is $l_a = l_b = l_c$, in

order to substitute into force density matrix **Q**, the *u*, *v* and *w* coordinate will be $u_1 = u_2 = \cdots = u_n$, $v_1 = v_2 = \cdots = v_n$ and $w_1 = w_2 = \cdots = w_n$. This leads to the third future of connectivity matrix which is;

iii) When *h* = 1, all nodes will converge at one point.

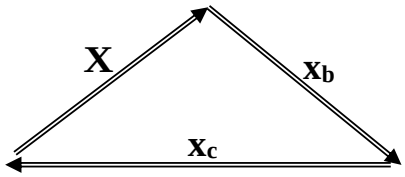

Figure 4.5: Circulating vector

When dealing with case 2), (when *n*=2), either two of l_a, l_b or l_c are determinate, in order to obtain the other one, the relation could be shown in Fig. 4.6 and is expressed in Eq. 4-23.

Figure 4.6: Vector converging at one point

$$l_c = \frac{l_a x_a + l_b x_b}{x_a + x_b} = \eta l_a + (1-\eta) l_b \qquad 4\text{-}23$$

For this case, the relation to the force density matrix **Q**, could be expressed as Eq. 4-21. All of the nodal vectors from $\mathbf{u}_1$ to $\mathbf{u}_n$ will be linear to vector $\mathbf{u}_{12}$ direction. This also explains the rest of the features of connectivity matrix which are;

iv) When *h* = 2, all nodes will be in a linear state.

v) When *h* = 3, all nodes is one a plane.

vi) When *h* = 4, all nodes will expand in a three dimensional space.

$$\begin{bmatrix} u_1 \\ u_2 \\ u_3 \\ u_4 \\ \vdots \\ u_n \end{bmatrix} = \begin{bmatrix} l_a \\ l_b \\ \eta_1 l_a + (1-\eta_1) l_b \\ \eta_2 l_a + (1-\eta_2) l_b \\ \vdots \\ \eta_n l_a + (1-\eta_n) l_b \end{bmatrix} \qquad 4\text{-}24$$

However, when considering Eq. 4-13, which is the singular matrix **Q** for simplex tensegrity case, the decisive configuration may have multiple axis of symmetry. If the symmetrical behavior is already known, it could be concluded that;

$$q_1 = q_2 = q_3 = q_4 = q_5 = q_6 = q_h \qquad 4\text{-}25$$

$$q_7 = q_8 = q_9 = q_v \tag{4-26}$$

$$q_{10} = q_{11} = q_{12} = q_c \tag{4-27}$$

Referring to Eq. 4-25 to Eq. 4-27, the force density matrix **Q** could be shown as the following.

$$\mathbf{Q} = \begin{bmatrix} Q & -q_h & -q_h & -q_c & 0 & -q_v \\ & Q & -q_h & -q_v & -q_c & 0 \\ & & Q & 0 & -q_v & -q_c \\ & & & Q & -q_h & -q_h \\ & \textit{Symmetry} & & & Q & -q_h \\ & & & & & Q \end{bmatrix} \tag{4-28}$$

$$\mathrm{Q} = 2q_h + q_v + q_c$$

In FDM, in order to obtain a cubical shape in a three dimensional space, the rank deficiency, h = 4 and the rank of the matrix will become 2. In addition, if the rotation based on node 1, the symmetrical behavior of nodal coordinate of node 2 to node 6 could be expressed in Eq. 4-29 to Eq. 4-31.

$$\begin{bmatrix} \boldsymbol{u}_1 \\ \boldsymbol{u}_2 \\ \boldsymbol{u}_3 \\ \boldsymbol{u}_4 \\ \boldsymbol{u}_5 \\ \boldsymbol{u}_6 \end{bmatrix} = \begin{bmatrix} 1 & 0 & -\frac{1}{2} & \frac{\sqrt{3}}{2} & -\frac{1}{2} & -\frac{\sqrt{3}}{2} & 1 & 0 & -\frac{1}{2} & \frac{\sqrt{3}}{2} & -\frac{1}{2} & -\frac{\sqrt{3}}{2} \\ 0 & 1 & -\frac{\sqrt{3}}{2} & -\frac{1}{2} & \frac{\sqrt{3}}{2} & -\frac{1}{2} & 0 & -1 & \frac{\sqrt{3}}{2} & \frac{1}{2} & -\frac{\sqrt{3}}{2} & \frac{1}{2} \end{bmatrix}^{\mathrm{T}} \begin{bmatrix} u_1 \\ v_1 \end{bmatrix} \tag{4-29}$$

$$\begin{bmatrix} u_1 \\ u_2 \\ u_3 \\ u_4 \\ u_5 \\ u_6 \end{bmatrix} = \begin{bmatrix} 1 & -\frac{1}{2} & -\frac{1}{2} & 1 & -\frac{1}{2} & -\frac{1}{2} \\ 0 & -\frac{\sqrt{3}}{2} & \frac{\sqrt{3}}{2} & 0 & \frac{\sqrt{3}}{2} & -\frac{\sqrt{3}}{2} \end{bmatrix}^{\mathrm{T}} \begin{bmatrix} u_1 \\ v_1 \end{bmatrix} \tag{4-30}$$

$$\begin{bmatrix} w_1 \\ w_2 \\ w_3 \\ w_4 \\ w_5 \\ w_6 \end{bmatrix} = \begin{bmatrix} 1 \\ 1 \\ 1 \\ -1 \\ -1 \\ -1 \end{bmatrix} w_1 \tag{4-31}$$

If the equilibrium condition is rewritten by the derivation of the force density for u and v direction as shown in Eq. 4-32;

$$\mathbf{U}^u = \mathbf{C}^u \mathbf{u}_1 \tag{4-32}$$

While for w direction, the equation could be expressed as;

$$\mathbf{U}^w = \mathbf{C}^w \mathbf{u}_1 \tag{4-33}$$

The relation between force density matrix **Q** and connectivity matrix **C** in self-equilibrium condition (when external force is zero) is shown from Eq. 4-34 to Eq. 4-36.

$$\mathbf{Q} \cdot \mathbf{u} = \overline{\mathbf{U}} \tag{4-34}$$

$$\begin{bmatrix}0\\0\end{bmatrix} = \mathbf{C}^{u\mathrm{T}}\mathbf{Q}\mathbf{C}^{u}\mathbf{u}_1 \qquad 4\text{-}35$$

$$0 = \mathbf{C}^{w\mathrm{T}}\mathbf{Q}\mathbf{C}^{w}w_1 \qquad 4\text{-}36$$

The equilibrium equation could be expressed as Eq. 4-37.

$$\mathbf{C}^{u\mathrm{T}}\mathbf{Q}\mathbf{C}^{u} = \begin{bmatrix} 1 & -1/2 & -1/2 & 1 & -1/2 & -1/2 \\ 0 & -\sqrt{3}/2 & \sqrt{3}/2 & 0 & \sqrt{3}/2 & -\sqrt{3}/2 \end{bmatrix} \begin{bmatrix} Q & -q_h & -q_h & -q_c & 0 & -q_v \\ & Q & -q_h & -q_v & -q_c & 0 \\ & & Q & 0 & -q_v & -q_c \\ & & & Q & -q_h & -q_h \\ & & & & Q & -q_h \\ & & & & & Q \end{bmatrix} \begin{bmatrix} 1 & 0 \\ -1/2 & -\sqrt{3}/2 \\ -1/2 & \sqrt{3}/2 \\ 1 & 0 \\ -1/2 & \sqrt{3}/2 \\ -1/2 & -\sqrt{3}/2 \end{bmatrix} \qquad 4\text{-}37$$

Symmetry

Also, the total force density of an elements on each node are shown in Eq. 4-38.

$$Q = 2q_h + q_v + q_c \qquad 4\text{-}38$$

For u and v direction, the equilibrium equation is shown in Eq. 4-39.

$$\mathbf{C}^{u\mathrm{T}}\mathbf{Q}\mathbf{C}^{u} = 9\begin{bmatrix} q_h + \dfrac{q_v}{2} & \dfrac{1}{2\sqrt{3}}q_v \\ \dfrac{1}{2\sqrt{3}}q_v & q_h + \dfrac{q_v}{6} + \dfrac{q_c}{3} \end{bmatrix} \qquad 4\text{-}39$$

As for w direction, the equation is as follow.

$$\mathbf{C}^{w\mathrm{T}}\mathbf{Q}\mathbf{C}^{w} = 12(q_v + q_c) = 0 \qquad 4\text{-}40$$

Since q_c represents the compressional member, the relation with the tensile q_v member could be shown as Eq. 4-41.

$$q_c = -q_v \qquad 4\text{-}41$$

Substituting Eq. 4-41 to Eq. 4-39;

$$\left(1 + \frac{\mathrm{Q}_v}{2}\right)\left(1 - \frac{\mathrm{Q}_v}{2}\right) - \frac{{\mathrm{Q}_v}^2}{6} = 1 - \left(\frac{1}{4} + \frac{1}{6}\right){\mathrm{Q}_v}^2 = 1 - \frac{1}{3}{\mathrm{Q}_v}^2 = 0 \qquad 4\text{-}42$$

Eventually, the result could be shown in Eq. 4-43.

$$\mathrm{Q}_v = \frac{q_h}{q_v} = -\sqrt{3} \qquad 4\text{-}43$$

To conclude, the ratio of force density for simplex tensegrity is shown in Eq. 4-44.

$$q_k : q_v : q_c = 1 : \sqrt{3} : -\sqrt{3} \qquad 4\text{-}44$$

Here, in order to obtain a cubical expansion in three dimensional space, the rank deficiency for the force density matrix **Q** should be h = 4. This is called "form condition" or "nondegenerate condition" in FDM, and the ratio of force density will be able to be obtained by completely satisfying these conditions.

4.3 Form-finding by TSM

4.3.1 The development of measure-potential element with virtual stiffness

The measure-potential element with virtual stiffness for tensegrity structure has been developed and it is also applicable for cable nets and membrane pneumatic structures. The proposed elements have the measure-potential; defined as a function of element area or element length. If the potential of a triangular element is proportionate to its area, then the element will behave as a soap film element. Therefore, the accuracy of the solution is simply depending on the performance of the geometrically nonlinear analysis.

As for the axial line elements, the potential is a proportion of (n+1)-th to the power of the element length while the axial force proportion is n-th to the power of its length; and for this, it is defined as "n-th axial line element". In the case of n=1, the stiffness equation becomes linear and the computational process may be equal to FDM. Furthermore, when the magnitude of n is equal to or greater than 2, the form-finding performance needs iterational process but as the structure deforms and expands in a three dimensional space, there are numerous possibilities for achieving an equilibrium shape.

4.3.2 Element potential function

In order to regulate the element behaviour in the local coordinate, the definition of measure-potential is expressed as a function of measurement such as element length or element area. The definition of element measure-potential is assumed to be equal to the element "virtual" stiffness. In addition, the definition does not relate to the material stiffness. Assume the element measure-potential as P, and the element measurement vector which is independent to each other as s, the element edge force could be expressed as the following equation.

$$\mathbf{S} = \frac{\partial P}{\partial \mathbf{s}} \qquad \text{4-45}$$

4.3.3 Axial line element

Consider an element is connected by two nodes, node 1 and node 2. Suppose that the element measure-potential is proportionate to the power of length of the line element, and then it can be expressed as;

$$P = Cl^{n+1} \tag{4-46}$$

The axial line element can be obtained by differentiating the equation displayed above.

$$N = nCl^{n} \tag{4-47}$$

C is a coefficient that is able to be set freely. If $\boldsymbol{\alpha}$ is the cosine vector for the axial line element which connects node 1 and node 2, then Eq. 2-3 could be re-expressed as:

$$\begin{bmatrix} \mathbf{D_1} \\ \mathbf{D_2} \end{bmatrix} = \begin{bmatrix} -\boldsymbol{\alpha} \\ \boldsymbol{\alpha} \end{bmatrix} N \tag{4-48}$$

Substituting Eq. 4-43 to Eq. 2-5, then the matrix could be expressed as;

$$\delta \begin{bmatrix} \mathbf{D_1} \\ \mathbf{D_2} \end{bmatrix} = \mathbf{K}_{\mathrm{T}}^{\mathrm{L}} \delta \begin{bmatrix} \mathbf{u_1} \\ \mathbf{u_2} \end{bmatrix} \tag{4-49}$$

$$\mathbf{K}_{\mathrm{T}}^{\mathrm{L}} = nCl^{n-2} \begin{bmatrix} \mathbf{e} + (n-2)\boldsymbol{\alpha}\boldsymbol{\alpha}^{\mathrm{T}} & -\mathbf{e} - (n-2)\boldsymbol{\alpha}\boldsymbol{\alpha}^{\mathrm{T}} \\ -\mathbf{e} - (n-2)\boldsymbol{\alpha}\boldsymbol{\alpha}^{\mathrm{T}} & \mathbf{e} + (n-2)\boldsymbol{\alpha}\boldsymbol{\alpha}^{\mathrm{T}} \end{bmatrix} \tag{4-50}$$

Referring to Eq. 4-47, in case of n = 2, the element forces become constant, and for Eq. 4-50, the tangent geometric stiffness for axial line element becomes equivalent to a truss element, thus the axial forces can be designated as a constant value. However, in case of n > 2, nonlinearity occurs and from here, the iterational process are required to converge the unbalanced forces. When the magnitude of n becomes larger, the length of all axial line elements achieved tends to be more uniform.

4.3.4 Truss element with real stiffness for struts

In order to perform a three dimensional truss analysis by TSM, the differentiation of the equilibrium condition equations should be done in order to obtain the tangent stiffness matrix. The nodal force vector and the equilibrium condition vector could be represented as the following equations.

$$\mathbf{D}_{ij} = [X_i \quad Y_i \quad Z_i \quad X_j \quad Y_j \quad Z_j]^{\mathrm{T}} \tag{4-51}$$

$$\boldsymbol{\alpha}_{ij} = [-\alpha_{ij} \quad -\beta_{ij} \quad -\gamma_{ij} \quad \alpha_{ij} \quad \beta_{ij} \quad \gamma_{ij}]^{\mathrm{T}} \tag{4-52}$$

Here, if the axial force N_{ij} that is subjected on the ij element, the equilibrium condition

equation could be shown as,

$$\mathbf{D}_{ij} = \boldsymbol{\alpha}_{ij} N_{ij} \qquad 4\text{-}53$$

By differentiating Eq. 4-53, the result could be shown as;

$$\boldsymbol{\delta}\mathbf{D}_{ij} = \boldsymbol{\delta}\boldsymbol{\alpha}_{ij} N_{ij} + \boldsymbol{\alpha}_{ij} \boldsymbol{\delta} N_{ij} \qquad 4\text{-}54$$

Eq. 4-54 exhibits a linear function of an infinitesimal displacement $\delta \boldsymbol{x}_{ij}$ for the nodal displacement vector, and both δN_{ij} and $\delta \boldsymbol{\alpha}_{ij}$ will be derived precisely. The element edge force equation is a linear function which consists of Young modulus E, cross sectional area A and element non-stressed length l_{oij}, described as the following equation.

$$\delta N_{ij} = \frac{\mathrm{EA}}{l_{0ij}} \delta l_{ij} \qquad 4\text{-}55$$

The length of the element could be expressed as the following equation.

$$l_{ij}{}^2 = x_{ij}{}^2 + y_{ij}{}^2 + z_{ij}{}^2 \qquad 4\text{-}56$$

For the increment δl_{ij} of the element length, could be obtained by the differentiation of Eq. 4-56.

$$\delta l_{ij} = \alpha_{ij} \delta x_{ij} + \beta_{ij} \delta y_{ij} + \gamma_{ij} \delta z_{ij} \qquad 4\text{-}57$$

Here, both sides of the equation is divided to l_{ij}, and considering the cosine vector between node i and j, $\delta x_{ij} = \delta x_j - \delta x_i$, $\delta y_{ij} = \delta y_j - \delta y_i$ and $\delta z_{ij} = \delta z_j - \delta z_i$, the compatibility equation could be shown as;

$$\delta l_{ij} = [-\alpha \quad -\beta \quad -\gamma \quad \alpha \quad \beta \quad \gamma]_{ij} \begin{bmatrix} \delta x_i \\ \delta y_i \\ \delta z_i \\ \delta x_j \\ \delta y_j \\ \delta z_j \end{bmatrix} \qquad 4\text{-}58$$

By substituting Eq. 4-52 to Eq. 4-54,

$$\boldsymbol{\alpha}_{ij} \boldsymbol{\delta} N_{ij} = \frac{\mathrm{EA}}{l_{0ij}} \boldsymbol{\alpha}_{ij} \boldsymbol{\alpha}_{ij}{}^{\mathrm{T}} \boldsymbol{\delta}\mathbf{x}_{ij} = \frac{\mathrm{EA}}{l_{0ij}} \begin{bmatrix} \boldsymbol{a} & -\boldsymbol{a} \\ -\boldsymbol{a} & \boldsymbol{a} \end{bmatrix}$$

$$\boldsymbol{a} = \begin{bmatrix} \alpha^2 & \alpha\beta & \alpha\gamma \\ \alpha\beta & \beta^2 & \beta\gamma \\ \alpha\gamma & \beta\gamma & \gamma^2 \end{bmatrix} \qquad 4\text{-}59$$

The equation shown above represents the stiffness equation of infinitesimal displacement theory using the displacement method. However, by applying the cosine vector components,

$$\alpha_{ij} = \frac{x_j - x_i}{l_{ij}} \quad 4\text{-}60 \qquad \beta_{ij} = \frac{y_j - y_i}{l_{ij}} \quad 4\text{-}61 \qquad \gamma_{ij} = \frac{z_j - z_i}{l_{ij}} \quad 4\text{-}62$$

Eq. 4-60 to 4-62 represents the cosine vector α, β and γ for the element. By

differentiating the above equation,

$$\delta\alpha_{ij} = \frac{1}{l_{ij}}[-(1-\alpha^2) \quad \alpha\beta \quad \alpha\gamma \quad (1-\alpha^2) \quad -\alpha\beta \quad -\alpha\gamma]_{ij}\begin{bmatrix}\delta x_i\\ \delta y_i\\ \delta z_i\\ \delta x_j\\ \delta y_j\\ \delta z_j\end{bmatrix} \qquad 4\text{-}63$$

Similarly,

$$\delta\beta_{ij} = \frac{1}{l_{ij}}[\alpha\beta \quad -(1-\beta^2) \quad \beta\gamma \quad -\alpha\beta \quad (1-\beta^2) \quad -\beta\gamma]_{ij}\begin{bmatrix}\delta x_i\\ \delta y_i\\ \delta z_i\\ \delta x_j\\ \delta y_j\\ \delta z_j\end{bmatrix} \qquad 4\text{-}64$$

$$\delta\gamma_{ij} = \frac{1}{l_{ij}}[\alpha\gamma \quad \beta\gamma \quad -(1-\gamma^2) \quad -\alpha\gamma \quad -\beta\gamma \quad (1-\gamma^2)]_{ij}\begin{bmatrix}\delta x_i\\ \delta y_i\\ \delta z_i\\ \delta x_j\\ \delta y_j\\ \delta z_j\end{bmatrix} \qquad 4\text{-}65$$

Here, if Eq. 4-63 to 4-65 are substituted into Eq. 4-54;

$$\boldsymbol{\delta\alpha}_{ij}N_{ij} = \frac{N_{ij}}{l_{ij}}\begin{bmatrix}\bar{\boldsymbol{a}} & -\bar{\boldsymbol{a}}\\ -\bar{\boldsymbol{a}} & \bar{\boldsymbol{a}}\end{bmatrix}_{ij}\begin{bmatrix}\delta x_i\\ \delta y_i\\ \delta z_i\\ \delta x_j\\ \delta y_j\\ \delta z_j\end{bmatrix} \qquad 4\text{-}66$$

$$\bar{\boldsymbol{a}} = \begin{bmatrix}(1-\alpha^2) & -\alpha\beta & -\alpha\gamma\\ -\alpha\beta & (1-\beta^2) & -\beta\gamma\\ -\alpha\gamma & -\beta\gamma & (1-\gamma^2)\end{bmatrix}$$

The equation is the tangent stiffness matrix for the truss element by the superposition function of Eq. 4-59 and Eq. 4-66. Here, $\mathbf{k_O}$ and $\mathbf{k_G}$ could be expressed as Eq. 4-67 and Eq. 4-68.

$$\mathbf{k_O} = \frac{\mathrm{EA}}{l_{0ij}}\begin{bmatrix}\alpha^2 & \alpha\beta & \alpha\gamma\\ \alpha\beta & \beta^2 & \beta\gamma\\ \alpha\gamma & \beta\gamma & \gamma^2\end{bmatrix} \qquad 4\text{-}67$$

$$\mathbf{k_G} = \frac{N_{ij}}{l_{ij}}\begin{bmatrix}(1-\alpha^2) & -\alpha\beta & -\alpha\gamma\\ -\alpha\beta & (1-\beta^2) & -\beta\gamma\\ -\alpha\gamma & -\beta\gamma & (1-\gamma^2)\end{bmatrix} \qquad 4\text{-}68$$

The element stiffness matrix $\mathbf{K_O}$ and the tangent geometric stiffness $\mathbf{K_G}$ are;

$$\mathbf{K_O} = \begin{bmatrix} \mathbf{k_O} & -\mathbf{k_O} \\ -\mathbf{k_O} & \mathbf{k_O} \end{bmatrix} \qquad 4\text{-}69$$

$$\mathbf{K_G} = \begin{bmatrix} \mathbf{k_G} & -\mathbf{k_G} \\ -\mathbf{k_G} & \mathbf{k_G} \end{bmatrix} \qquad 4\text{-}70$$

The tangent stiffness equation for the truss element could be shown as the following equation.

$$\delta \begin{bmatrix} \mathbf{D}_i \\ \mathbf{D}_j \end{bmatrix} = \left\{ \begin{bmatrix} \mathbf{k_G} & -\mathbf{k_G} \\ -\mathbf{k_G} & \mathbf{k_G} \end{bmatrix} + \begin{bmatrix} \mathbf{k_O} & -\mathbf{k_O} \\ -\mathbf{k_O} & \mathbf{k_O} \end{bmatrix} \right\} \begin{bmatrix} \delta\mathbf{u}_i \\ \delta\mathbf{u}_j \end{bmatrix} \qquad 4\text{-}71$$

Eq. 4-71 could also be expressed as;

$$\delta\mathbf{D} = (\mathbf{K_O} + \mathbf{K_G})\delta\mathbf{u} \qquad 4\text{-}72$$

4.4 Comparison of FDM and measure-potential element with virtual stiffness

Table 4.1: Comparison of axial line element by both methods

Subject	**FDM**	**Measure-potential element**
Designation for power of element length	1st degree	Any degree
Structural analysis	Linear	Nonlinear
The process of obtaining the ratio between force density	Nonlinear calculation	Unnecessary

Table 4.1 shows the comparison of the two different approaches for form-finding of tensegrity structure; one is by using FDM, and the other is by using the measure-potential element in TSM. In FDM, the force density that divided axial forces by the element length is defined as constant. Therefore, when the measure potential element is defined as that the axial forces are proportionate to element length, both approach becomes the same linear procedure. In FDM, however, the calculation of feasible force density ratio among all the elements using nonlinear equations is required to find a feasible shape. The condition of feasible force density ratio requires that rank deficiency of the connectivity matrix becomes more than 4. Therefore, the accuracy of FDM may depend on the nonlinear process provided by the eigenvalue analysis or the dynamic

relaxation.

In contrast, the measure-potential element, which used in the TSM algorithm, can designate freely its coefficients relating the axial force and the power value of element length. This is based on the versatility of TSM that can obtain strict equilibrium solutions adjusting to defined element behavior. Therefore, iterational process becomes common between the measure-potential elements and the actual elements with real material.

4.5 Path finding method

The equilibrium equation for nonlinear Newton potential could be expressed as the following,

$$F(\mathbf{u}, f) = \mathbf{0} \qquad 4\text{-}73$$

Here, the function $F(\mathbf{u},f)$ comprises of a nonlinear function of vectors which includes $\mathbf{u}$, the n-th column of displacement vector and f as the load parameter. The equilibrium equation indicated in Eq. 4-73 shows that with n amount of displacement and one load parameter, the total of unknown parameter becomes n+1, which exceeds the total of n column value. Therefore, in order to solve Eq. 4-73, some requirement had to be applied to overcome this excessive value. In order to execute a path finding process, there are three methods that can be classified which is load control method, displacement control method and arc length method.

By the addition of an extra requirement, solution that satisfies the equilibrium equation could be achieved by repeating the mentioned process by interpolating the load–displacement curve for a specific equilibrium state. This process could obtain an equilibrium path numerically which fulfils the objective of the path finding process. The procedure to obtain an equilibrium path could be made by the following procedures;

1) The derivation of tangent stiffness matrix and equilibrium equation.
2) Obtaining equilibrium path from an equilibrium phase.
3) Investigate the stability or irregularity of the equilibrium phase position.

In this study, the conversion of load and displacement control is the main method used and is executed depending on the tangent value achieved form the load–displacement curve. If the current equilibrium phase reaches nearby the load extremum, displacement control is executed and if it surpasses the extremum, then load control is switched back and this procedure is repeated continuously all along the path finding analysis.

4.6 Bifurcation path pursuing procedure

In a common path finding analysis, while pursuing the primary path, there are many bifurcation points connecting to secondary path which are neglected during the analysis [8]. A point of bifurcation also should be considered in order to examine and classify morphologies that may emerge. As the secondary path is pursued, irregularity or unexpected structural morphology could be discovered. The possibility of a bifurcation point existence could be determined when the number of negative eigenvalue of the tangent stiffness matrix changes; either increases or decreases, and some modification had to be done in order to pursue the secondary path. In this study, when an equilibrium state reaches a point where the number of negative eigenvalue changes, the procedure to pursue a bifurcation point will be stated as follows;

1) Setting connectivity; coefficients for element behaviour C, n in Eq. 4-46 and extensional stiffness EA in Eq. 4-54; stable support conditions; and primary positions of nodes.

2) Execution of first iteration phase with external forces on control points: Depending on conditions of primary positions in 1) and magnitude of external forces, different solution on different path may be obtained. Therefore, multiple numbers of paths which are independent to each other can be found without processing bifurcation analysis. The obtained solution can be adopted as the primary shape for the path finding.

3) Searching the path by incremental analysis from the starting point of the solution that is obtained in 1): The loading control is adopted when the tangent value is small. The control method is switched appropriately on the path finding process.

4) Specifying the bifurcation point and switching into bifurcation path: The number of negative eigenvalue of the tangent stiffness matrix is monitored in every incremental step during the path finding process. When the number changes along the path, it is considered as the bifurcation point (except where it is the extremum). Furthermore, the bifurcation paths are found by switching method to add the small disturbance displacements calculated by the eigenvector. This is a general type of bifurcation analysis, for example, as mentioned in [8].

4.7 Numerical example

4.7.1 The shape determination of tensegrity tower under gravitational influence

A full scale experiment is not comparable when validating the analysis accuracy of form-finding with the application of element with virtual stiffness. Therefore, the author's measure-potential element is evaluating its availability by comparison with the general procedure of FDM.

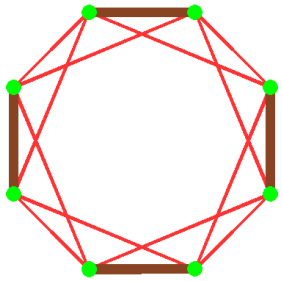

(a) Plan view

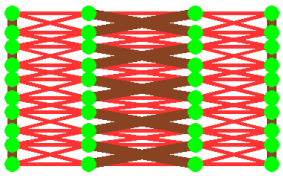

(b) Side view

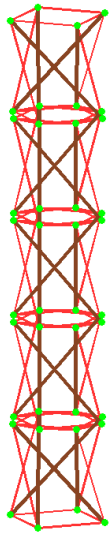

(c) Bird's eye view

Figure 4.7: Five storey tensegrity tower

As mentioned earlier in this chapter, tensegrity structure could produce numerous amount of equilibrium shapes, even with the same initial condition or configuration (the coefficient C and n in Eq. 4-46, loading condition and connectivity). The total number of equilibrium shapes will increase exponentially with the increment of the total nodes and elements, especially for a vast tensegrity model which has a large amount of nodes with high degree of freedom, the equilibrium solution would be endless (infinity).

In this subsection, the connectivity of the tower consists of four compressional members and twelve tensional members for each storey. The non-stressed length of the compressional member is 1[m] each. In addition, the tower is formed by a square shaped simplex tensegrity for each storey. Fig. 4.7(b) shows the side view of the tower where the elements are piled up accordingly, and it also shows the connectivity of each nodes. This is the initial stage for the analysis where the boundary condition for all nodes are free nodes and nodal force is zero. Fig. 4.7(c) shows the equilibrium shape for the tensegrity tower. Here, the tower is given a stable support condition for the four nodes

at the bottom part of the lowest layer of the tensegrity tower. Here, the tower is given a stable support condition for the four nodes at the bottom part of the lowest layer of the tensegrity tower. A value of 0.3[N] of load in vertical direction is applied on every node and is constant along the analysis (is considered to be equivalent to the self-weight of the structure), to simulate a form-finding of tensegrity tower under gravitational influence. The objective of this analysis is to obtain the equilibrium solution which is equivalent to Snelson's tower [11]. In addition, the extensional stiffness for the strut is EA=2×10^9[N], for the tensional members, the C is set as 10 and it also applies a 2nd degree of axial line element.

Firstly, the influence of initial configurations on equilibrium solutions of the tensegrity tower is investigated, which the geometrically nonlinear analysis has been done exhaustively. The angle of struts is set from θ=0° to θ=90° increased to 3° of each increment step, and the distance between layers is set between 0[m] to 9[m] increased to 0.3[m] gradually. The total number of combination of these different configurations is 900. These 900 different primary positions of nodes produce 285 different equilibrium solutions corresponding to one mechanical condition. Fig. 4.8 shows the total potential energy Π of an equilibrium solution which also could be shown in the following equation.

$$\Pi = U + P - V \qquad 4\text{-}74$$

Where U is the strain energy for the strut, P is the axial line element potential and V is the loss potential of the external force. The relation between total potential energy and the incidence rate of equilibrium solution is checked, and the rate which is more than 1% is shown in this analysis. Furthermore, Fig. 4.9 shows the side view of the morphology of equilibrium solutions with the incidence rates which are more than 2%.

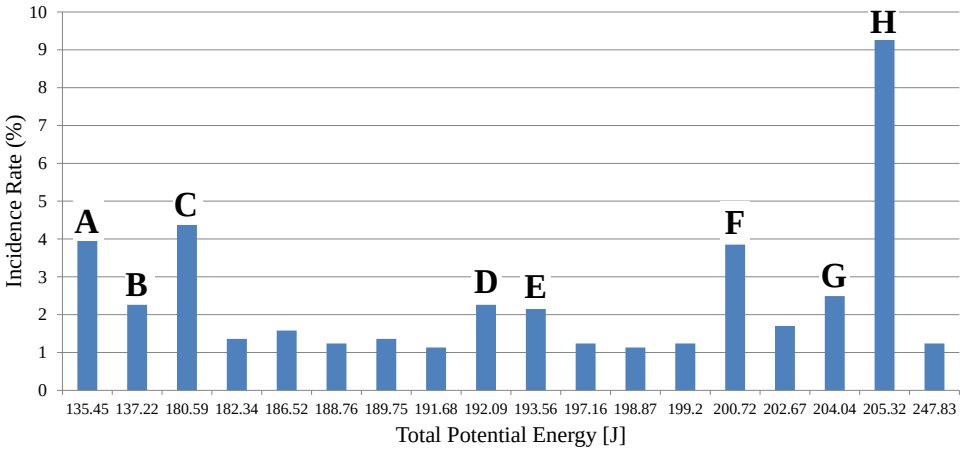

Figure 4.8: The relation of incidence rate and total potential energy for equilibrium solutions

In Fig. 4.9, the boundary condition of each nodes are marked as; the blue nodes are restrained in vertical direction, the pink nodes are perfectly fixed and the green nodes are the control nodes which are grouped together and displaced with the same amount for each steps. These green nodes will be on the crown position when the target solution is obtained. Based on the analyzed result, when the total potential energy of the tensegrity tower was comparatively high, the highest incidence rate (H) occurred, which was 9.3%. However, when the total potential energy was the lowest, as exhibited by solution (A), the incidence rate was 4.0%, which was the third highest rate between all solutions.

From the result, although the potential energy is low, the solution is not necessarily prominent, thus, the correlative relation between energy and incidence rate could not be

Solution A

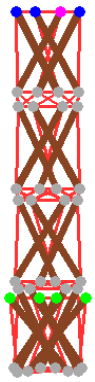

Solution B

Total potential energy	:	135.45[J]	Total potential energy	:	137.22[J]
Height	:	4.33[m]	Height	:	2.85[m]
Incidence Rate	:	4.0%	Incidence Rate	:	2.3%

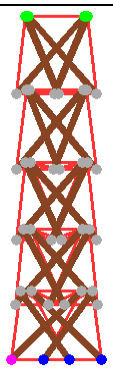

Solution C

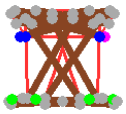

Solution D

Total potential energy	:	180.59[J]	Total potential energy	:	192.09[J]
Height	:	-3.19[m]	Height	:	0.59[m]
Incidence Rate	:	4.4%	Incidence Rate	:	2.3%

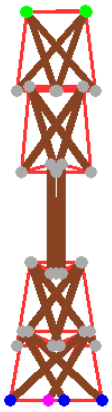

Solution E

Solution F

Total potential energy	:	193.56[J]	Total potential energy	:	200.72[J]
Height	:	-3.59[m]	Height	:	-0.84[m]
Incidence Rate	:	2.2%	Incidence Rate	:	3.9%

Solution G

Solution H

Total potential energy	:	204.04[J]	Total potential energy	:	205.32[J]
Height	:	0.66[m]	Height	:	-0.28[m]
Incidence Rate	:	2.5%	Incidence Rate	:	9.3%

Figure 4.9: Deformation diagram of tensegrity tower under gravitational influence

defined precisely. Here, the proportion of morphology, symmetricity or shape-continuity are more likely to have much higher correlative relation, rather than the relation of incidence rate and potential energy. However, the incidence rate for the target solution, (C) (when total potential energy is 180.59[J]) is 4.4%, which shows that with the adjustment of initial configuration randomly, the heuristic search procedure is proven to be inefficient.

In order to pursue the target solution more efficiently, several techniques could be considered which are;

1) Applying compulsory displacement to the nodes that are restricted by boundary condition and the control nodes on the crown section.
2) The control node is displaced downwards until sign of inversion occurs for the value of the reaction force.
3) Release the boundary condition of the control nodes.

All of the above mentioned techniques could be considered in order to pursue the target solution as shown in Fig. 4.9 (C).

4.7.2 Equilibrium path finding of tensegrity tower

As shown in subsection **4.7.1**, when compulsory displacement is applied on the control nodes gradually, the equilibrium solutions with "zero reaction forces" can be recognized to be in self-reliant condition. While pursuing the solution, if small amount of increment is applied, the snap-through phenomena does not occur and the tensegrity tower will deform continuously. In this analysis, the system of "truss and axial line elements" produces the equilibrium paths which may be an analogy to of the elastic buckling of actual structures. According to the above consideration, in this subsection, two cases of path finding procedure are examined as follows; one is the case that the constant nodal forces are applied on all nodes in the vertical downwards direction to simulate the behavior under gravitational influence. And the other is the case of the behavior without gravity in order to observe equilibrium solution of pure tensegrity.

(a) Plan view (b) Side view

Figure 4.10: The initial configuration for a double storey tensegrity tower

For this analysis, a double storey tensegrity tower (Fig. 4.10) is applied for the form-finding analysis. The extensional stiffness for the strut is EA=2×10^9[N], for the tensional members, the *C* is set as 10 and it also applies a 2nd degree of axial line element. In Fig. 4.10, the support condition at the bottom part of the tower are set as fixed in all direction for the pink node and vertically restrained for the blue nodes, while the nodes on the crown part are the control nodes. The other nodes of the rest of the tensegrity tower are set as free nodes. Path finding is pursued as mentioned in section **4.5**. The procedure for path finding is classified into two control methods [12], which are load control when the tangent of the load–displacement curve is high, and displacement control when the tangent of the load–displacement curve is low; and both methods are freely to be switched while monitoring the tangent of the curve. In addition, the compulsory displacements subjected on the control nodes are equal throughout the calculation and only symmetrical solution is searched for this analysis. Bifurcation path and side toppling of the tower will be discussed in subsection **4.7.5**.

4.7.3 Equilibrium solution under gravitational influence

All nodes are subjected equally with 1[N] of nodal force in vertical downward direction. The initial configuration for this tower, the angle of struts is set from θ=0° to θ=90° increased to 3° of each increment step, and the distance between layers is set between 0[m] to 9[m] increased to 0.3[m] gradually. The total number of different conditions for primary positions are also 900, and 20 equilibrium shapes are obtained. The solutions with symmetry shapes are extracted from the obtained solutions (the total of 20) as shown in Fig. 4.14, in which the total potential energy is exhibited from low order which are marked as (A) to (N), and each of the graphics show the side view and plan view. When examined the incidence rate of the solutions in Fig. 4.14 similarly to the previous procedure, the solution (I) has the highest incidence rate which is 50.6%, and also exhibits a well-proportioned morphology. Therefore, the solution (I) is the predominant morphology, even if this tensegrity tower has a comparatively low degree of freedom.

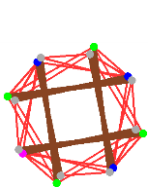
Plan view

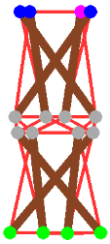
Side view

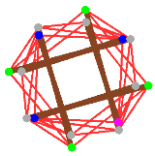
Plan view

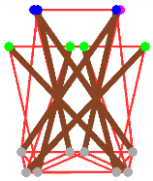
Side view

Solution (A)			Solution (B)		
Potential energy	:	50.24[J]	Potential energy	:	56.18[J]
Height	:	1.70[m]	Height	:	0.21[m]
Incidence rate	:	2.7%	Incidence rate	:	4.8%

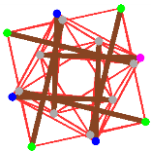
Plan view

Side view

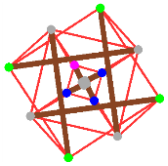
Plan view

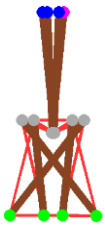
Side view

Solution (C)			Solution (D)		
Potential energy	:	57.73[J]	Potential energy	:	58.09[J]
Height	:	1.90[m]	Height	:	1.93[m]
Incidence rate	:	0.2%	Incidence rate	:	0.6%

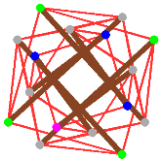
Plan view

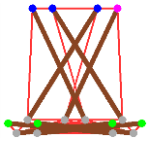
Side view

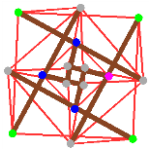
Plan view

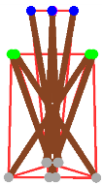
Side view

Solution (E)			Solution (F)		
Potential energy	:	61.90[J]	Potential energy	:	64.63[J]
Height	:	0.81[m]	Height	:	0.28[m]
Incidence rate	:	1.9%	Incidence rate	:	0.1%

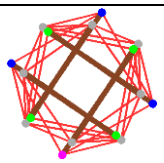
Plan view

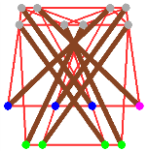
Side view

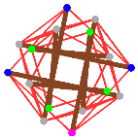
Plan view

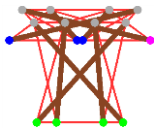
Side view

Solution (G)			Solution (H)		
Potential energy	:	67.82[J]	Potential energy	:	69.20[J]
Height	:	0.24[m]	Height	:	0.61[m]
Incidence rate	:	0.3%	Incidence rate	:	1.7%

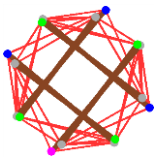
Plan view

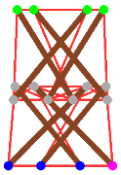
Side view

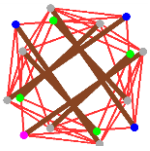
Plan view

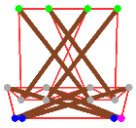
Side view

Solution (I)			Solution (J)		
Potential energy	:	73.67[J]	Potential energy	:	74.95[J]
Height	:	-1.21[m]	Height	:	-0.82[m]
Incidence rate	:	50.6%	Incidence rate	:	4.9%

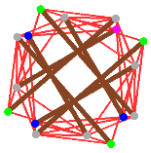
Plan view

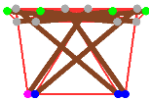
Side view

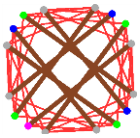
Plan view

Side view

Solution (K)			Solution (L)		
Potential energy	:	78.89[J]	Potential energy	:	79.76[J]
Height	:	-0.57[m]	Height	:	-0.23[m]
Incidence rate	:	3.2%	Incidence rate	:	17.3%

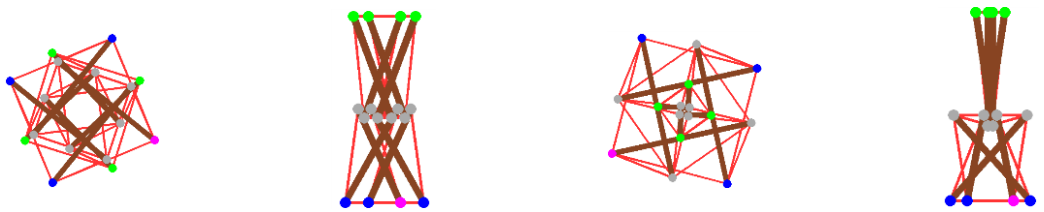

Plan view　　Side view　　Plan view　　Side view

Solution (M)			Solution (N)		
Potential energy	:	85.85[J]	Potential energy	:	86.58[J]
Height	:	-1.62[m]	Height	:	-1.63[m]
Incidence rate	:	8.1%	Incidence rate	:	0.1%

Figure 4.11: Equilibrium shapes for the double storey tensegrity tower

If horizontal instability such as side-toppled morphology is excluded, it is suggested that the morphology (solution (I)) has a high stability rate where elements in between the storey support against the gravitational force by tensional forces. However, the solution does not have the lowest total potential energy compared to the other solutions, and the correlative relation between incidence rate and potential energy also could not be proven.

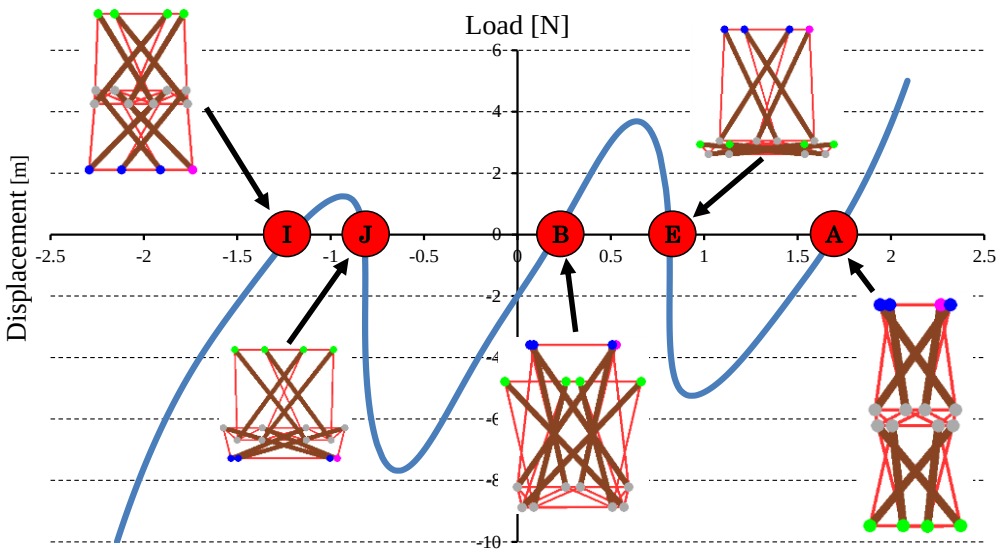

Fig 4.12: The equilibrium path that contains solution (A), (B), (E), (I) and (J)

As shown in Fig 4.12, starting from solution (I) (where the total potential energy is Π=73.67[J]), the path finding is started by using load control in both plus and minus directions. The y-axis represents the nodal force, where a load of W[N] is subjected on the control node in the vertical direction, and simultaneously all nodes are subjected

with 1[N] of nodal force in the same direction. The *x*-axis represents the distance between the control node and the fixed nodes in the vertical direction and here, the *y*-direction downwards is plus direction. In the path, other than solution (I), there exist other equilibrium solutions when W=0[N] which are (J), (B), (E) and (A). Since all of the solutions are in the same path, the group seems to have a relatively high incidence rate.

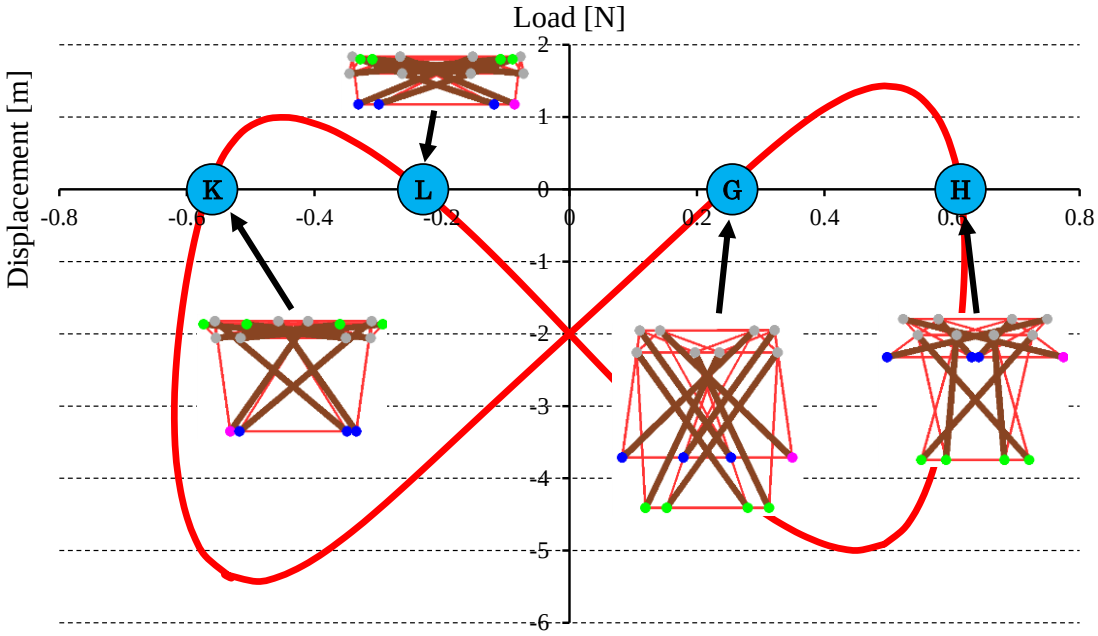

Figure 4.13: The equilibrium path that contains solution (G), (H), (K) and (L)

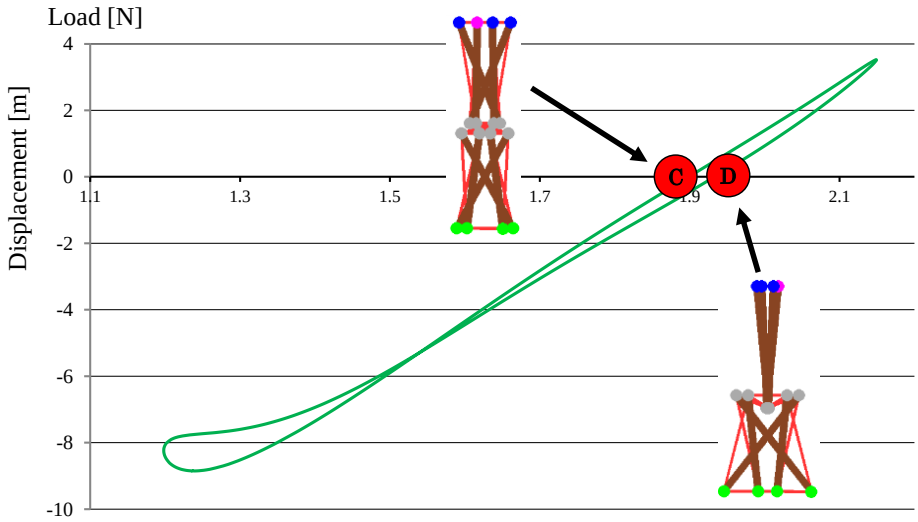

Figure 4.14: The equilibrium path that contains solution (C) and (D)

The solution (L) has the second highest incidence rate of 17.3%, with total potential energy Π=79.76[J]. As shown in Fig. 4.13, when the path is pursued from solution (L),

the path exhibits a "∞" shape circulated path, and another three equilibrium shapes were obtained which are marked as (G), (H) and (K). When pursuing solution (C), solution (D) was obtained and the path forms a loop shape as shown in Fig. 4.14.

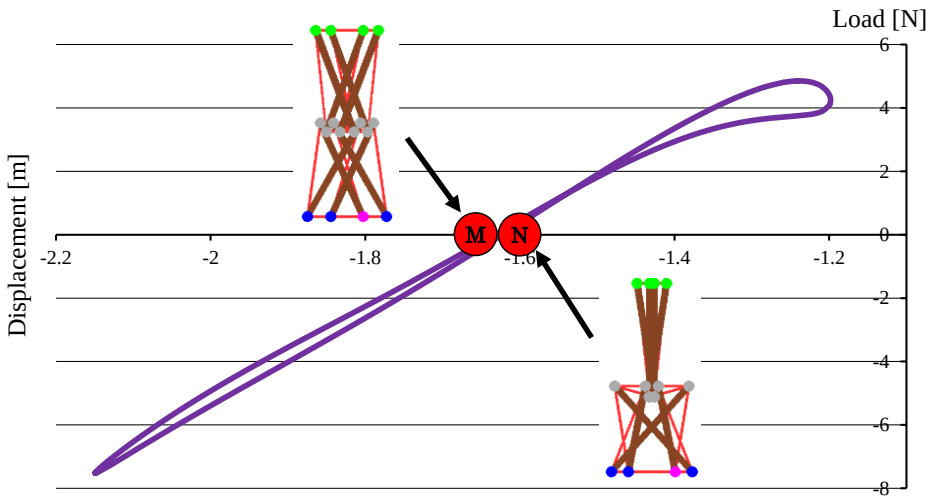

Figure 4.15: The equilibrium path that contains solution (M) and (N)

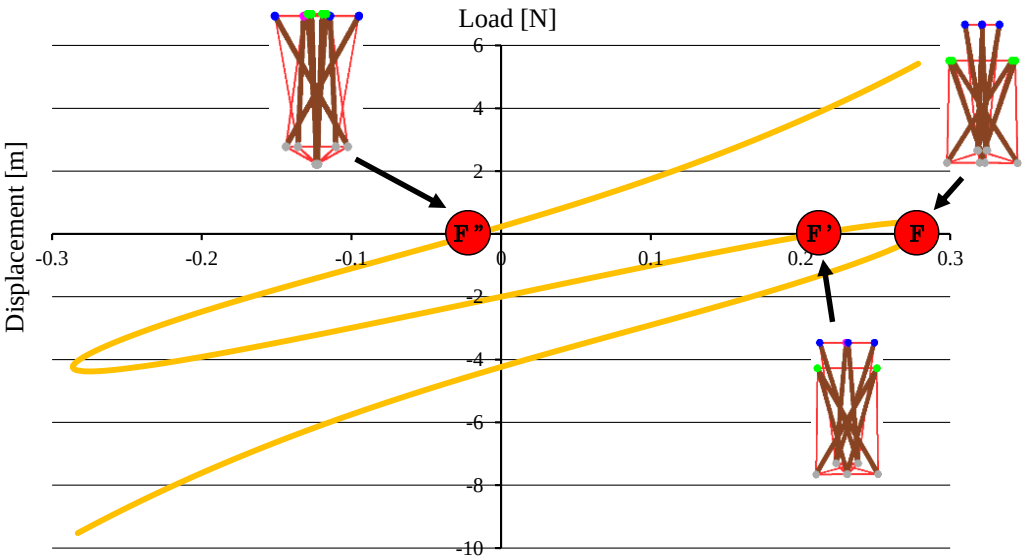

Figure 4.16: The equilibrium path that contains solution (F), (F') and (F")

Moreover, the path that contains solution (M) and (N) also forms a loop shape path, as shown in Fig. 4.15. Here, solution (C) and (M), (D) and (N) show a vertically symmetrical shape mutually to each other. Fig. 4.16 shows the path which contains solution (F), and while pursuing the path, solution (F') and (F") were obtained which did not appear when the path was pursued exhaustively. Fig. 4.17 shows the total path obtained in this analysis.

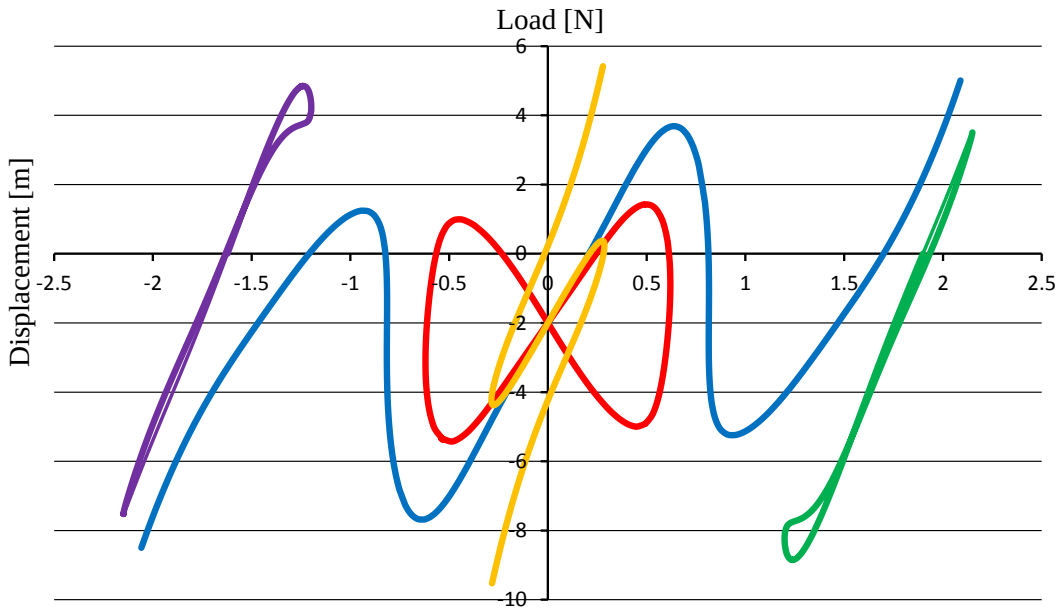

Figure 4.17: The total equilibrium paths for double storey tensegrity tower under gravitational influence

A total of five independent paths were achieved with multiple equilibrium shapes (when W=0[N]) and each shape was characterized in each path. The classification of symmetrical shapes consistency should be verified mathematically.

4.7.4 Self-equilibrium shapes for pure tensegrity

In this analysis, the element initial configuration, connectivity, boundary condition, analysis condition and algorithm, are the same as stated in subsection **4.7.5**. However, nodal forces are not applied on every node except the control node. Based on these analysis conditions, the self-equilibrium shapes (when W=0[N]) of pure tensegrity are investigated. In this case, within the 900 cases of primary positions which are searched exhaustively, there are only 6 of self-equilibrium shapes which were obtained in the two paths as shown in Fig. 4.18.

Here, when the load and displacement are zero, there are two different shapes existing with different morphologies where all nodes are in the same plane level with the fixed nodes. The gravitational influence is neglected in this analysis, and both paths are perfectly symmetrical sideways (if the point of origin is the center axis). Compared to the paths in Fig. 4.17 where gravitational influence is considered, both paths in this analysis perfectly went through the point of origin while obtaining a symmetrical shape, and the total number of extremum point is comparatively less than the previous analysis,

which also exhibits a simple path behavior. The gravitational influence may affect the complexity of the equilibrium paths obtained from the numerical analysis. This also shows the difficulty in the application of the structure.

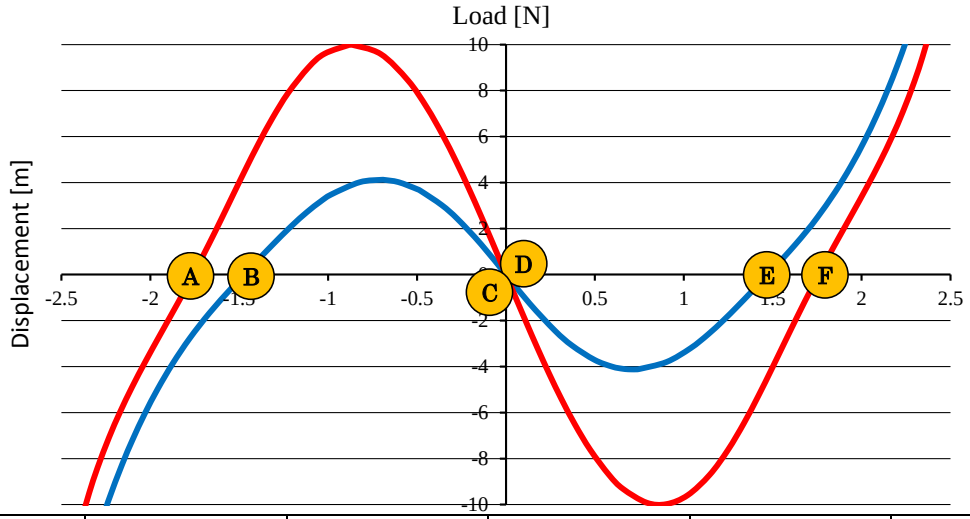

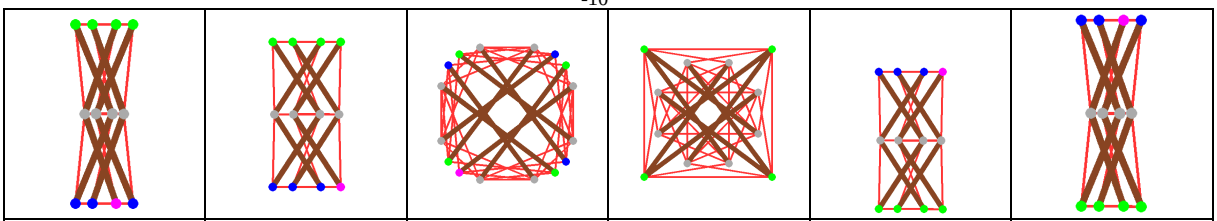

Solution (A)	Solution (B)	Solution (C)	Solution (D)	Solution (E)	Solution (F)

Figure 4.18: Equilibrium paths and self-equilibrium solutions for double storey pure tensegrity tower

4.7.5 Double storey tensegrity tower with a single control node

For the next numerical analysis, a double storey tensegrity tower is also applied. The connectivity between struts and axial line elements are shown in Fig. 4.19 (a) and (b), where struts and axial line elements are linked together to form a circular shape and connected to a middle node for upper and lower part for each level. Also, the middle nodes are connected vertically between the upper and lower part for each storey. Meanwhile, Fig. 4.19 (c) is the deformational shape of the tower after subjected to a particular amount of load.

The tensegrity tower is made up of 24 nodes, 10 struts and 62 axial line elements. An initial load with the capacity of 2[kN] in vertical direction is subjected on the middle node of the upper level of the tower (control point) and the load–displacement control is manoeuvred properly for this path finding analysis. The support condition at the

bottom part of the tower are set as fixed at all direction for node (A) and vertically restrained for the rest of the nodes (B), (C), (D) and (E). All other nodes on the rest of the tower are set as free node. When the control point is subjected to 2[kN] of initial load, the tower deforms to an initial shape and unbalanced force is converged in 13 steps. From here, load or displacement control is executed with incremental value of 0.02[kN] of load and 0.02[m] of displacement for each step.

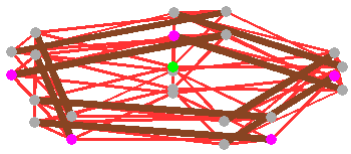

(a) Bird's eye view

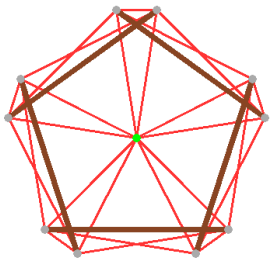

(b) Plan view

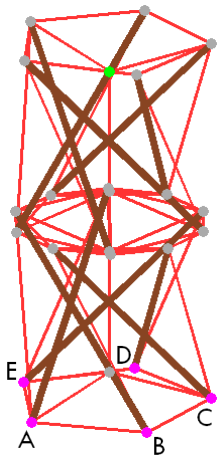

(c) 3D view

Figure 4.19: Initial configuration, connectivity and equilibrium shape of double storey tensegrity tower

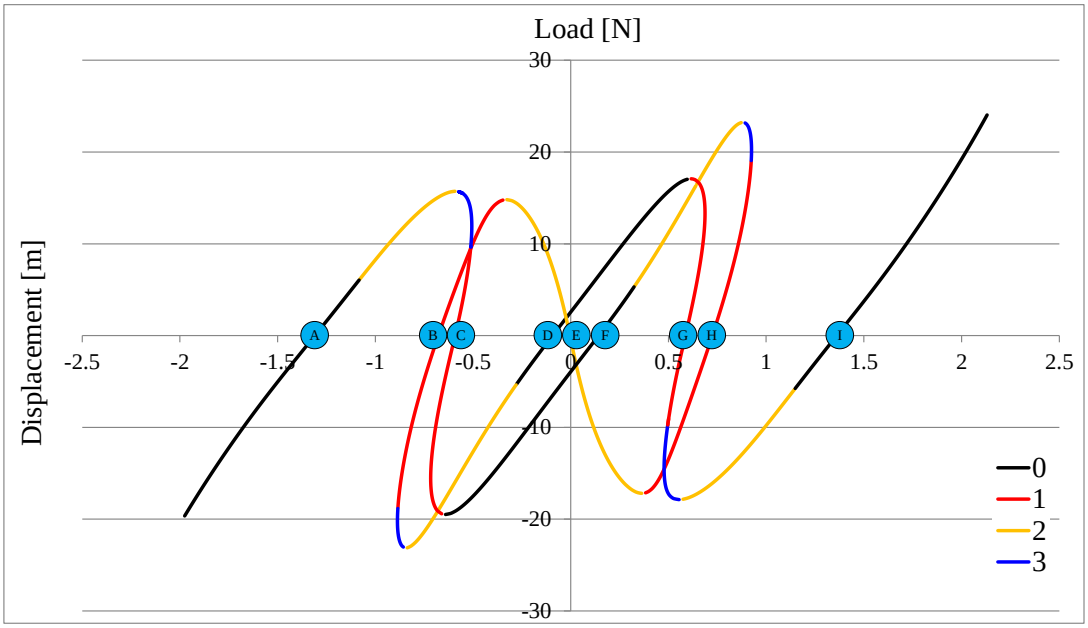

Figure 4.20: Main paths of the tensegrity tower

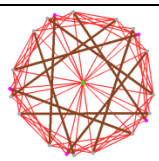 Plan view 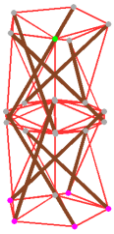 3D view	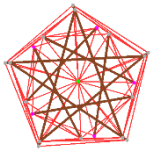 Plan view 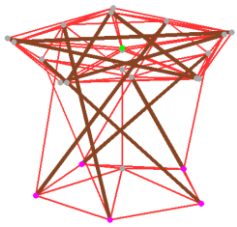 3D view	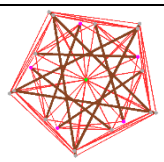 Plan view 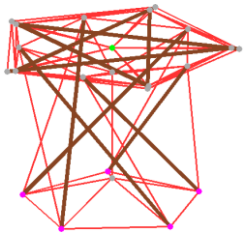 3D view
Solution (A)	Solution (B)	Solution (C)
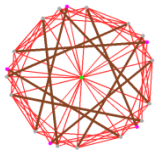 Plan view 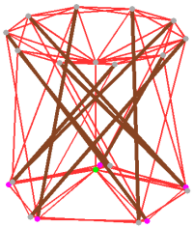 3D view	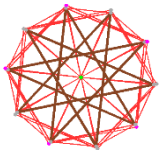 Plan view 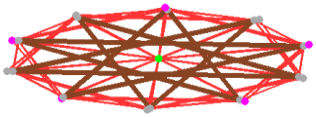 3D view	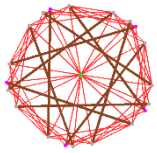 Plan view 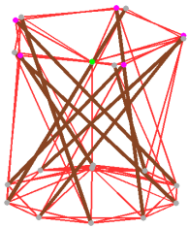 3D view
Solution (D)	Solution (E)	Solution (F)
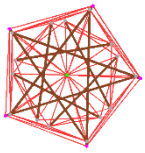 Plan view 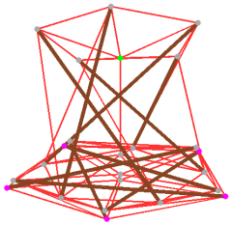 3D view	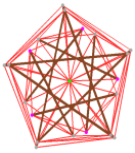 Plan view 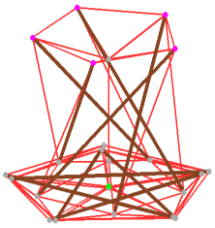 3D view	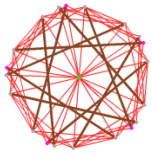 Plan view 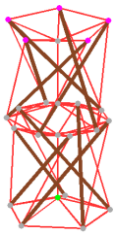 3D view
Solution (G)	Solution (H)	Solution (I)

Figure 4.21: Equilibrium solutions obtained in the main path

In this analysis, variations of equilibrium shapes were successfully achieved from the simulation, and the location of each shapes are marked from (A) to (I), as shown in Fig. 4.20. The equilibrium shapes are schematically and orderly displayed in Fig. 4.21, showing the plan and 3D views for each morphology. Generally, a relatively sideways symmetrical path has also been achieved in this analysis. As shown in Fig. 4.20 and Fig. 4.21, equilibrium solutions (A), (B), (C) and (D) are the inverted projection of the (F), (G), (H) and (I) solutions and are diametrically symmetrical. Solution (E) is a totally flat equilibrium solution where the control node is levelled to the restrained nodes.

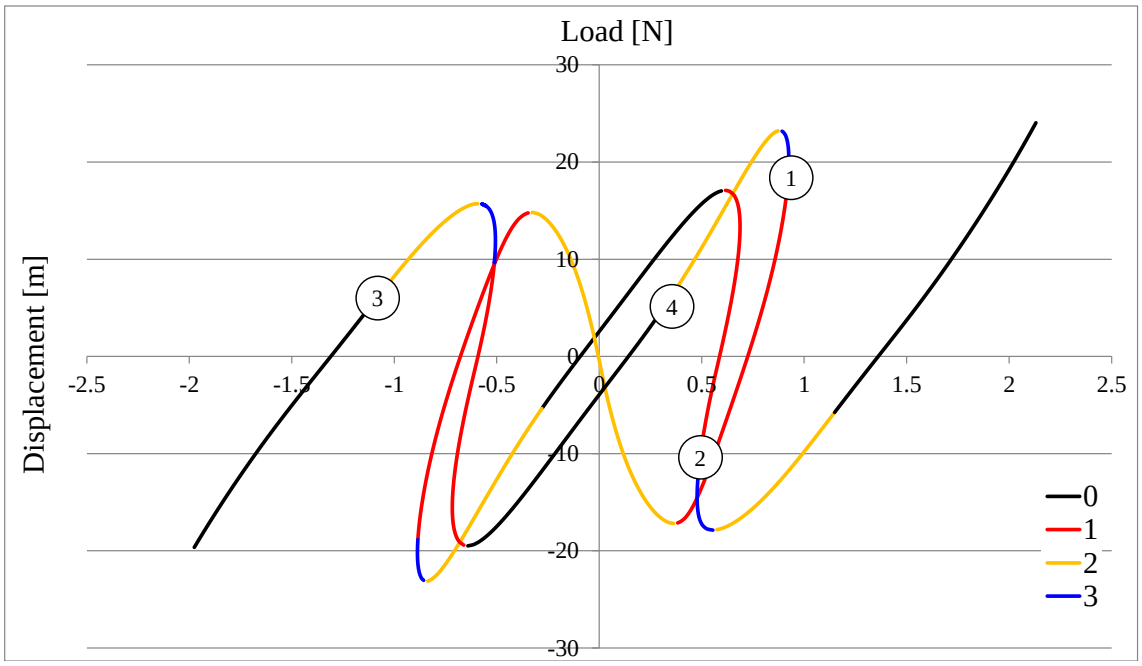

Figure 4.22: Bifurcation points obtained from the main path

In this analysis, a total of four bifurcation points were achieved from the main path and marked as point ① to ④ as shown in Fig. 4.22. Also, the main path exhibits a symmetrical behavior, and the incremental step has been done in a very small amount gradually, and the splitting point of two individual bifurcation paths which were adjacent to the bifurcation point were observed. The bifurcation path was pursued starting from point ①. As shown in Fig. 4.23, when a certain amount of eigenvector was applied at all nodes when reaching the bifurcation point, the tensegrity tower starts to topple sideways and the deformation behavior has been observed. The bypass was marked as ①-a which connects point ①'-a, and along this bypass, the total of three equilibrium shapes were obtained and marked as solution (J), (K) and (L) in Fig. 4.23, and the irregular equilibrium shapes are shown in Fig. 4.24.

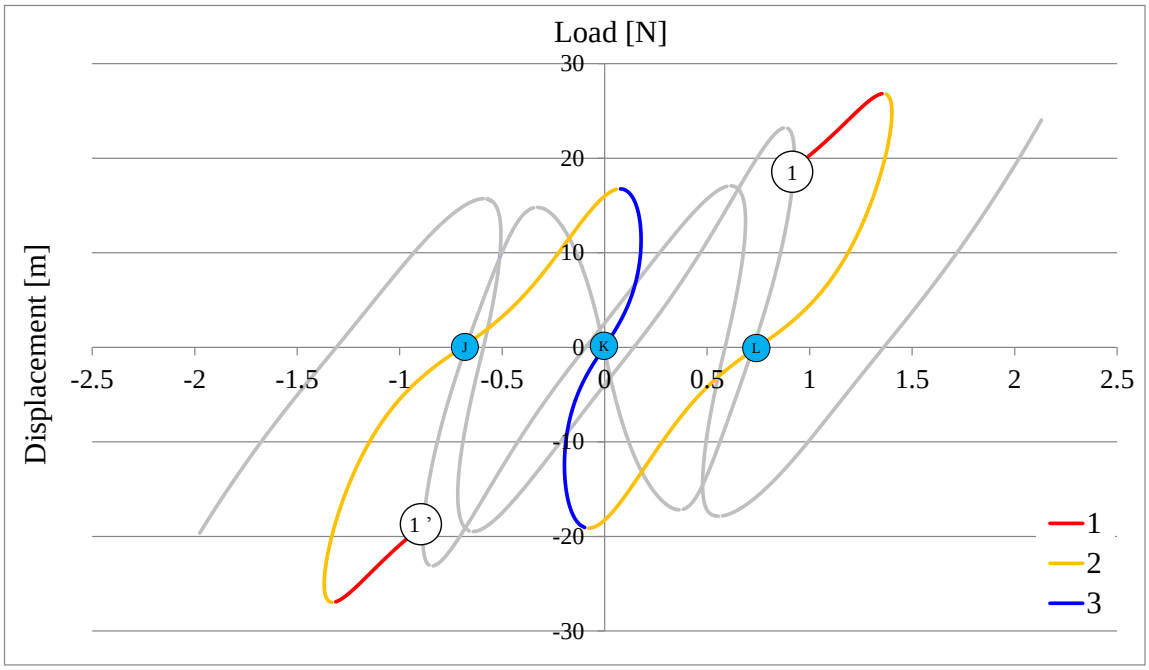

Figure 4.23: Bypass that connects ①-a and ①’-a

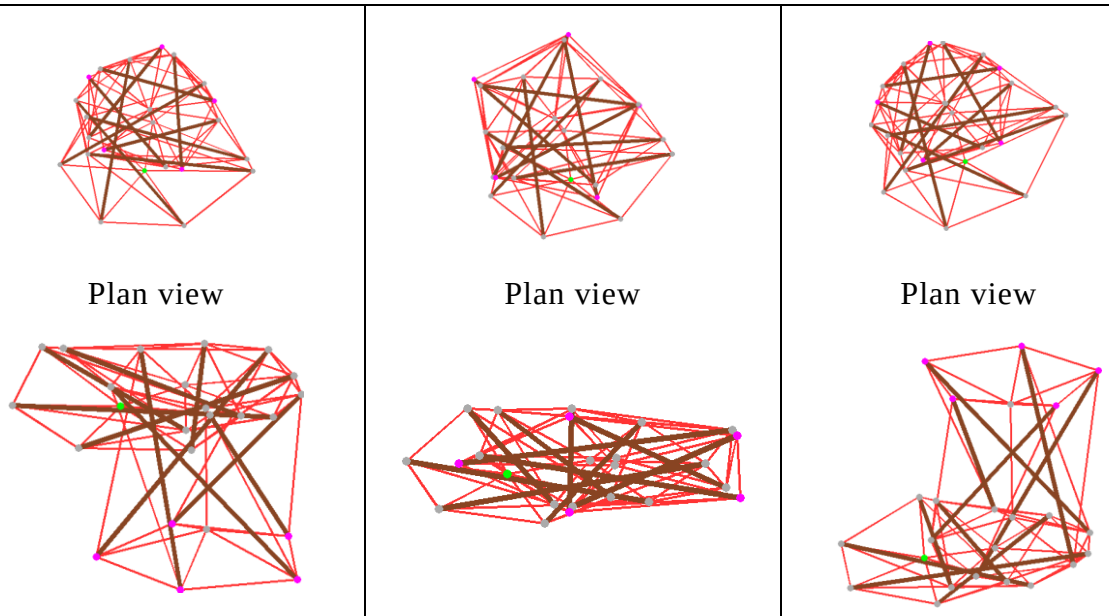 Plan view 3D view	Plan view 3D view	Plan view 3D view
Solution (J)	Solution (K)	Solution (L)

Figure 4.24: Equilibrium solutions obtained from bypass ①–a to ①’-a

Also, from the same point ①, the strut of the tensegrity tower elongate until it becomes a single redundant line if the load is applied continuously for bifurcation path ①-b and ①'-b, as shown in Fig. 4.25. When pursuing the bifurcation point ②, only one equilibrium shape was obtained from the bypass which connects point ② and point ②’. As shown in Fig. 4.26, the bypass passes the point of origin and the equilibrium

shape, marked as solution (M) shows an irregular flat shape, and also exhibit the decrement of symmetricity.

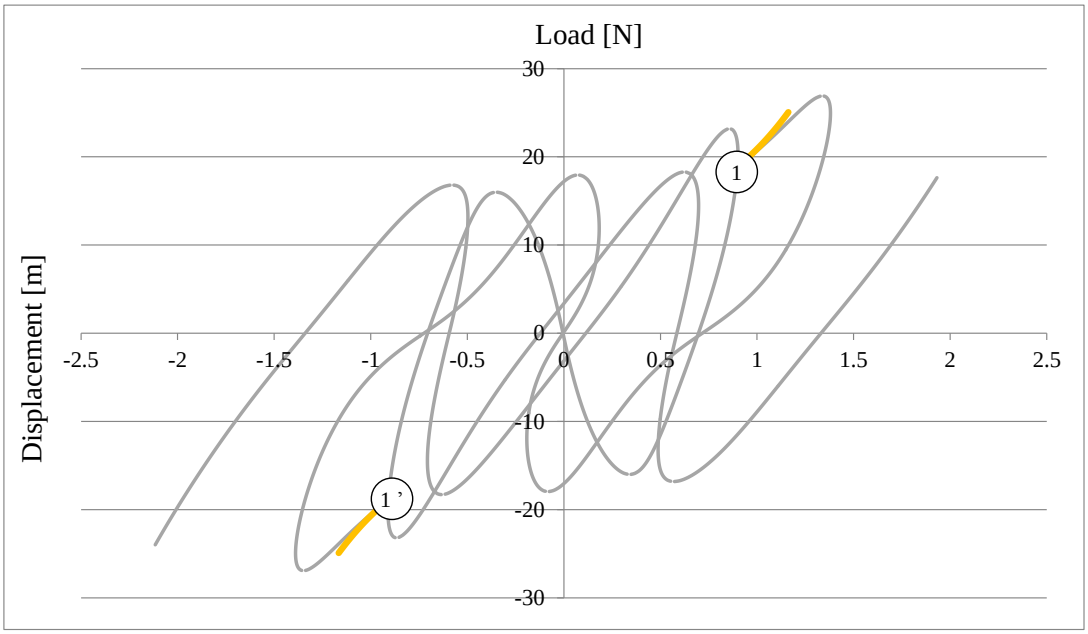

Figure 4.25: The bifurcation paths from bifurcation point ①-b and ①’-b

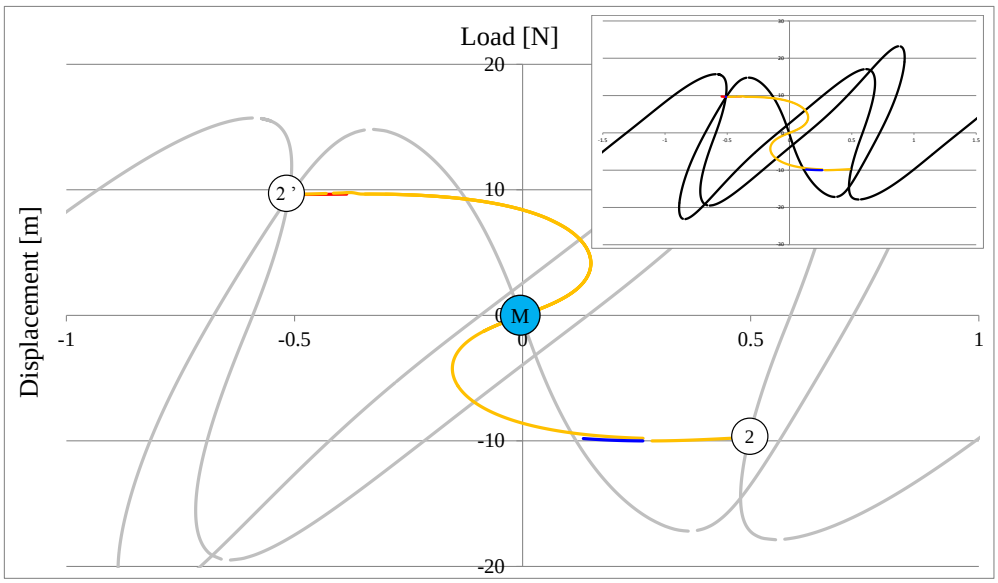

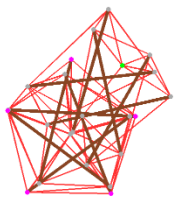

Plan view

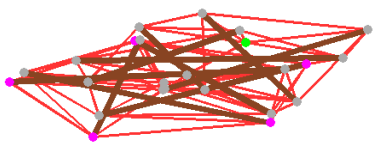

3D view

Solution (M)

Figure 4.26: The bypass that connects point ② to ②’

Further, when pursuing the bifurcation point ③-a and point ④-a, two relatively

identical bifurcation path emerged, as shown in Fig. 4.27. From point ③-a, a bypass that connects point ④'-a, and an equilibrium shape was obtained (solution (N)). While for point ④-a, the bypass connects point ③'-a, and an equilibrium shape was also obtained and marked as solution (O). Both equilibrium solutions achieved from this bifurcation paths also shows the loss of symmetricity. However, both solutions are symmetrical vertically, as shown in the 3D deformation diagram in the Fig. 4.27.

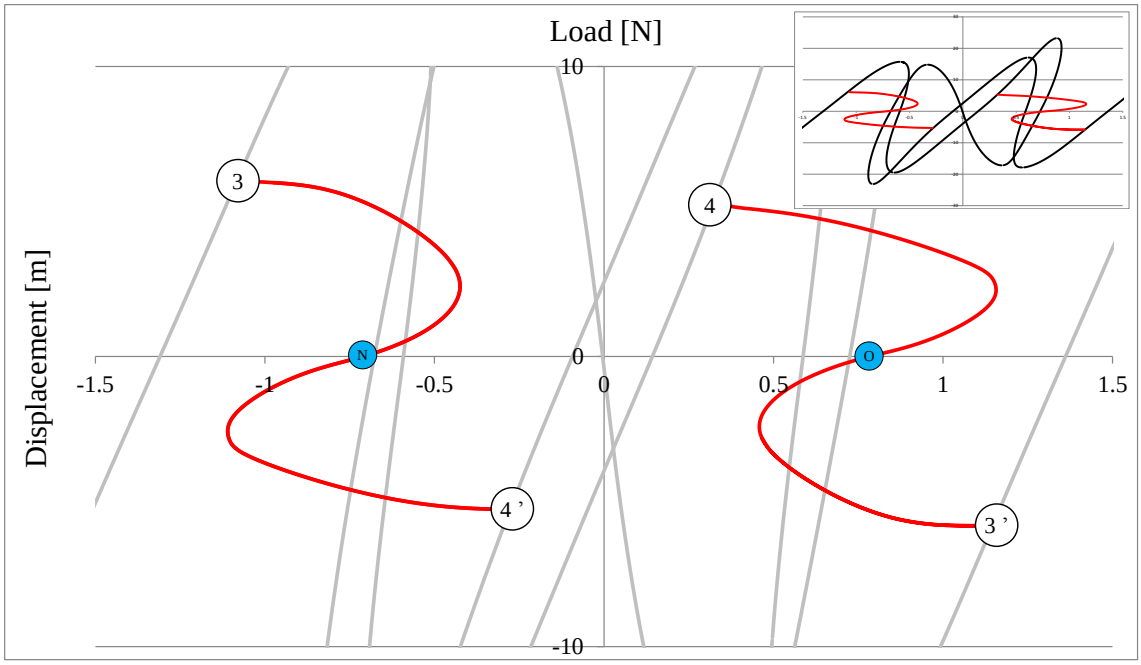

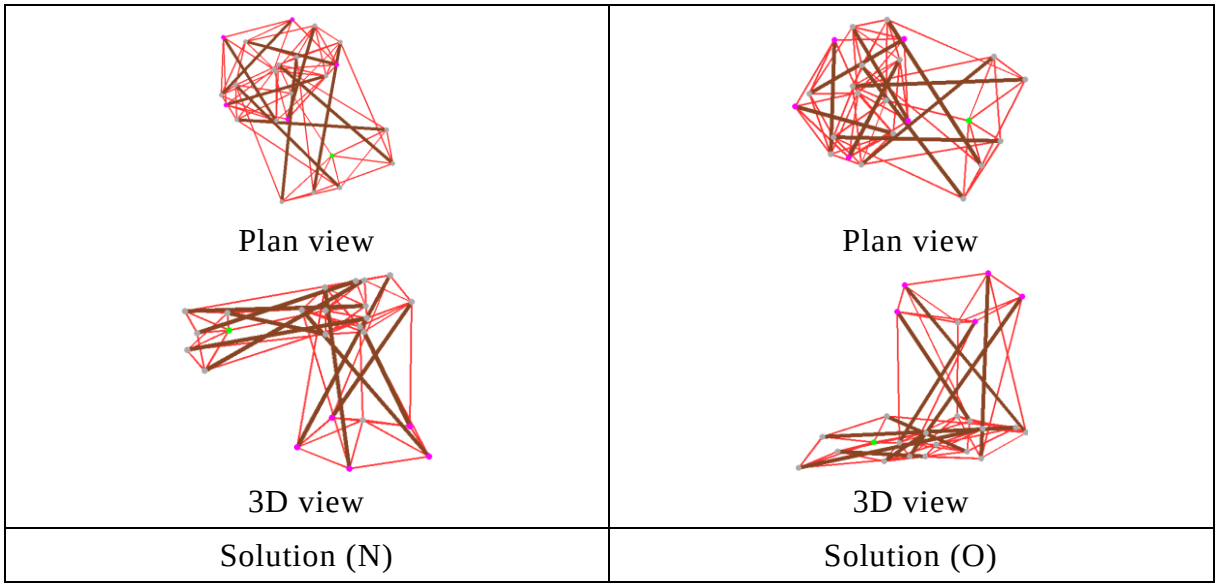

Figure 4.27: The bypass that connects point ③-a to ④'-a and ④'-a to ③'-a

Furthermore, when pursuing the same points, a bypass that connects point ③-b and point ④'-b emerges and obtained solution (P), while for point ④, the bifurcation path

produced two equilibrium shapes (solution (Q) and (R)), and the path becomes linear when it passes point ①, as shown in Fig. 4.28.

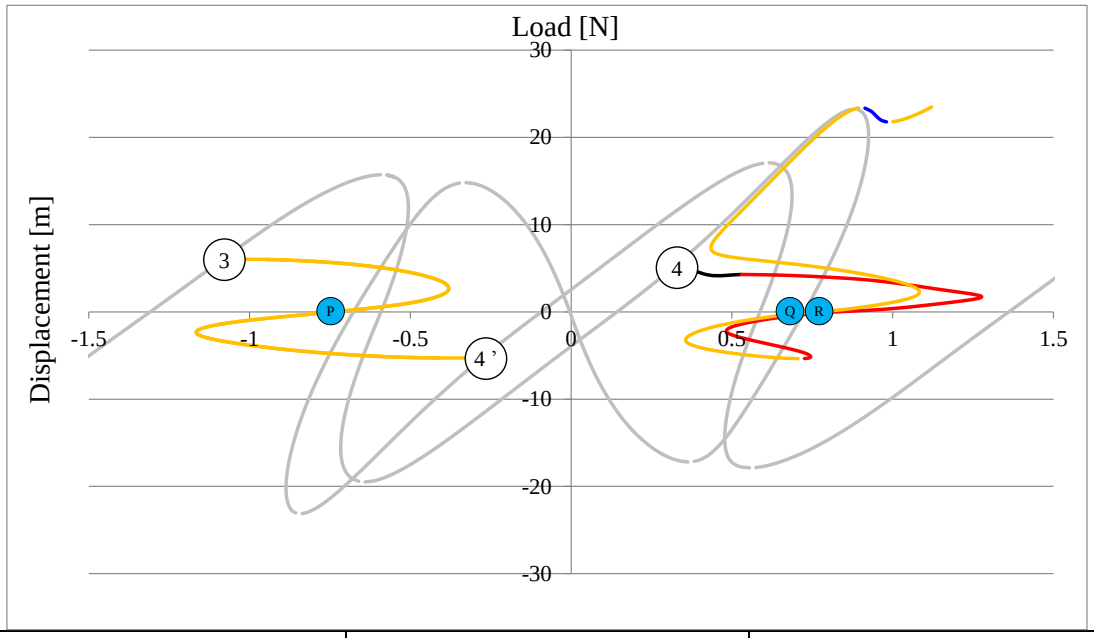

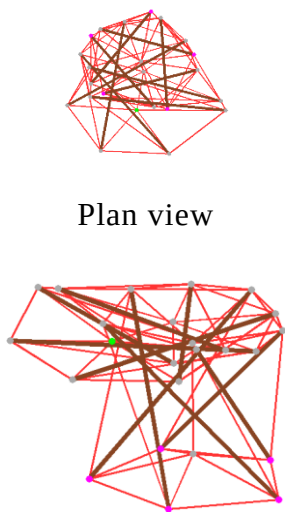 Plan view 3D view	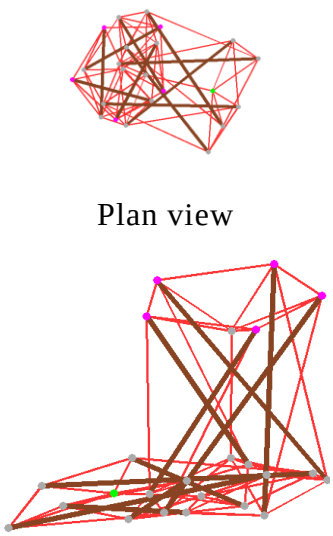 Plan view 3D view	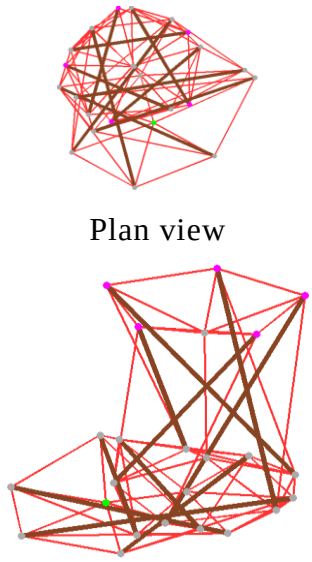 Plan view 3D view
Solution (P)	Solution (Q)	Solution (R)

Figure 4.28: The bypass that connects point ③-b to ④’-b, from point ④-b and equilibrium solutions obtained from the paths

Fig. 4.29 shows the summary of the total paths that were obtained in this analysis, where the total of 18 self-equilibrium shapes were achieved. The bifurcation paths that splits from the main paths are independent and show individual characteristics. Also, for this analysis, a rather stiffer tensegrity tower has been applied, which has the total

of 72 axial line elements and 10 struts were applied to the tensegrity tower. However, the main and bifurcation paths were successfully obtained for this analysis, while achieving symmetrical and irregular equilibrium shapes throughout the analysis.

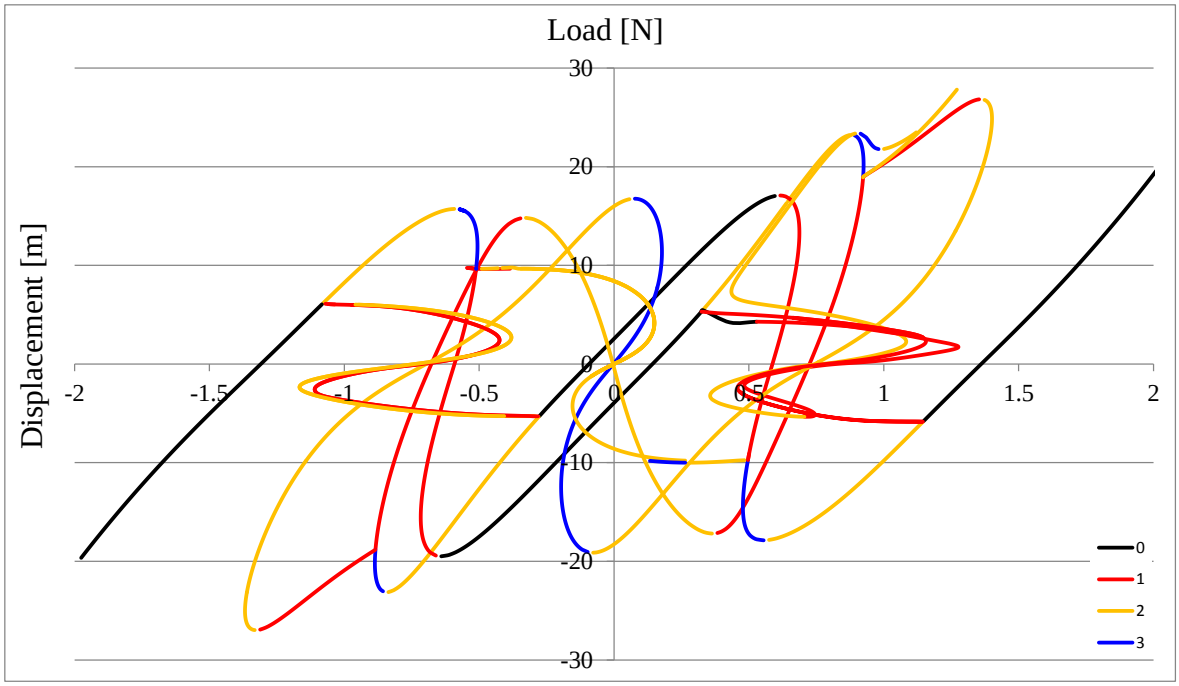

Figure 4.29: The total paths for the double storey tensegrity tower with a single control node

4.8 Discussion

Based on the findings from the numerical analyses, the characteristics of equilibrium solutions of tensegrity tower have become more evident. A rational procedure for form-finding have been developed by the application of “the measure-potential elements” for the tensional members and of “the truss elements” for compressional members. The TSM makes all solutions perfectly satisfy the “perfect equilibrium”, even if in case of many elements and/or complex element connectivity.

In **4.7.1**, the relation between incidence rate and the total potential energy for the tensegrity tower has been studied in order to examine the mechanical background of the appearance of each equilibrium solution. This suggests that the form-finding procedure by the geometrically nonlinear analysis may have a characteristic of chaos, so it is difficult to predict the shape of the solution only from initial conditions. On the other hand, it could be concluded that the proportion of morphology, symmetricity or shape-continuity are more likely to have much higher correlative relation, compared to the

relation between incidence rate and the potential energy. In addition, the target solution could be obtained easily and definitely, if an initial geometry can be set relatively close to the target, by applying compulsory displacement gradually.

Based on the knowledge mentioned above, path finding analysis is executed to ensure the positions of all the equilibrium solutions on the "load–displacement curves" including bifurcation paths, as shown in **4.7.2**, there were two analyses which were executed for tensegrity tower. Firstly, a double storey tensegrity tower was applied to execute the form-finding analysis in **4.7.3**. Here, the aim is to extract symmetrical equilibrium solution from the curve, a total of 16 equilibrium shapes were successfully obtained from the total of 5 independent main paths. Within the equilibrium solutions, solution (I) shows the highest incidence rate (50.6%) with the potential energy of 73.67[J], which is not the lowest compared to other obtained solutions, but has the most well-proportioned shape. This also shows that the correlative relation between incidence rate and the total potential energy could not be defined clearly. Using the same tensegrity tower model, another analysis was executed to examine the deformation behavior without gravitational influence as shown in subsection **4.7.4**. By neglecting the gravitational influence, a pair of perfectly symmetrically sideways paths have been achieved, although the total number of self-equilibrium shapes is significantly fewer than the case of gravitational influence (total of 6 self-equilibrium shapes).

In the subsequent form-finding analysis in subsection **4.7.5**, a double storey tensegrity tower with a single control node has been applied for determining all possible paths that may exist. In the analysis, a total of 9 symmetrical shapes were obtained from the main paths, and the existence of 4 bifurcation points were confirmed on the curve by examination of eigenvector of the tangent stiffness matrix. In this analysis, a total of 18 irregular equilibrium shapes have been confirmed, while all possible paths have been extracted. Each obtained bifurcation paths have its own identity, whether act as a bypass or elongates until it becomes a linear line. Here, the equilibrium shapes, symmetrical or irregular could be classified by the total number of negative eigenvalue. By examining the behavior of each shape, a better form-finding procedure could be proposed for future studies.

The application of measure-potential elements and truss elements in form-finding of tensegrity structure by TSM has been shown to be effective. If the determined shapes are substituted by element with real stiffness, a simulation of deformational behavior for tensegrity tower with extremely large displacement could be realized. When executing the simulation, the consideration of contact between elements should also be

a main focus. As shown in all the analyses of this chapter, the deformation of tensegrity tower is very random and unpredictable, and the probability of contact between elements in tensegrity are very high. Therefore, a much complex consideration should be made for the case, which may lead to the simulation for a real behavior of tensegrity structure.

References

[1] **F. Bossens, R. A. de Callafon, R. E. Skelton**: Modal analysis of a tensegrity structure – an experimental study. *Dynamic Systems and Control Group, University of California, U.S.A.*

[2] **S. Mizuho, S. Saijo, S. Hirai,** (2008): Experimental study of deformable clawing robot with tensegrity structure. *The 26th Annual Conference of the Robotics Society of Japan*.

[3] **K. Kawaguchi, T. Kawata,** (2008): Group theory approach of a tensegrity model with mechanisms. *J. Struct. Constr. Eng., Architectural Institute of Japan*, vol. 73 no. 631, pp. 1561–1568.

[4] **N. Vassart, R. Motro,** (1999): Multiparameter form finding method: application to tensegrity systems. *International Journal of Space Structures*, vol. 14. no. 2, pp. 147–154.

[5] **J. Zhang, M. Ohsaki,** (2005): A method for the form-finding problem of tensegrity structure by eigenvalue analysis of equilibrium matrix. *Architectural Institute of Japan*, pp. 943–944.

[6] **S. Okazawa, F. Fujii,** (1997): An eigenvalue-control to trace the equilibrium path to compute an elastoplastic bifurcation point. *Journal of Structural Engineering*, vol. 43A, pp. 311–320.

[7] **M. Asai, F. Fujii, K. Ikeda,** (1999): Reduction technique in bifurcation problems of symmetric structures using eigenvectors. *Journal of Structural Engineering*, vol. 45A, pp. 263–270.

[8] **H. Noguchi, T. Hisada,** (2000): Development of a new branch-switching algorithm in nonlinear FEM using scaled corrector. *The Japan Society of Mechanical Engineers*, vol. 92 No. 196, pp. 2191–2198.

[9] **H. Obiya, K. Ijima, N. Kawasaki, T. Matsunaga, A. Matsuo,** (2010): Form-finding of tensegrity structures with rigid bodies and axial line element. *Journal of Applied Mechanic*, vol. 13, pp. 47–56.

[10] **R. R. Pandia, S. D. Guest,** (2006): Using symmetry for tensegrity form-finding. *Journal of the International Association for Shell and Spatial Structures*, vol. 47 no. 3.

[11] **K. Snelson,** (2009): Force made visible. *Hard Press Editions*.

[12] **K. Kadota, H. Obiya, K. Ijima, S. Iguchi, H. Hateruma,** (2005): Path finding with multi-bifurcation by characteristics of the tangent stiffness method. *Journal of Structures and Materials in Civil Engineering*, vol. 21, pp. 57–64.

[13] **I. Saiki, K. Sudo, K. Ikeda, T. Iwakuma,** (2006): An improvement of the stiffness

modification method to find bifurcated paths at a multiple bifurcation point. *Journal of JSCE*, vol. 62 No.4, pp. 782–793.

List of symbols

Symbol		Description
$\mathbf{Q}$	:	Force density matrix
$\mathbf{C}$	:	Connectivity matrix
$\mathbf{x}$	:	Nodal coordinate vector
$\mathbf{D}$	:	Nodal force vector
$\mathbf{J}$	:	Element edge force–nodal force transformation matrix
$\mathbf{S}$	:	Element edge force vector
$\mathbf{u}$	:	Nodal coordinate vector
$\mathbf{X}$	:	Force vector
$\mathbf{L}$	:	Element length vector
$\bar{\mathbf{U}}$	:	Nodal force vector in self-equilibrium state
$\mathbf{s}$	:	Element measurement vector
$\boldsymbol{\alpha}$	:	Cosine vector
$\mathbf{K}_{\mathrm{T}}^{\mathrm{L}}$	:	Element stiffness matrix for axial line element
$\mathbf{e}$	:	Unit matrix
$\mathbf{K}_{\mathrm{G}}$	:	Tangent geometric stiffness matrix
$\mathbf{K}_{\mathrm{O}}$	:	Element stiffness matrix
f_{ix}	:	Nodal force
q_h	:	Tension members that form the upper and lower triangles
q_v	:	Tension members that connect upper and lower nodes
q_c	:	Compressional members that connect upper and lower nodes
q	:	Force density ratio
u	:	Nodal coordinate in u-direction
v	:	Nodal coordinate in v-direction
w	:	Nodal coordinate in w-direction
N	:	Axial force
l	:	Element length
α	:	Cosine vector in u-direction
β	:	Cosine vector in v-direction
γ	:	Cosine vector in w-direction
h	:	Rank of matrix
r	:	Rank deficiency

List of symbols

Symbol		Description
P	:	Element measure potential
C	:	Element force coefficient
n	:	Element force multiplier
i	:	The i edge of an element
j	:	The j edge of an element
X	:	Force component in x-direction
Y	:	Force component in y-direction
Z	:	Force component in z-direction
x	:	Nodal coordinate in x-direction
y	:	Nodal coordinate in y-direction
z	:	Nodal coordinate in z-direction
l_{0ij}	:	Non-stressed element length
f	:	Variable function of load and displacement control

Chapter 5
Frictionless Contact Analysis Comprising Axial Force Element and Frame Element with Large Displacement

5.1 Introduction

When performing a deformational analysis for tensegrity, the nonlinearity that may occur is not only caused by the geometrical characteristics of the element, but also by the contact problem amongst elements or nodes. Contact problem is a complex nonlinear case and it is important to consider how to express the phenomena with the application of digitalized data. There are four types of contact phenomena that are adoptable, which are node–surface contact, node–element contact, contact between nodes and contact between surfaces.

In this chapter, the author will perform two cases of contact analysis. One is contact between elements and the other is node–element contact. For the case of contact between elements, a three dimensional contact analysis axial force element is applied, and the geometrically nonlinear algorithm for contact between elements is developed [1]. The aim is to produce the algorithm by using non-compressible element to simulate cables which constitute tensegrity. In this analysis, a cable element can involve multiple sliding nodes which simulate contact points between elements. Here, the contact judgment is determined when element passes through each other and the judgment is defined by a simple inner product and scalar triple product for the contacted elements. In addition, the reaction force produced by the contact node is defined as the contact force and in case of sign inversion of the contact force, the contact judgment is released and the elements are treated as a non-contact element or normal element.

For the other case, a node–element contact analysis is also presented in this chapter. A plane frame element is applied for the analysis, where the element is formed by two edges and a contact node. Same as the contact case between tensional elements, the contact judgment is performed by the inner product for node–element contact. When sign inversion of the contact force happens, the node is released and the element is treated as a common plane frame element.

A common problem occurs when a contact node slides and is close to an element edge. As explained in chapter 1, the unbalanced force is unable to be converged due to the limitation in boundary condition. It makes the element force stiffness matrix singular that the distance between a contact node and an element edge approach to zero. Therefore, it leads to the divergence of the unbalanced force.

To solve this problem, the shear deformation in Timoshenko beam is considered, as a countermeasure, in the element force equation. By introducing the shear deformation to the element force equation, the “critical area” [2] where the unbalanced force hardly converges can be made significantly less than those of the Euler–Bernoulli beam, as shown in several examples in this chapter.

The “passing through” of a contact node is also studied, by a simple algorithm for the inner and outer vector product, which produced stable convergence results, including at the tip of the element. In addition, the algorithm for the “passing through” of the contact node to the next element was easier to implement and much more accurate at all the edges of the elements. In a study on frictionless node–element contact [3], the author proposed an algorithm that combines a contact element with the next non-contact element that the contact node is about to “passing through”. The equilibrium state was

successfully achieved by this technique, although its reliability is low due to the change of mesh configuration, which affects the entire scheme. In another study by Tsutsui et al. [2], an element force equation based on a cantilever beam coordinate was used to improve the "passing through". The introduced equation enabled the convergence of the unbalanced force when the contact node was relatively close to the edge of the element—a configuration that had not been previously achieved. Furthermore, the findings of this study would facilitate further studies on node–element contact because its definitions and analytical results are precise, reliable, and very robust.

5.2 The derivation of tangent stiffness equation for three dimensional contact case comprising axial force elements

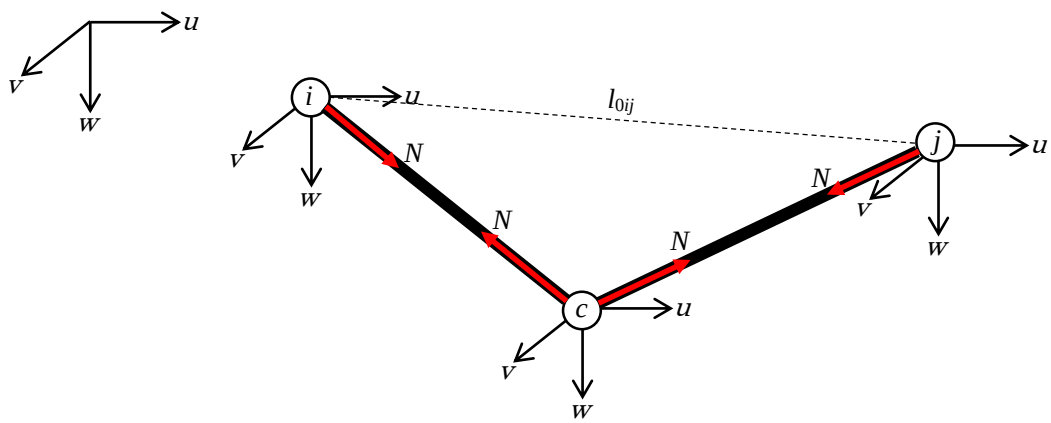

Figure 5.1: Equilibrium condition of a contact element

Here, the tangent stiffness equation for a three dimensional axial force element (truss element) will be derived. The tangent stiffness equation could be obtained by differentiating the equilibrium equation as shown in Eq. 2-3 and Eq. 2-4. The derivation is similar to what was stated in chapter 2. Here, Fig. 5.1 shows a contact element consisting of three nodes, and the relation between element edges *i* and *j* and the contact node c could be shown in Eq. 5-1 to 5-4.

$$\mathbf{D}_{ic} = [U_i \quad V_i \quad W_i \quad U_c \quad V_c \quad W_c]^{\mathrm{T}} \tag{5-1}$$

$$\boldsymbol{\alpha}_{ic} = [-\alpha_{ic} \quad -\beta_{ic} \quad -\gamma_{ic} \quad \alpha_{ic} \quad \beta_{ic} \quad \gamma_{ic}]^{\mathrm{T}} \tag{5-2}$$

$$\mathbf{D}_{cj} = [U_c \quad V_c \quad W_c \quad U_j \quad V_j \quad W_j]^{\mathrm{T}} \tag{5-3}$$

$$\boldsymbol{\alpha}_{cj} = [-\alpha_{cj} \quad -\beta_{cj} \quad -\gamma_{cj} \quad \alpha_{cj} \quad \beta_{cj} \quad \gamma_{cj}]^{\mathrm{T}} \tag{5-4}$$

In this case, the contact node is considered as a sliding node, which exhibits the equivalent amount of axial force, of both sides of *ic* and *cj* section. In this case, the axial

force N according to the equilibrium condition is shown as Eq. 5-5 to Eq. 5-7.

$$\mathbf{D}_{icj} = [U_i \quad V_i \quad W_i \quad U_c \quad V_c \quad W_c \quad U_j \quad V_j \quad W_j]^{\mathrm{T}} \tag{5-5}$$

$$\boldsymbol{\alpha}_{icj} = [-\alpha_{ic} \quad -\beta_{ic} \quad -\gamma_{ic} \quad \alpha_{ic} - \alpha_{cj} \quad \beta_{ic} - \beta_{cj} \quad \gamma_{ic} - \gamma_{cj} \quad \alpha_{cj} \quad \beta_{cj} \quad \gamma_{cj}]^{\mathrm{T}} \tag{5-6}$$

$$\mathbf{D}_{icj} = \boldsymbol{\alpha}_{icj} \cdot N \tag{5-7}$$

By the differentiation of the equilibrium equation for the contact element, shown in Eq. 5-7, the deformed quantity could be expressed as Eq. 5-8.

$$\delta\mathbf{D}_{icj} = \delta\boldsymbol{\alpha}_{icj} \cdot N + \boldsymbol{\alpha}_{icj} \cdot \delta N \tag{5-8}$$

The right side of the equation represents the fluctuation of nodal displacement vector $\delta\mathbf{u}_{icj}$. It is expressed as a linear equation and δN and δl_{ij} will be derived formally. The element force equation is also a linear equation, and the equation is formed by the Young's modulus E, cross sectional area A and non-stressed length l_{0ij} and could be expressed as;

$$N = \frac{\mathrm{EA}}{l_{0ij}} \delta l_{ij} \tag{5-9}$$

Here, the increment of the length δl_{ij} could be shown as;

$$\delta l_{ij} = \delta l_{ic} + \delta l_{cj} \tag{5-10}$$

For the *ic* and *cj* section, the length increment could be shown as the following equations.

$$\delta l_{ic} = {u_{ic}}^2 + {v_{ic}}^2 + {w_{ic}}^2 \tag{5-11}$$

$$\delta l_{cj} = {u_{cj}}^2 + {v_{cj}}^2 + {w_{cj}}^2 \tag{5-12}$$

By the differentiation of Eq. 5-11 and Eq. 5-12, while considering $\delta u_{ic}=\delta u_c-\delta u_i$, $\delta v_{ic}=\delta v_c-\delta v_i$, $\delta w_{ic}=\delta w_c-\delta w_i$, $\delta u_{cj}=\delta u_j-\delta u_c$, $\delta v_{cj}=\delta v_j-\delta v_c$ and $\delta w_{cj}=\delta w_j-\delta w_c$, the length increment could be shown in a matrix form as shown in Eq. 5-13.

$$\delta l_{ij} = \begin{bmatrix} -\alpha_{ic} \\ -\beta_{ic} \\ -\gamma_{ic} \\ \alpha_{ic} - \alpha_{cj} \\ \beta_{ic} - \beta_{cj} \\ \gamma_{ic} - \gamma_{cj} \\ \alpha_{cj} \\ \beta_{cj} \\ \gamma_{cj} \end{bmatrix}^{\mathrm{T}} \begin{bmatrix} \delta u_i \\ \delta v_i \\ \delta w_i \\ \delta u_c \\ \delta v_c \\ \delta w_c \\ \delta u_j \\ \delta v_j \\ \delta w_j \end{bmatrix} \tag{5-13}$$

Here, by substituting Eq. 5-2 and Eq. 5-4 into Eq. 5-14, the element stiffness for *ic* and *cj* section could be shown as;

$$\boldsymbol{\alpha}_{icj} \cdot \delta N = \frac{\mathrm{EA}}{l_{0ij}} \boldsymbol{\alpha}_{icj} \cdot {\boldsymbol{\alpha}_{icj}}^{\mathrm{T}} \cdot \delta\mathbf{u}_{icj} \tag{5-14}$$

By substituting the differentiation of Eq. 5-2 and Eq. 5-4, the super positioning of the equations represents the geometric stiffness. The geometric stiffness for contact element

is shown in Eq. 5-15 and Eq. 5-16.

$$\delta\boldsymbol{\alpha}_{ic}\cdot N=\frac{N}{l_{ic}}\begin{bmatrix}1-\alpha^2 & -\alpha\beta & -\alpha\gamma & -(1-\alpha^2) & \alpha\beta & \alpha\gamma\\ & 1-\beta^2 & -\beta\gamma & \alpha\beta & -(1-\beta^2) & \beta\gamma\\ & & 1-\gamma^2 & \alpha\gamma & \beta\gamma & -(1-\gamma^2)\\ & & & 1-\alpha^2 & -\alpha\beta & -\alpha\gamma\\ & \textit{Symmetry} & & & 1-\beta^2 & -\beta\gamma\\ & & & & & 1-\gamma^2\end{bmatrix}_{ic}\begin{bmatrix}\delta u_i\\ \delta v_i\\ \delta w_i\\ \delta u_c\\ \delta v_c\\ \delta w_c\end{bmatrix} \qquad 5\text{-}15$$

$$\delta\boldsymbol{\alpha}_{cj}\cdot N=\frac{N}{l_{cj}}\begin{bmatrix}1-\alpha^2 & -\alpha\beta & -\alpha\gamma & -(1-\alpha^2) & \alpha\beta & \alpha\gamma\\ & 1-\beta^2 & -\beta\gamma & \alpha\beta & -(1-\beta^2) & \beta\gamma\\ & & 1-\gamma^2 & \alpha\gamma & \beta\gamma & -(1-\gamma^2)\\ & & & 1-\alpha^2 & -\alpha\beta & -\alpha\gamma\\ & \textit{Symmetry} & & & 1-\beta^2 & -\beta\gamma\\ & & & & & 1-\gamma^2\end{bmatrix}_{cj}\begin{bmatrix}\delta u_c\\ \delta v_c\\ \delta w_c\\ \delta u_j\\ \delta v_j\\ \delta w_j\end{bmatrix} \qquad 5\text{-}16$$

Here, the geometric stiffness of the *ic* and *cj* section could simplified as;

$$\delta\boldsymbol{\alpha}_{icj}\cdot N=\delta\boldsymbol{\alpha}_{ic}\cdot N+\delta\boldsymbol{\alpha}_{cj}\cdot N \qquad 5\text{-}17$$

The tangent stiffness equation for the contact element could be formed by the super position of Eq. 5-14 to Eq. 5-17.

5.3 Numerical Example

In this section, several numerical analyses for contact between elements are presented. The numerical examples are based on the derivation of tangent geometric stiffness of three dimensional axial force elements in section **5.2**. Also, these analyses will exhibit the behavior of axial force element in pre-contact and post contact mode where, a slipping node is/are created when the contact judgment is determined. In addition, a simple contact between two elements is showed in subsection **5.3.1**, followed by multiple contact analysis in subsection **5.3.2**. The analyses results are shown in graphical sketches accordingly.

5.3.1 Contact between two axial force elements

In this analysis, a simple contact between two elements is executed and the analysis model is shown in Fig. 5.2. In this analysis, the upper element A (marked in red color) is subjected with compulsory displacement in *w* direction (downwards) until it contacts with the lower element B (marked as black color). The nodes on element A and B are fixed in all direction.

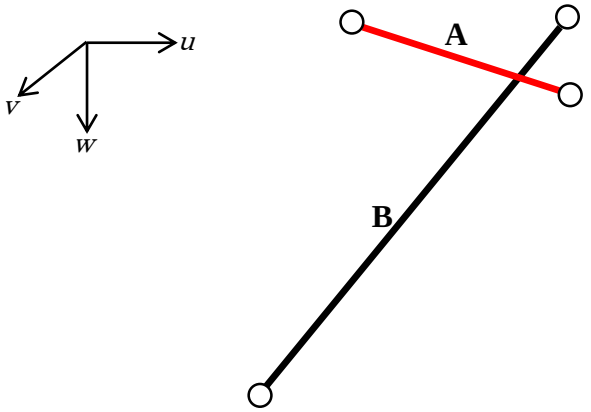

Fig 5.2: Analysis model

<u>Initial data</u>:			
Total nodes	:	4	nodes
Total elements	:	2	elements
Non-stressed element length A, l_A	:	2.000	[m]
Non-stressed element length B, l_B	:	3.605	[m]
<u>Analysis condition</u>:			
Cross sectional area, A	:	1.0×10^{-4}	[cm^2]
Tensional Young Modulus, E	:	1.0×10^{8}	[N/cm^2]
Compressional Young Modulus, E	:	1.0×10^{-4}	[N/cm^2]
Allowable unbalanced force	:	1.0×10^{-8}	[N]
Compulsory displacement	:	0.3	[m]/step

Using the initial condition, the contact between elements analysis is performed and the results are shown in Fig. 5.3. The deformations of both elements are shown continuously from step (2) to (9). From the initial configuration, a compulsory displacement is applied on both edges of element A, vertically downwards with the increment of 0.3[m] per each step.

Step	The convergence of unbalanced force	Deformation diagram
2	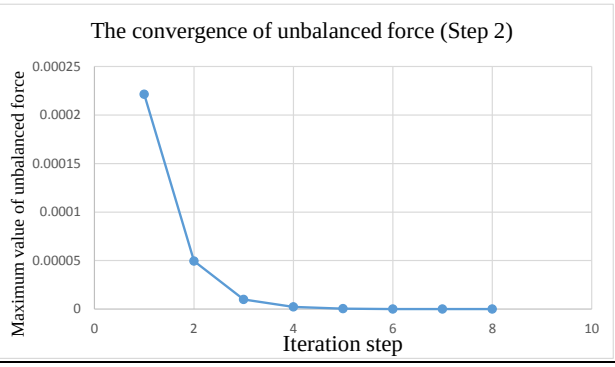	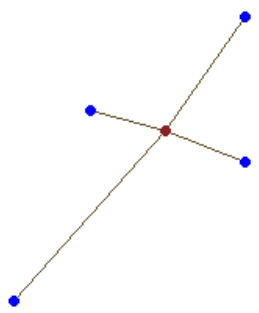

3	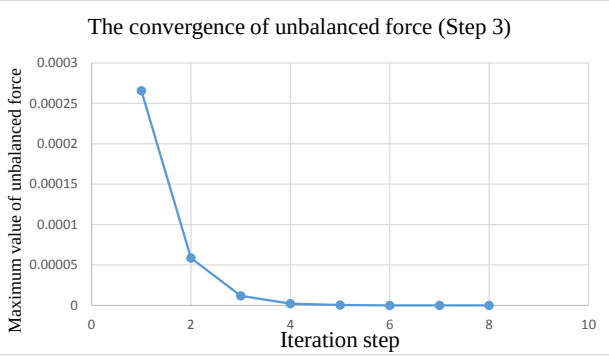 The convergence of unbalanced force (Step 3) Maximum value of unbalanced force 0.0003 0.00025 0.0002 0.00015 0.0001 0.00005 0 0 2 4 6 8 10 Iteration step	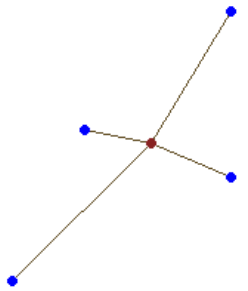
4	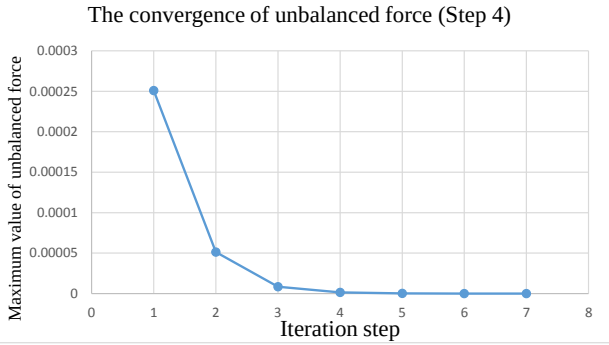 The convergence of unbalanced force (Step 4) Maximum value of unbalanced force 0.0003 0.00025 0.0002 0.00015 0.0001 0.00005 0 0 1 2 3 4 5 6 7 8 Iteration step	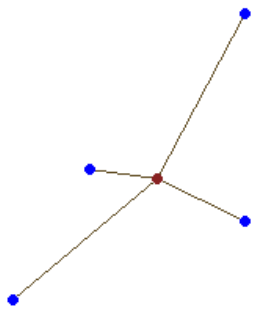
5	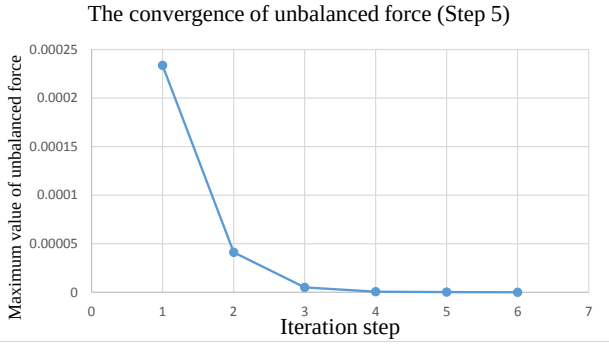 The convergence of unbalanced force (Step 5) Maximum value of unbalanced force 0.00025 0.0002 0.00015 0.0001 0.00005 0 0 1 2 3 4 5 6 7 Iteration step	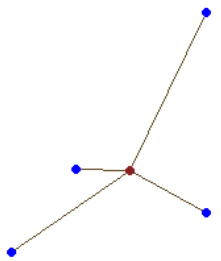
6	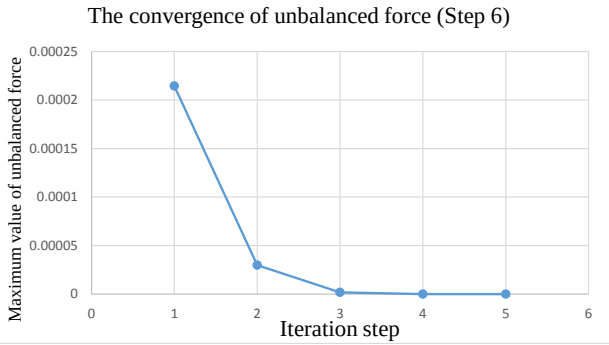 The convergence of unbalanced force (Step 6) Maximum value of unbalanced force 0.00025 0.0002 0.00015 0.0001 0.00005 0 0 1 2 3 4 5 6 Iteration step	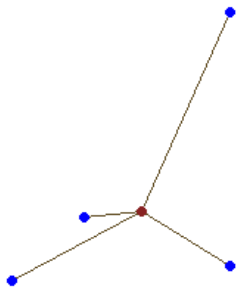
7	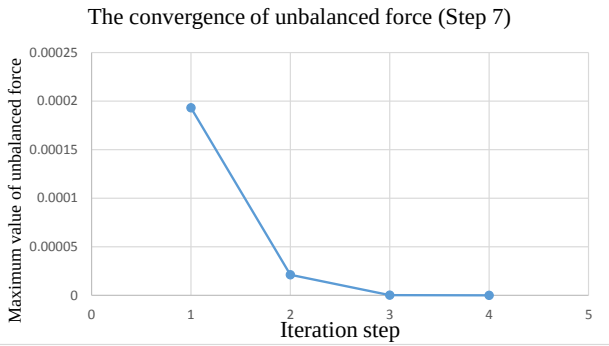 The convergence of unbalanced force (Step 7) Maximum value of unbalanced force 0.00025 0.0002 0.00015 0.0001 0.00005 0 0 1 2 3 4 5 Iteration step	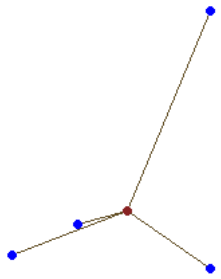

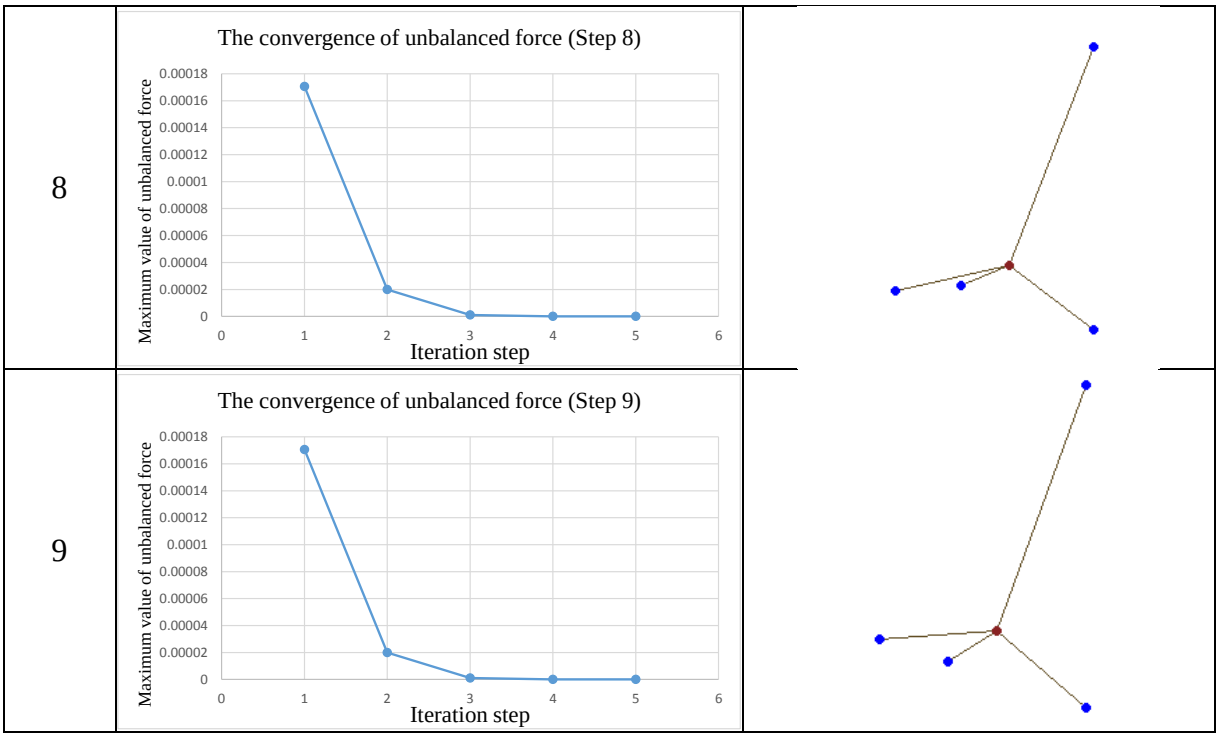

Figure 5.3: The convergence of unbalanced force and the deformation diagrams

Here, contact occurs in step (2), and both elements start to deform slightly. By increasing the compulsory displacements, referring to the deformation graph, when contact occurs, a brown node (sliding node) is created, in order to simulate the contact behavior. By the creation of sliding node, the axial force between contact node and both element edges for A and B are the same, as the contact node behaves as a roller node arbitrary to the direction of both elements. The analysis also shows a stable and rapid convergence of unbalanced force, which also exhibits the superiority of TSM.

Based on the analysis result, it could be concluded that the implementation of sliding node could simulate the behavior of contact between elements. This analysis is the simplest case of a frictionless contact between elements, and in this case, non-compressible elements were applied. The analysis exhibits a simple contact between elements with large deformation, while the unbalanced force was rapidly converged less than ten iteration steps.

5.3.2 Multiple contact analysis

For the next numerical analysis, a mesh shape model is applied to simulate multiple contact analysis. Fig. 5.4(a), (b) and (c) show the initial configuration of the mesh shape model. In Fig 5.4(a), the blue nodes marked from (A) to (O) clock wisely is the

restrained in all direction nodes, while the red nodes are sliding nodes. The analysis conditions for this analysis are shown as the followings;

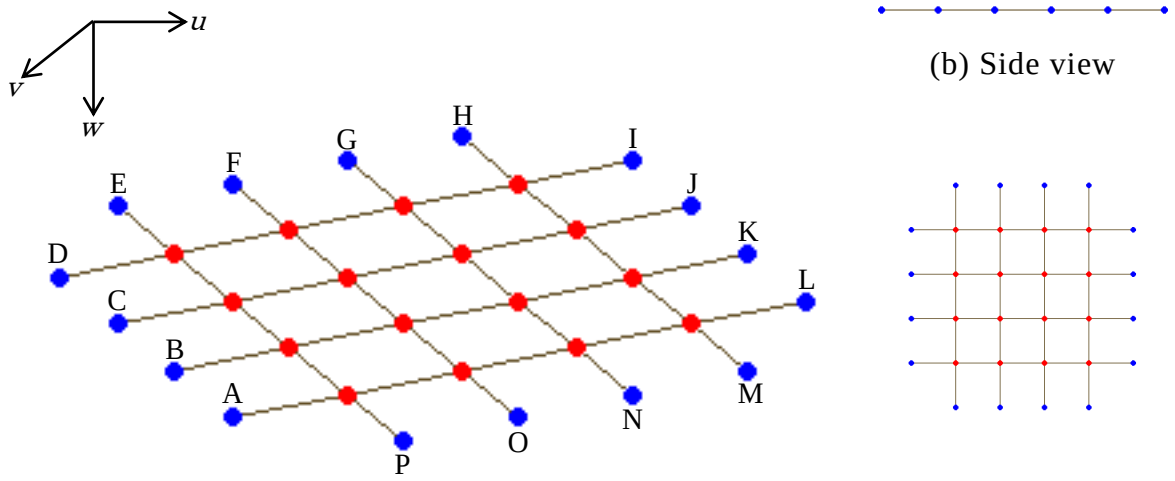

(b) Side view

(a) Bird's eye view

(c) Plan view

Figure 5.4: Initial configuration of wire mesh

<u>Initial data</u>:

Total nodes	:	32	nodes
Total elements	:	8	elements
Non-stressed of all elements length	:	15.000	[m]

<u>Analysis condition</u>:

Cross sectional area, A	:	1.0×10^{-4}	[cm^2]
Tensional Young Modulus, E	:	1.0×10^{8}	[N/cm^2]
Compressional Young Modulus, E	:	1.0×10^{-4}	[N/cm^2]
Allowable unbalanced force	:	1.0×10^{-6}	[N]
Compulsory displacement	:	0.2	[m]/step

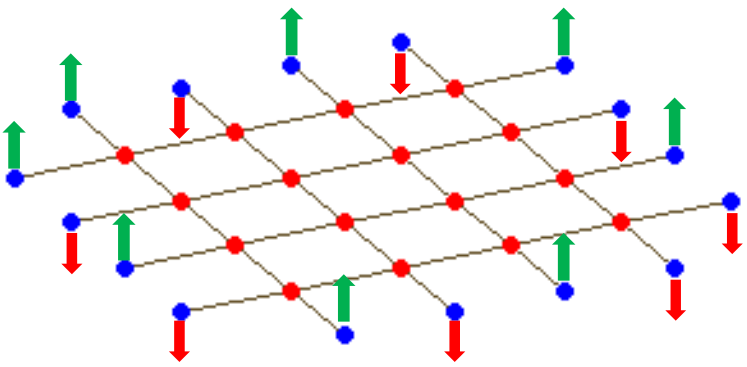

Figure 5.5: Compulsory displacement on each nodes

As shown in Fig. 5.4(a) and Fig. 5.5, compulsory displacements are applied on all restrained nodes, where nodes marked with (A),(C),(F),(H),(J),(L),(M) and (O) are applied in vertically downwards direction with 0.2[m] per step. While for nodes marked with (B),(D),(E),(G),(I),(K),(N) and (P), the compulsory displacement are applied in vertically upwards direction with -0.2[m] per step. The deformation of the mesh is shown gradually in Fig. 5.6. Here, a specific deformation scheme is shown by three different angles which are in side view, plan view and bird's eye view.

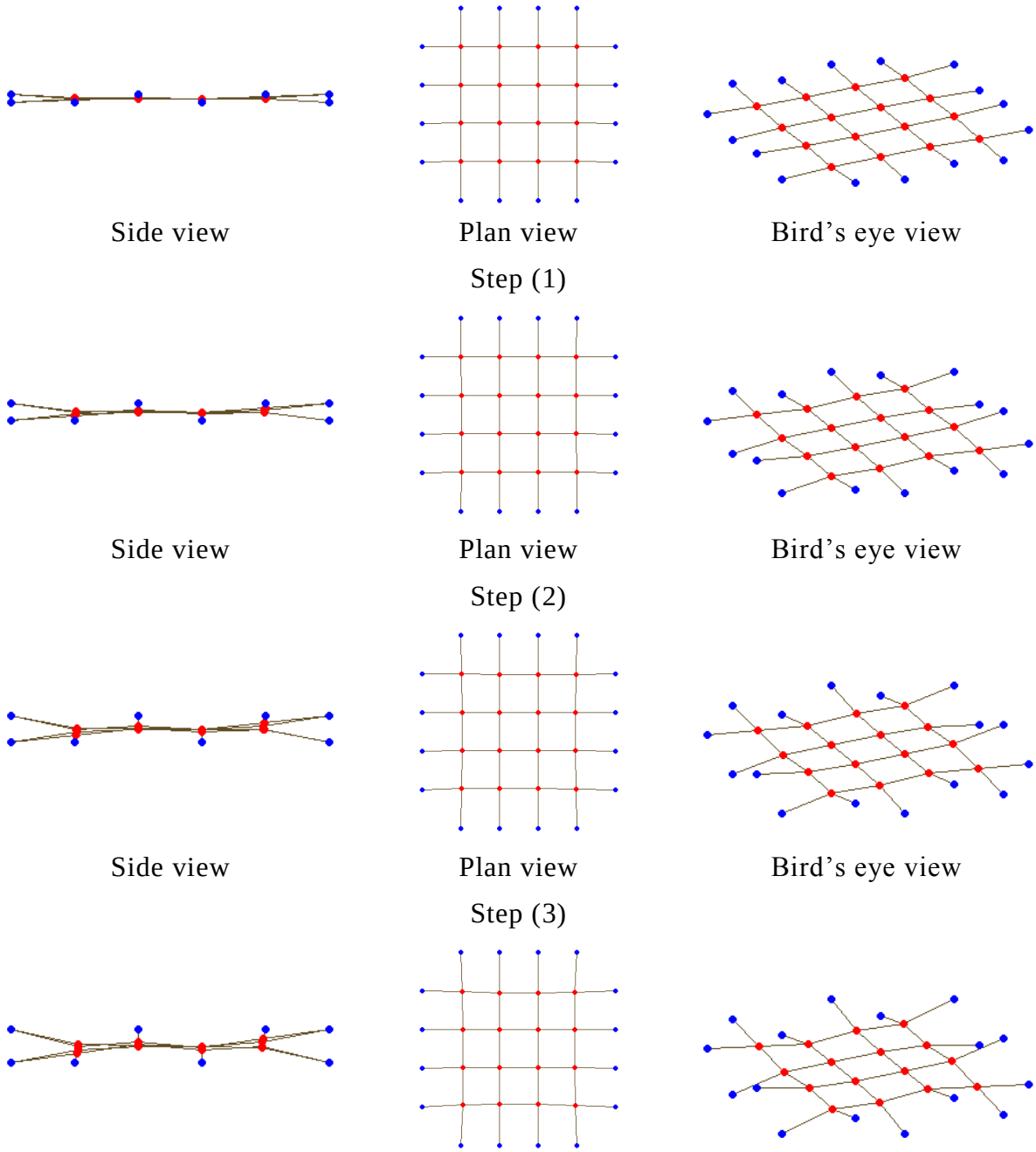

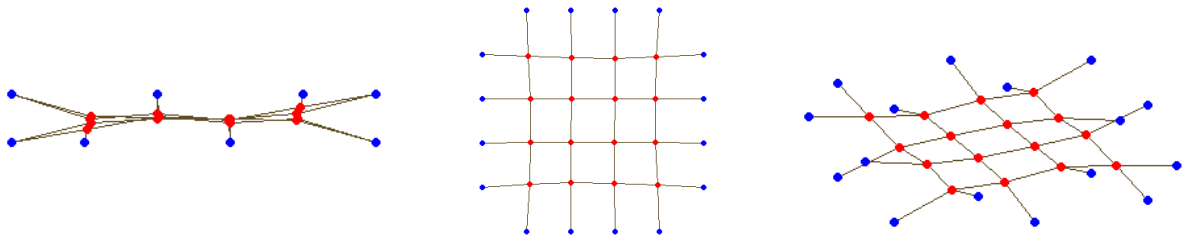

Side view Plan view Bird's eye view

Step (5)

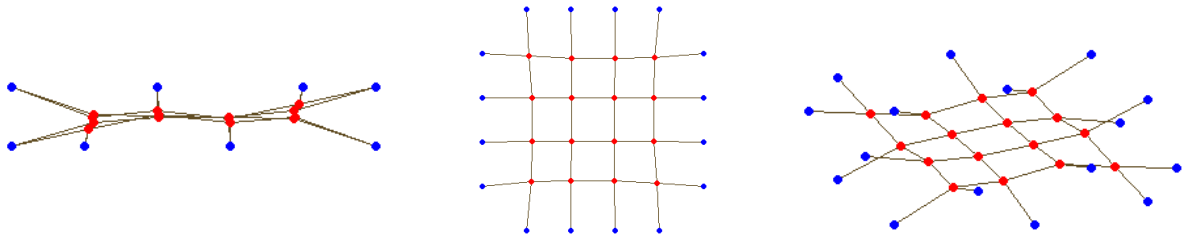

Side view Plan view Bird's eye view

Step (6)

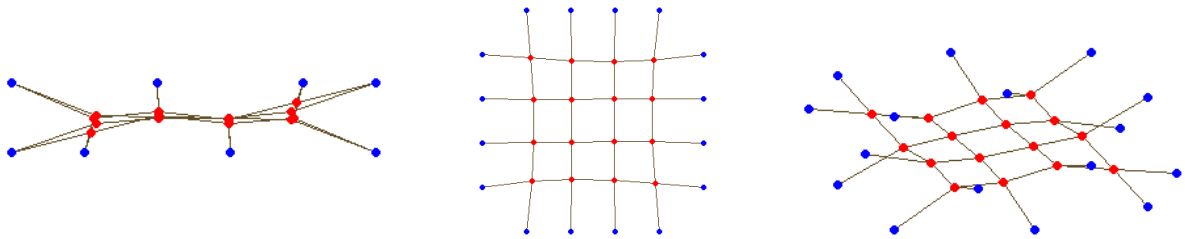

Side view Plan view Bird's eye view

Step (7)

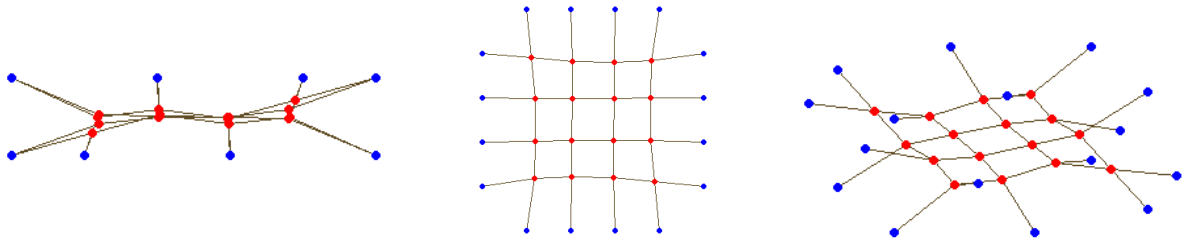

Side view Plan view Bird's eye view

Step (8)

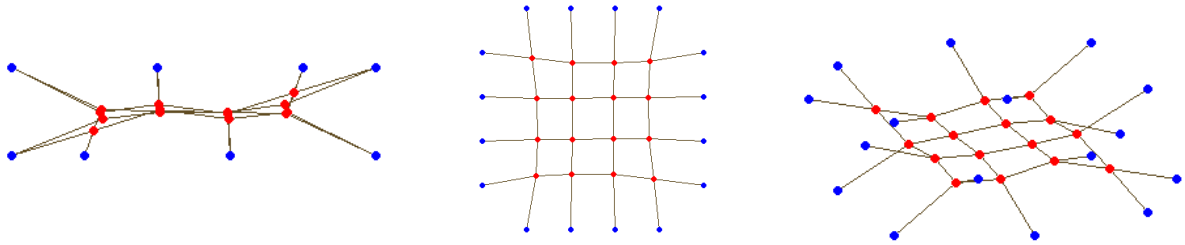

Side view Plan view Bird's eye view

Step (9)

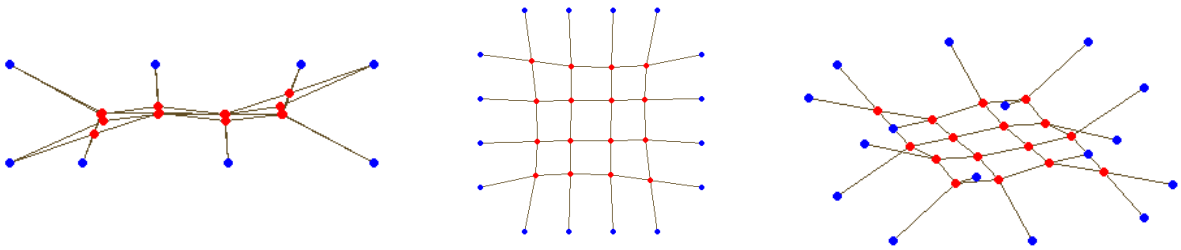

Side view Plan view Bird's eye view

Step (10)

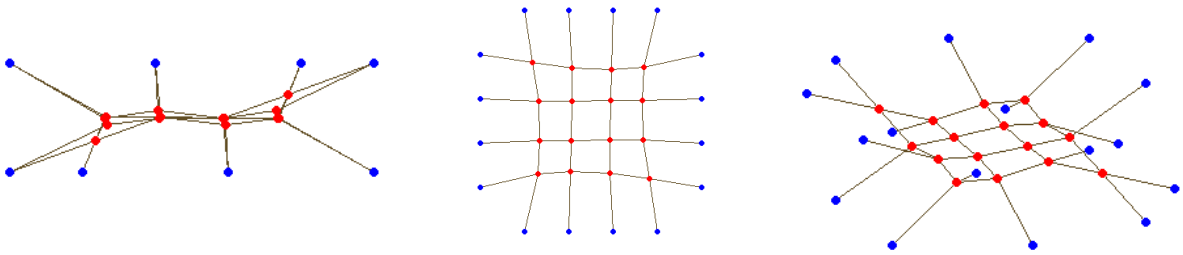

Side view Plan view Bird's eye view

Step (11)

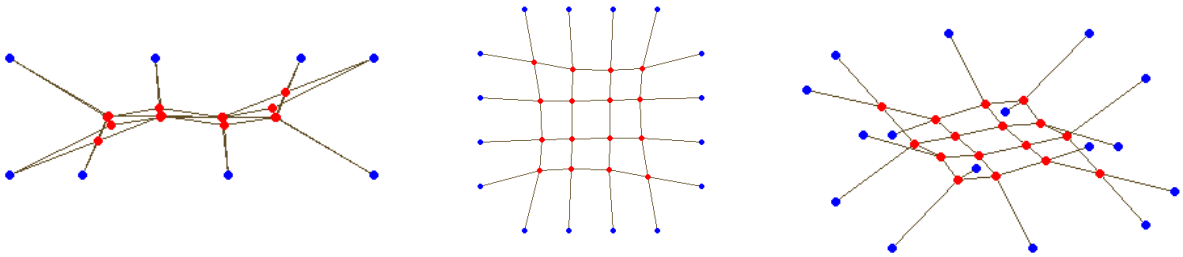

Side view Plan view Bird's eye view

Step (12)

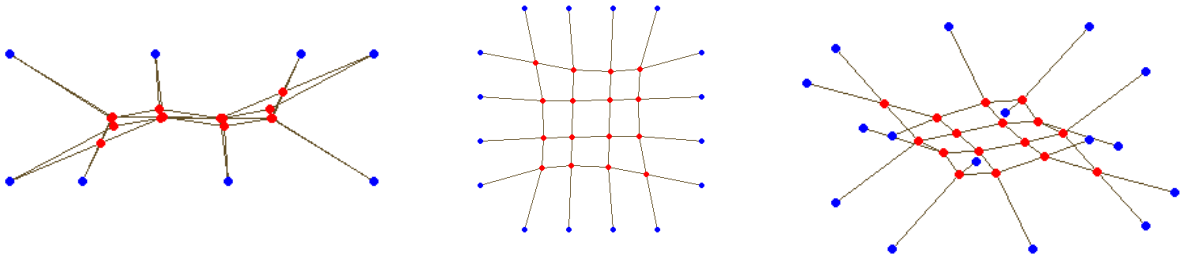

Side view Plan view Bird's eye view

Step (13)

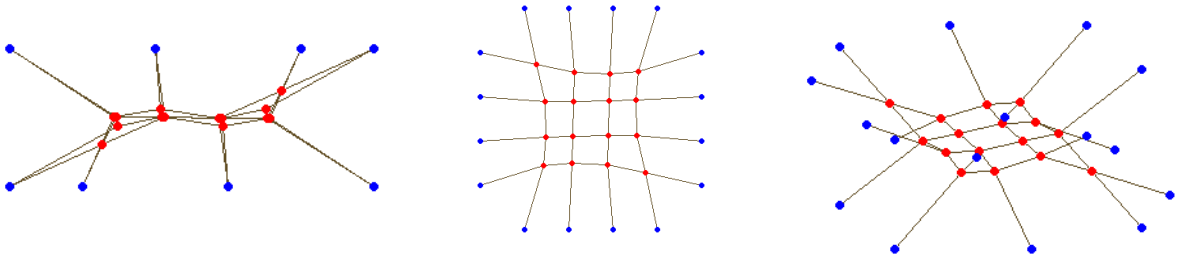

Side view Plan view Bird's eye view

Step (14)

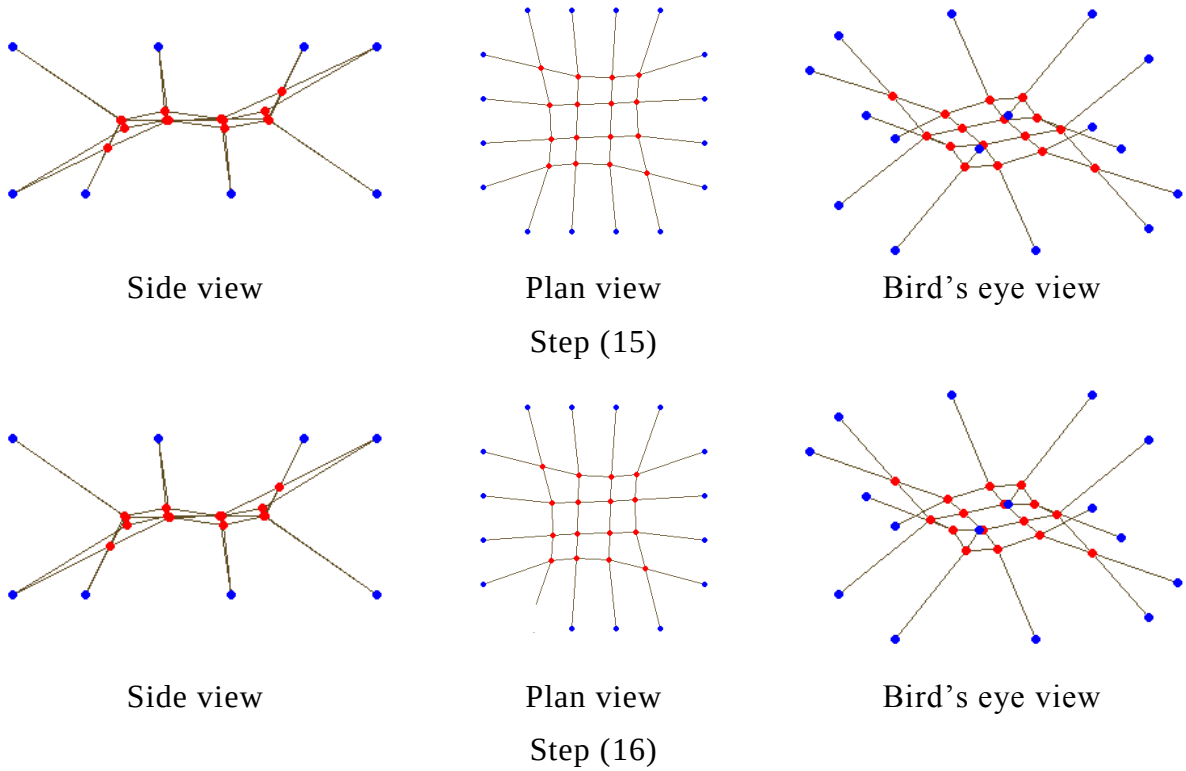

Figure 5.6: Deformation diagrams of the wire mesh

As shown in Fig. 5.6(1), the mesh starts to deform as compulsory displacements were applied on each restrained nodes. The compulsory displacements were applied gradually until step (16), where all elements were in tensional mode and could be observed in every deformation diagrams. Similar to the analysis stated in **5.3.1**, the unbalanced forces were also converged in less than ten iteration steps throughout the entire analysis, although the element configurations were more complex than the previous one.

5.4 Contact of a plane frame element

Here, the differential of equilibrium equation will be performed to derive an interaction process in order to obtain tangent geometric stiffness for contact phenomena. Figure 5.7 represents element force for contact problem in global coordinate system. For this beam coordinate, contact node influences the deformation of the element as the group of forces that includes edge moments and axial force. Fig. 5.8 represents nodal forces for contact node and both element edges for a plane frame structure. For this case, rotation component for the contact node is neglected and the degree of freedom for the node is two. The edge force vector for this combination of element edge forces and

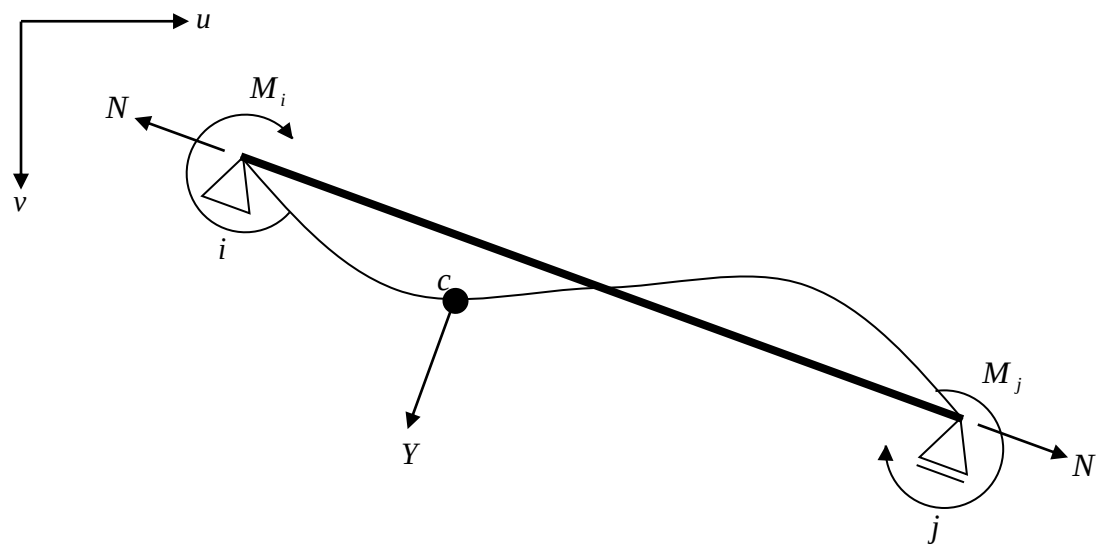

Figure 5.7: Element edge forces and contact force

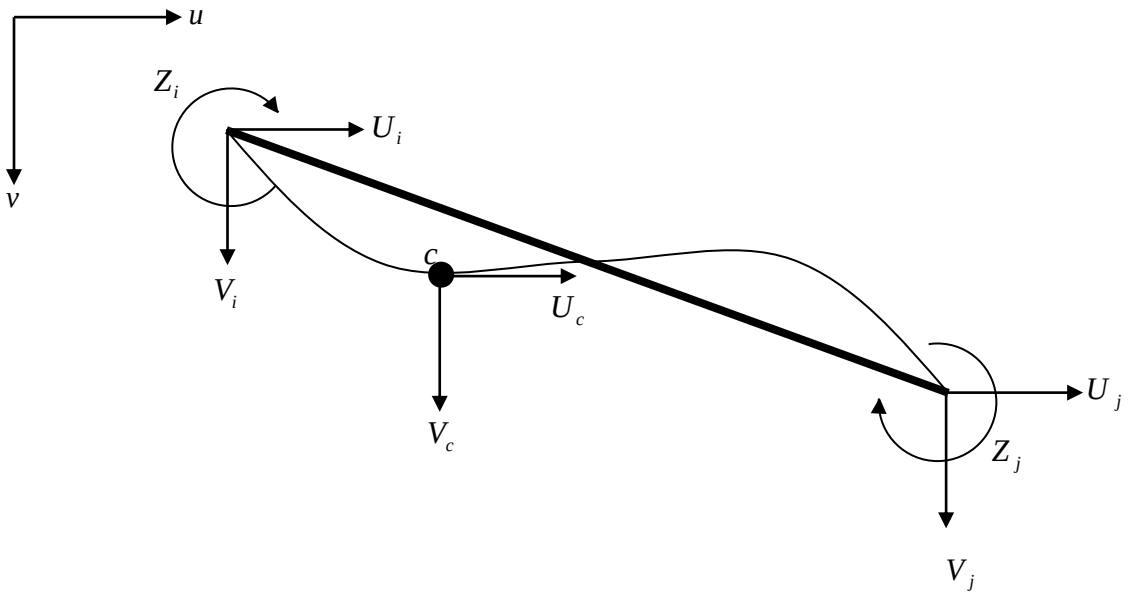

Figure 5.8: Nodal forces for contact node and both element edges

contact force is expressed as;

$$\mathbf{S} = [N \quad M_i \quad M_j \quad Y]^{\mathrm{T}} \qquad 5\text{-}18$$

Here, similar to the procedure in chapter 1, node *i* is a pin fixed node, node *j* is movable in element axial direction or a roller node and node *c* is all fixed node. Fig. 5.8 also shows the local coordinate system for beam element, the expression for nodal force that works on these nodes can be expressed as;

$$\mathbf{D} = [U_i \quad V_i \quad Z_i \quad U_j \quad V_j \quad Z_j \quad U_c \quad V_c]^{\mathrm{T}} \qquad 5\text{-}19$$

According to Fig. 5.9, element length is *l*, length between *i* edge and contact node *c* is l_i and the length between j edge and contact node c is l_j, and the cosine vector between

both edges is $\{\alpha,\beta\}$, between i edge and contact node c is $\{\alpha_{ci},\beta_{ci}\}$, between j edge and contact node c is $\{\alpha_{jc},\beta_{jc}\}$. The equilibrium equation between element force vector and nodal force vector can be expressed in the matrix form.

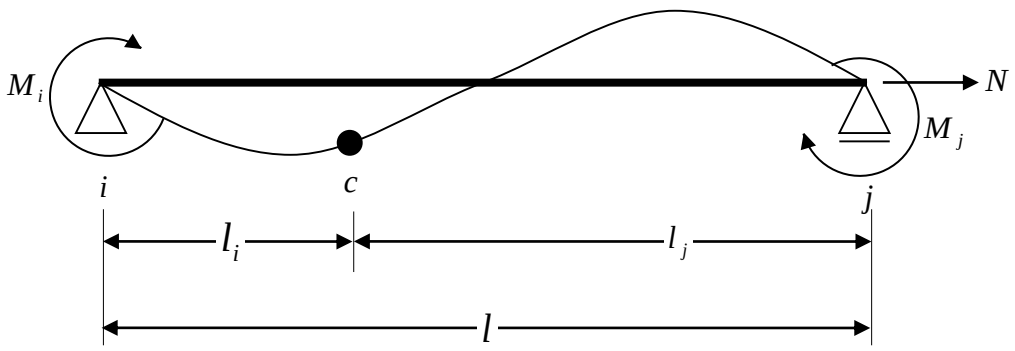

Figure 5.9: Element length, and length between contact node and both edges

$$\begin{bmatrix} U_i \\ V_i \\ Z_i \\ U_j \\ V_j \\ Z_j \\ U_c \\ V_c \end{bmatrix} = \begin{bmatrix} -\alpha & -\frac{\beta}{l} & -\frac{\beta}{l} & \frac{\beta}{l}l_j \\ -\beta & \frac{\alpha}{l} & \frac{\alpha}{l} & -\frac{\alpha}{l}l_j \\ 0 & 1 & 0 & 0 \\ \alpha & \frac{\beta}{l} & \frac{\beta}{l} & \frac{\beta}{l}l_i \\ \beta & -\frac{\alpha}{l} & -\frac{\alpha}{l} & -\frac{\alpha}{l}l_i \\ 0 & 0 & 1 & 0 \\ 0 & 0 & 0 & -\beta \\ 0 & 0 & 0 & \alpha \end{bmatrix} \begin{bmatrix} N \\ M_i \\ M_j \\ Y \end{bmatrix} \qquad 5\text{-}20$$

$$u_{ij} = u_j - u_i \qquad 5\text{-}21 \qquad\qquad v_{ij} = v_j - v_i \qquad 5\text{-}22$$

$$u_{ic} = u_i - u_c \qquad 5\text{-}23 \qquad\qquad v_{ic} = v_i - v_c \qquad 5\text{-}24$$

$$u_{jc} = u_c - u_j \qquad 5\text{-}25 \qquad\qquad v_{jc} = v_c - v_j \qquad 5\text{-}26$$

If the node coordinates are expressed as in Eq. 5-21 to Eq. 5-26, differential for each matrix component in Eq. 5-20 are derived as follows.

$$\delta l = \alpha\delta u_{ij} + \beta\delta v_{ij} \qquad 5\text{-}27$$

$$\delta\alpha = \frac{1}{l}\left(\beta^2\delta u_{ij} + \alpha\beta\delta v_{ij}\right) \qquad 5\text{-}28$$

$$\delta\beta = \frac{1}{l}\left(-\alpha\beta\delta u_{ij} + \alpha^2\delta v_{ij}\right) \qquad 5\text{-}29$$

$$\delta\left(\frac{\alpha}{l}\right) = \frac{1}{l^2}\left((\beta^2 - \alpha^2)\delta u_{ij} - 2\alpha\beta\delta v_{ij}\right) \qquad 5\text{-}30$$

$$\delta\left(\frac{\beta}{l}\right) = \frac{1}{l^2}\left(-2\alpha\beta\delta u_{ij} - (\beta^2 - \alpha^2)\delta v_{ij}\right) \qquad 5\text{-}31$$

$$\delta\left(\frac{\alpha}{l}l_i\right)=\frac{1}{l^2}[\delta u_i \quad \delta v_i \quad \delta u_j \quad \delta v_j \quad \delta u_c \quad \delta v_c]\begin{bmatrix}\alpha\alpha_{ci}l_{ci}-\alpha^2 l_j-(\beta^2-\alpha^2)l_i\\ \alpha\beta_{ci}l_{ci}-\alpha\beta l_j+2\alpha\beta l_i\\ \alpha\alpha_{jc}l_{jc}+\alpha^2 l_j+(\beta^2-\alpha^2)l_i\\ \alpha\beta_{jc}l_{jc}+\alpha\beta l_j-2\alpha\beta l_i\\ -\alpha\alpha_{jc}l_{jc}-\alpha\alpha_{ci}l_{ci}\\ -\alpha\beta_{jc}l_{jc}-\alpha\beta_{ci}l_{ci}\end{bmatrix} \qquad 5\text{-}32$$

$$\delta\left(\frac{\beta}{l}l_i\right)=\frac{1}{l^2}[\delta u_i \quad \delta v_i \quad \delta u_j \quad \delta v_j \quad \delta u_c \quad \delta v_c]\begin{bmatrix}-\alpha\beta l_j+\alpha_{ci}\beta l_{ci}+2\alpha\beta l_i\\ -\beta^2 l_j+\beta\beta_{ci}l_{ci}+(\beta^2-\alpha^2)l_i\\ \alpha\beta l_j+\alpha_{jc}\beta l_{jc}-2\alpha\beta l_i\\ \beta^2 l_j+\beta\beta_{jc}l_{jc}-(\beta^2-\alpha^2)l_i\\ -\alpha_{ci}\beta l_{ci}-\alpha_{jc}\beta l_{jc}\\ -\beta\beta_{ci}l_{ci}-\beta\beta_{jc}l_{jc}\end{bmatrix} \qquad 5\text{-}33$$

$$\delta\left(\frac{\alpha}{l}l_j\right)=\frac{1}{l^2}[\delta u_i \quad \delta v_i \quad \delta u_j \quad \delta v_j \quad \delta u_c \quad \delta v_c]\begin{bmatrix}-\alpha^2 l_i-\alpha\alpha_{ci}l_{ci}-(\beta^2-\alpha^2)l_j\\ -\alpha\beta l_i-\alpha\beta_{ci}l_{ci}+2\alpha\beta l_j\\ \alpha^2 l_i-\alpha\alpha_{jc}l_{jc}+(\beta^2-\alpha^2)l_j\\ \alpha\beta l_i-\alpha\beta_{jc}l_{jc}-2\alpha\beta l_i\\ \alpha\alpha_{ci}l_{ci}+\alpha\alpha_{jc}l_{jc}\\ \alpha\beta_{ci}l_{ci}+\alpha\beta_{jc}l_{jc}\end{bmatrix} \qquad 5\text{-}34$$

$$\delta\left(\frac{\beta}{l}l_j\right)=\frac{1}{l^2}[\delta u_i \quad \delta v_i \quad \delta u_j \quad \delta v_j \quad \delta u_c \quad \delta v_c]\begin{bmatrix}-\alpha\beta l_i+\alpha_{ci}\beta l_{ci}+2\alpha\beta l_j\\ -\beta^2 l_i+\beta\beta_{ci}l_{ci}+(\beta^2-\alpha^2)l_j\\ \alpha\beta l_i+\alpha_{jc}\beta l_{jc}-2\alpha\beta l_j\\ \beta^2 l_i+\beta\beta_{jc}l_{jc}-(\beta^2-\alpha^2)l_j\\ \alpha_{ci}\beta l_{ci}+\alpha_{jc}\beta l_{jc}\\ \beta\beta_{ci}l_{ci}+\beta\beta_{jc}l_{jc}\end{bmatrix} \qquad 5\text{-}35$$

The tangent geometric stiffness for contact element $\mathbf{K_{GC}}$ is obtained in the similar way as for the plane frame structure, which is done by differentiating equilibrium equation. Also in this case, element force is considered to be constant; the expression of tangent geometric stiffness is as follows.

$$\mathbf{k}_{\mathbf{G}_C}=\begin{bmatrix}k_{G11} & k_{G12} & 0 & k_{G14} & k_{G15} & 0 & k_{G17} & k_{G18} & 0\\ & k_{G22} & 0 & k_{G24} & k_{G25} & 0 & k_{G27} & k_{G28} & 0\\ & & 0 & 0 & 0 & 0 & 0 & 0 & 0\\ & & & k_{G44} & k_{G45} & 0 & k_{G47} & k_{G48} & 0\\ & & & & k_{G55} & 0 & k_{G57} & k_{G58} & 0\\ & & & & & 0 & 0 & 0 & 0\\ & \textit{Symmetry} & & & & & 0 & 0 & 0\\ & & & & & & & 0 & 0\\ & & & & & & & & 0\end{bmatrix} \qquad 5\text{-}36$$

$$Q_i=Y\frac{l_j}{l}-\frac{M_i+M_j}{l} \qquad 5\text{-}37$$

$$Q_j = Y\frac{l_i}{l} - \frac{M_i + M_j}{l} \qquad 5\text{-}38$$

$$\mathbf{K}_{\mathbf{G_c}} = \begin{bmatrix} \mathbf{k}_{\mathbf{G}_C} & -\mathbf{k}_{\mathbf{G}_C} \\ -\mathbf{k}_{\mathbf{G}_C} & \mathbf{k}_{\mathbf{G}_C} \end{bmatrix} \qquad 5\text{-}39$$

$$k_{G11} = \beta^2\frac{N}{l} - 2\alpha\beta\frac{M_i + M_j}{l^2} - \left(\alpha\beta l_i + \alpha_{ci}\beta l_{ci} - 2\alpha\beta l_j\right)\frac{Y}{l^2} \qquad 5\text{-}40$$

$$k_{G12} = \alpha\beta\frac{N}{l} + \left(\alpha^2 - \beta^2\right)\frac{M_i + M_j}{l^2} - \left\{\beta^2 l_i + \beta\beta_{ci} l_{ci} - \left(\beta^2 - \alpha^2\right) l_j\right\}\frac{Y}{l^2} \qquad 5\text{-}41$$

$$k_{G14} = -\beta^2\frac{N}{l} + 2\alpha\beta\frac{M_i + M_j}{l^2} + \left(\alpha\beta l_i - \alpha_{jc}\beta l_{jc} - 2\alpha\beta l_j\right)\frac{Y}{l^2} \qquad 5\text{-}42$$

$$k_{G15} = \alpha\beta\frac{N}{l} - \left(\alpha^2 - \beta^2\right)\frac{M_i + M_j}{l^2} + \left\{\beta^2 l_i + \beta\beta_{jc} l_{jc} - \left(\beta^2 - \alpha^2\right) l_j\right\}\frac{Y}{l^2} \qquad 5\text{-}43$$

$$k_{G17} = \left(\alpha_{ci}\beta l_{ci} - \alpha_{jc}\beta l_{jc}\right)\frac{Y}{l^2} \qquad 5\text{-}44$$

$$k_{G18} = \left(\beta\beta_{ci} l_{ci} - \beta\beta_{jc} l_{jc}\right)\frac{Y}{l^2} \qquad 5\text{-}45$$

$$k_{G22} = \alpha^2\frac{N}{l} + 2\alpha\beta\frac{M_i + M_j}{l^2} + \left\{\alpha\beta\left(l_i - 2l_j\right) + \alpha\beta_{ci} l_{ci}\right\}\frac{Y}{l^2} \qquad 5\text{-}46$$

$$k_{G24} = \alpha\beta\frac{N}{l} - \left(\alpha^2 - \beta^2\right)\frac{M_i + M_j}{l^2} + \left\{\alpha^2\left(l_j - l_i\right) - \beta^2 l_j + \alpha\alpha_{jc} l_{jc}\right\}\frac{Y}{l^2} \qquad 5\text{-}47$$

$$k_{G25} = -\alpha^2\frac{N}{l} - 2\alpha\beta\frac{M_i + M_j}{l^2} + \left\{\alpha\beta\left(2l_j - l_i\right) + \alpha\beta_{jc} l_{jc}\right\}\frac{Y}{l^2} \qquad 5\text{-}48$$

$$k_{G27} = \alpha^2\frac{Y}{l^2} \qquad 5\text{-}49$$

$$k_{G28} = \alpha\beta\frac{Y}{l^2} \qquad 5\text{-}50$$

$$k_{G44} = \beta^2\frac{N}{l} - 2\alpha\beta\frac{M_i + M_j}{l^2} + \left\{\alpha\beta\left(l_j - 2l_i\right) + \alpha_{jc}\beta l_{jc}\right\}\frac{Y}{l^2} \qquad 5\text{-}51$$

$$k_{G45} = \alpha\beta\frac{N}{l} - \left(\alpha^2 - \beta^2\right)\frac{M_i + M_j}{l^2} + \left\{\alpha^2 l_i - \beta^2\left(l_j - l_i\right) + \beta\beta_{jc} l_{jc}\right\}\frac{Y}{l^2} \qquad 5\text{-}52$$

$$k_{G47} = \alpha\beta\frac{Y}{l^2} \qquad 5\text{-}53$$

$$k_{G48} = \beta^2\frac{Y}{l^2} \qquad 5\text{-}54$$

$$k_{G55} = \alpha^2 \frac{N}{l} - 2\alpha\beta \frac{M_i + M_j}{l^2} + \{\alpha\beta(2l_i - l_j) - \alpha\beta_{jc} l_{jc}\} \frac{Y}{l^2} \qquad 5\text{-}55$$

$$k_{G57} = -\alpha^2 \frac{Y}{l^2} \qquad 5\text{-}56$$

$$k_{G58} = -\alpha\beta \frac{Y}{l^2} \qquad 5\text{-}57$$

The matrix element for the element geometric stiffness is shown in Eq. 5-40 to Eq. 5-57. Referring to Eq. 5-36, geometric stiffness matrix for one contact element which consists of three nodes is a 9×9 matrix. The rotation component for the contact node is neglected and has no influence to the calculations. By adapting the contact node's degree of freedom into the geometric stiffness matrix, zero values had to be added to the rotation component.

5.5 Definition of contact element behavior for contact problem

In this subsection, the application of principle of super position for interposing contact phenomena will be performed. The concept of this interposing process for plane frame beam element loaded with end moments is shown in Fig. 5.10.

EI = Bending stiffness

EA = Extensional stiffness

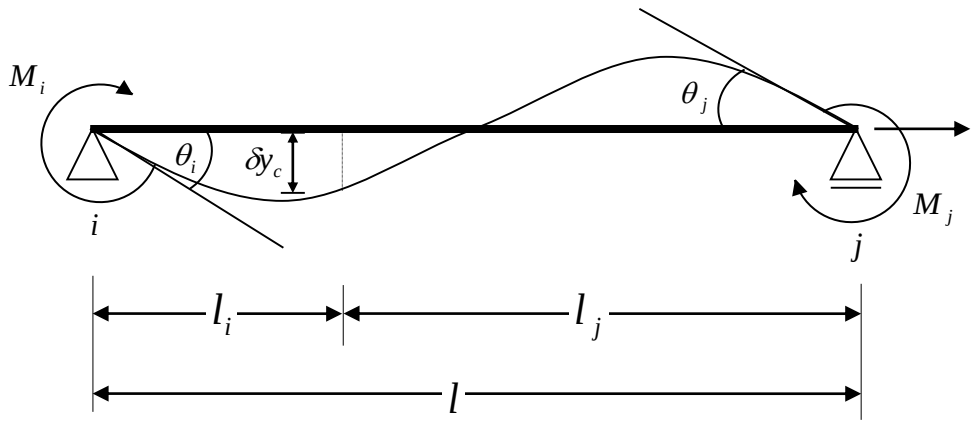

Figure 5.10: Deformation of the plane frame beam

$x \to l$

$$\delta y_c = \frac{1}{\mathrm{EI}} \left(\frac{M_i + M_j}{6l} x^3 - \frac{M_i}{2} x^2 + \frac{(2M_i - M_j)l}{6} x \right) \qquad 5\text{-}58$$

$$\theta_i = \frac{2M_i - M_j}{6\mathrm{EI}} l \qquad 5\text{-}59$$

$$\theta_i = \frac{2M_j - M_i}{6\mathrm{EI}} l \qquad 5\text{-}60$$

The deflection amount when $x=l_i$ is calculated by equation Eq. 5-58, and deflection angles for both ends are shown in equations Eq. 5-59 and Eq. 5-60.

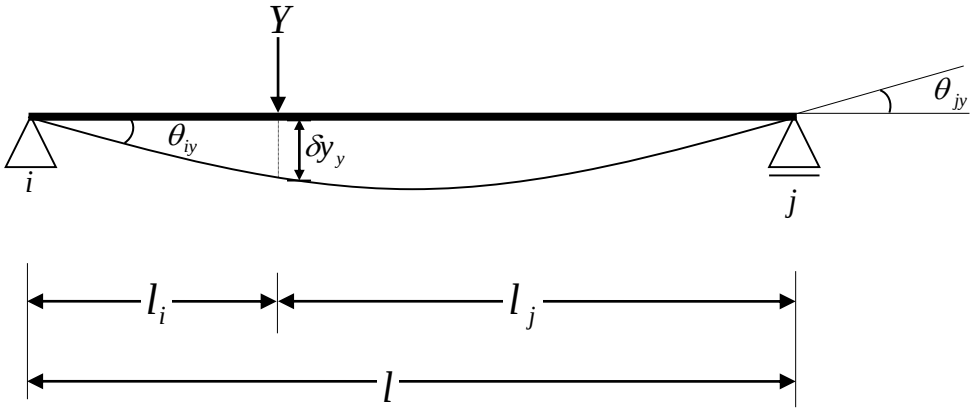

Figure 5.11: Deformation of the plane frame beam by the contact force

$$\delta y_y = \frac{{l_i}^2 {l_j}^2}{3\mathrm{EI}l} Y \qquad 5\text{-}61$$

$$\theta_{iy} = \frac{l_i l_j}{6\mathrm{EI}} \left(1 + \frac{l_j}{l}\right) Y \qquad 5\text{-}62$$

$$\theta_{jy} = -\frac{l_i l_j}{6\mathrm{EI}} \left(1 + \frac{l_i}{l}\right) Y \qquad 5\text{-}63$$

Case B is shown in Fig. 5.11, the deflection value after external force Y applied at the same distance ($x=l_i$), is shown in equation Eq. 5-61. Deflection angles for both ends for this case are calculated by equations Eq. 5-62 and Eq. 5-63.

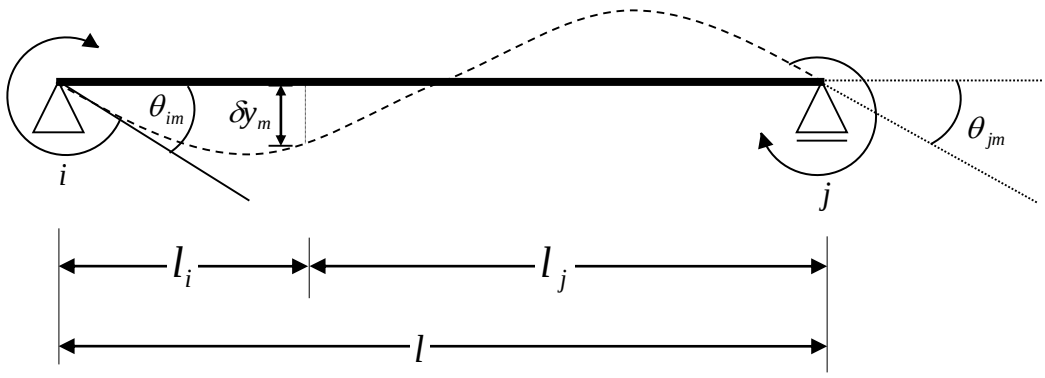

Figure 5.12: Beam deformation combined by the principle of super position

If the deflection value for both cases A and B are the same, according to principle of superposition, the total displacement value when $x=l_i$ and deflection angles for both

ends can be expressed as in Eq. 5-64, Eq. 5-65 and Eq. 5-66.

$$\delta y_m = \frac{l_i l_j}{6\mathrm{EI}}\left(1+\frac{l_j}{l}\right)M_i - \frac{l_i l_j}{6\mathrm{EI}}\left(1+\frac{l_i}{l}\right)M_j \qquad 5\text{-}64$$

$$\theta_{im} = \frac{l}{3\mathrm{EI}}M_i - \frac{l}{3\mathrm{EI}}M_j \qquad 5\text{-}65$$

$$\theta_{jm} = -\frac{l}{3\mathrm{EI}}M_i + \frac{l}{3\mathrm{EI}}M_j \qquad 5\text{-}66$$

Here, as shown in Fig 5.13, if horizontal force works on the contact node, equations Eq.5-58 to Eq. 5-66 and equations Eq. 5-67 to Eq. 5-69 can be expressed in the matrix form (see Eq. 5-70.).

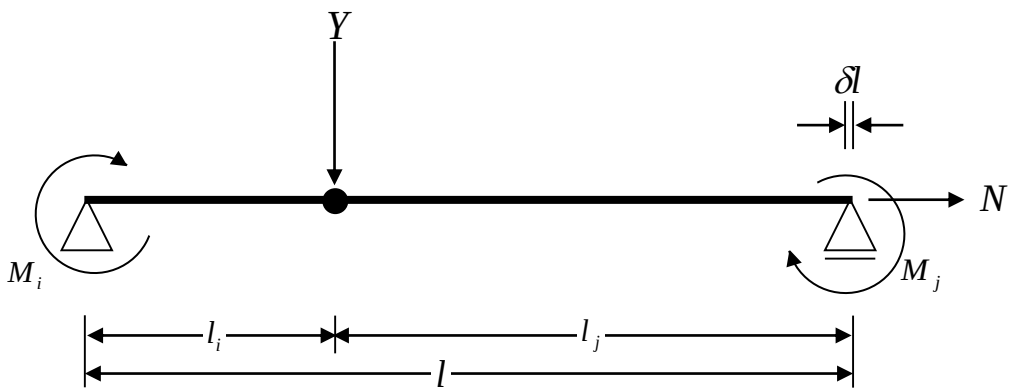

Figure 5.13: Forces working on a contacted plane frame beam

$$\delta y = \delta y_y + \delta y_m \qquad 5\text{-}67$$

$$\theta_i = \theta_{iy} + \theta_{im} \qquad 5\text{-}68$$

$$\theta_j = \theta_{jy} + \theta_{jm} \qquad 5\text{-}69$$

$$\begin{bmatrix}\delta l\\ \theta_i\\ \theta_j\\ \delta y\end{bmatrix} = \begin{bmatrix}\frac{l}{\mathrm{EA}} & 0 & 0 & 0\\ 0 & \frac{l}{3\mathrm{EI}} & -\frac{l}{6\mathrm{EI}} & \frac{l_i l_j}{6\mathrm{EI}}\left(1+\frac{l_j}{l}\right)\\ 0 & -\frac{l}{6\mathrm{EI}} & \frac{l}{3\mathrm{EI}} & -\frac{l_i l_j}{6\mathrm{EI}}\left(1+\frac{l_j}{l}\right)\\ 0 & \frac{l_i l_j}{6\mathrm{EI}}\left(1+\frac{l_j}{l}\right) & -\frac{l_i l_j}{6\mathrm{EI}}\left(1+\frac{l_i}{l}\right) & \frac{{l_i}^2{l_j}^2}{3\mathrm{EI}l}\end{bmatrix}\begin{bmatrix}N\\ M_i\\ M_j\\ Y\end{bmatrix} \qquad 5\text{-}70$$

$$\begin{bmatrix}N\\ M_i\\ M_j\\ Y\end{bmatrix} = \begin{bmatrix}\frac{\mathrm{EA}}{l} & 0 & 0 & 0\\ 0 & \frac{4l_{ic}+3l_{jc}}{l_{ic}}k_a & \frac{9{l_0}^2-{l_{ic}}^2{l_{jc}}^2}{{l_{ic}}^2{l_{jc}}^2}k_a & -\frac{3l_{jc}{l_0}^2}{{l_{ic}}^2{l_{jc}}^2}k_a\\ 0 & \frac{9{l_0}^2-{l_{ic}}^2{l_{jc}}^2}{{l_{ic}}^2{l_{jc}}^2}k_a & \frac{4l_{jc}+3l_{ic}}{l_{jc}}k_a & \frac{3l_{ic}{l_0}^2}{{l_{ic}}^2{l_{jc}}^2}k_a\\ 0 & -\frac{3l_{jc}{l_0}^2}{{l_{ic}}^2{l_{jc}}^2}k_a & \frac{3l_{ic}{l_0}^2}{{l_{ic}}^2{l_{jc}}^2}k_a & \frac{3{l_0}^4}{{l_{ic}}^3{l_{jc}}^3}k_a\end{bmatrix}\begin{bmatrix}\delta l\\ \theta_i\\ \theta_j\\ \delta y\end{bmatrix} \qquad 5\text{-}71$$

$$k_a = \frac{\mathrm{EI}}{l_0} \qquad 5\text{-}72$$

Eq. 5-71 and Eq. 5-72 are the element force equations for a contact element using Euler–Bernoulli beam in a simply supported beam coordinate. The equation shown in Eq. 5-71 consists by axial force N, edge moments M_i and M_j, and contact force Y. Using this beam coordinate, it is assumed that the contact force, Y is within the range of the beam (Fig. 5.13), and creates geometric and kinematic variables as expressed in details in Eq. 5-67 to Eq. 5-69. The expression of a contact element using this beam coordinate is an idealization of the simplest yet accurate frictionless node–element contact.

5.6 The application of Timoshenko beam in node–element contact analysis

The Timoshenko beam was initially idealized to handle shear deformation and rotational inertia for short beam. Here, the theory describes that when the ratio of beam depth to the beam length (span) becomes higher, the shear deformation coefficient q_s, as shown in Eq. 5-73 could not be neglected. Based on the beam theory, in a node–element contact, when the contact node approaches the element edge, the effective distance between the contact node and the edge would decrease. Therefore, by applying the short beam theory for node–element contact case, the aim is to achieve convergence solution when the contact node approaches the element edges.

$$q_s = \frac{12\mathrm{EI}}{GA_e l^2} \qquad 5\text{-}73$$

Due to the sliding of the contact point toward element edges, when the distance between the contact node to the element edges either ic or jc section, the unbalanced force is not able to be converged when considering the element force equation by Euler–Bernoulli theory as shown in Eq. 5-71. The sliding of the contact node towards the element edge may reduce the l_{ic} or l_{jc} in Eq. 5-71 to zero which leads to the “division by zero” of the element force equation matrices. Therefore, it is difficult to achieve equilibrium when the contact node approaches the element edge owing to the non-convergence of the unbalanced force. As the contact node approaches the element edge and the distance decreases, the author describes the section where the unbalanced force is hardly to be converged as the “critical area”. The “critical area” has been an obstacle to perform “passing through” or “sliding through” of the contact node to the next non-contact element.

Here, the derivation of Timoshenko beam for node–element contact will be done. Firstly, the fundamental assumption of the Euler–Bernoulli and the Timoshenko beam is the plane cross section remains plane throughout the beam deformation. In Timoshenko beam, the cross section rotates due to the effect of shear deformation and no longer normal to the neutral axis. Furthermore, it is also assumed that the beam deformation is produced by two components, namely the bending and shear deformations. Here, the author will relate these two components to derive the element force equation for node–element contact based on Timoshenko beam.

5.7 The arbitrary point load on a simply supported beam

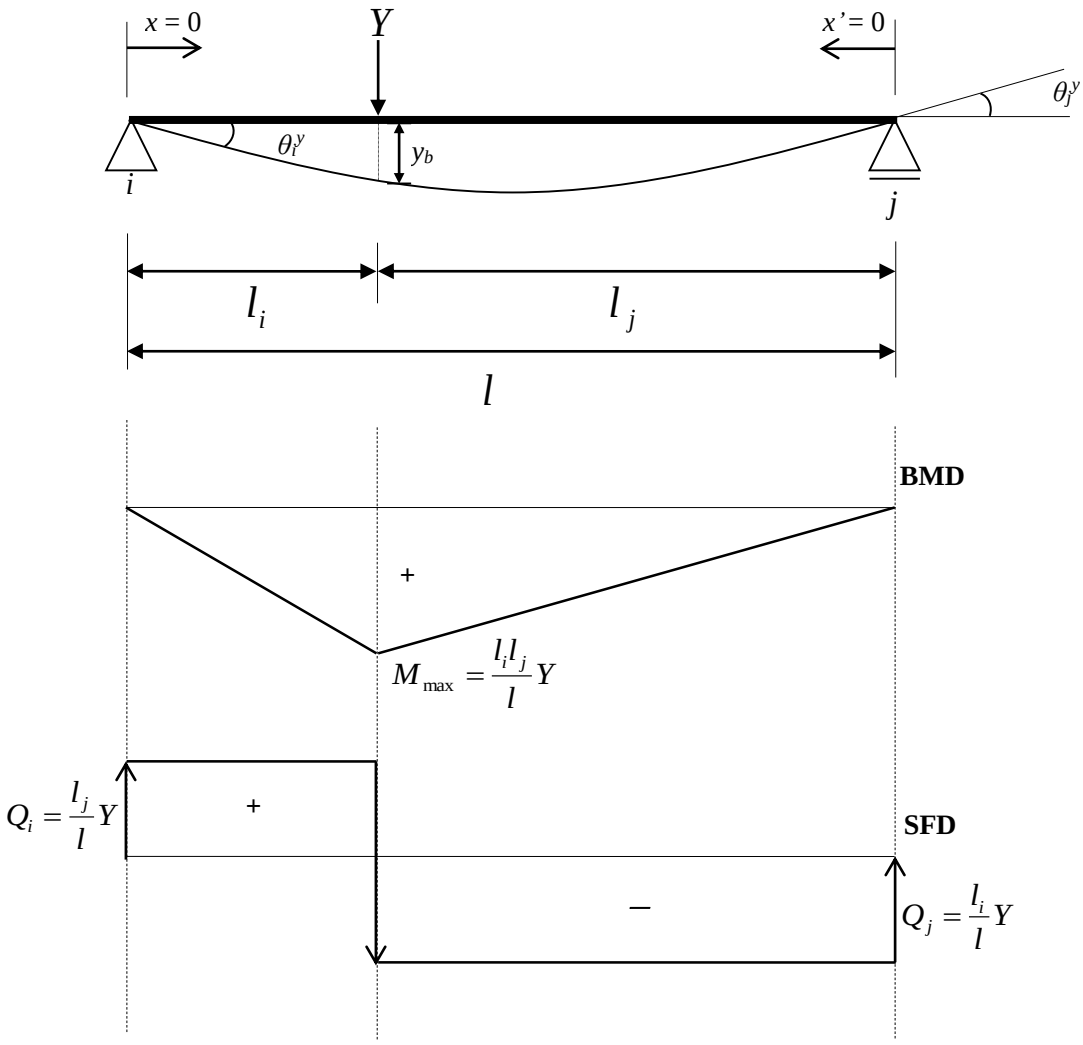

Figure 5.14: The BMD and SFD of a simply supported beam

According to the shear force diagram (SFD) in Fig. 5.14, the deformation caused by

shear effect when the flexural load (contact force, Y) is subjected creates a discontinuity of the shear distribution and should be handled separately into l_i and l_j sections. In addition, the point where the flexural load is subjected could be also considered as the position of the contact node. Here, considering the l_i section from the range x=0 to x=l_i, the shear force could be represented as;

$$Q_i = Y\frac{l_j}{l} = \mathrm{G}A_e\gamma_i \qquad 5\text{-}74$$

Here, the relation between the shear strain and the contact force could be shown is shown in Eq. 5-75.

$$\gamma_i = \frac{l_j}{\mathrm{G}A_e l}Y \qquad 5\text{-}75$$

Furthermore, the deflection due to contact force in Fig. 5.13 when x=l_i or x'=l_j could also be defined as Eq. 5-76,

$$y = \frac{l_i l_j}{\mathrm{G}A_e l}Y \qquad 5\text{-}76$$

Here, when considering the plane frame beam, the relation between the shear Q and edge moments M_i and M_j for Timoshenko case could be shown as;

$$Q = -\frac{M_i + M_j}{l} = \mathrm{G}A_e\gamma \qquad 5\text{-}77$$

By super positioning Eq. 5-75 to Eq. 5-77 according to the derivation made in Eq. 5-70, the bending and shear deformation component could be shown in Eq. 5-78. Eq. 5-78 shows the super positioning result for node–element contact when shear deformation is taken into account. As shown in the equation, if the shear deformation component in the matrices is neglected, the equation is similar to the Euler–Bernoulli case, in the previous section. Here, by inversing the matrix equation (Eq. 5-78), the element force equation for node–element contact by Timoshenko beam theory could be shown in Eq. 5-79 to Eq. 5-82.

$$\begin{bmatrix}\delta l\\ \theta_i\\ \theta_j\\ \delta y\end{bmatrix} = \begin{bmatrix}\frac{l}{\mathrm{EA}} & 0 & 0 & 0\\ 0 & \frac{l}{3\mathrm{EI}}+\frac{1}{\mathrm{G}A_e l} & -\frac{l}{6\mathrm{EI}}+\frac{1}{\mathrm{G}A_e l} & \frac{l_i l_j}{6\mathrm{EI}}\left(1+\frac{l_j}{l}\right)\\ 0 & -\frac{l}{6\mathrm{EI}}+\frac{1}{\mathrm{G}A_e l} & \frac{l}{3\mathrm{EI}}+\frac{1}{\mathrm{G}A_e l} & -\frac{l_i l_j}{6\mathrm{EI}}\left(1+\frac{l_i}{l}\right)\\ 0 & \frac{l_i l_j}{6\mathrm{EI}}\left(1+\frac{l_j}{l}\right) & -\frac{l_i l_j}{6\mathrm{EI}}\left(1+\frac{l_i}{l}\right) & \frac{{l_i}^2{l_j}^2}{3\mathrm{EI}l}+\frac{l_i l_j}{\mathrm{G}A_e l}\end{bmatrix}\begin{bmatrix}N\\ M_i\\ M_j\\ Y\end{bmatrix} \qquad 5\text{-}78$$

$$\begin{bmatrix} N \\ M_i \\ M_j \\ Y \end{bmatrix} = \begin{bmatrix} \frac{\mathrm{EA}}{l_0} & 0 & 0 & 0 \\ 0 & \left(4\Omega + 3l_{ic}{l_{cj}}^3 - 108\Psi^2\right)k_b & \left\{9\left({l_0}^2 - l_{cj}\Psi\right) - \Omega\right\}k_b & -3l_0\left(l_0 l_{cj} + 6\Psi\right)k_b \\ 0 & \left\{9\left({l_0}^2 - l_{cj}\Psi\right) - \Omega\right\}k_b & \left(4\Omega + 3{l_{ic}}^3 l_{cj} - 108\Psi^2\right)k_b & 3l_0(l_0 l_{ic} + 6\Psi)k_b \\ 0 & -3l_0\left(l_0 l_{cj} + 6\Psi\right)k_b & 3l_0(l_0 l_{ic} + 6\Psi)k_b & \frac{3l_0\left({l_0}^3 + 12 l_0\Psi\right)}{l_{ic} l_{cj}}k_b \end{bmatrix} \begin{bmatrix} \delta l \\ \theta_i \\ \theta_j \\ \delta y \end{bmatrix} \qquad 5\text{-}79$$

Where;

$$k_b = \frac{\mathrm{EI}}{l_0\Omega} \qquad 5\text{-}80$$

$$\Psi = \frac{\mathrm{EI}}{\mathrm{GA}_e} \qquad 5\text{-}81$$

$$\Omega = \left(l_{ic} l_{cj}\right)^2 + 3\Psi\left({l_0}^2 + l_{ic} l_{cj}\right) + 36\Psi^2 \qquad 5\text{-}82$$

In this case, k_b (Eq. 5-80) is the bending stiffness for Timoshenko beam. Ψ in Eq. 5-81 is the shear deformation coefficient while A_e is the effective cross sectional area. For the geometrical parameters, l_0 is the non-stressed beam length, l_{ic} is the distance between the contact node and i edge, and l_{cj} is the distance between the contact node and the j edge.

In this section, the element force equation of node–element contact for the Timoshenko beam is expressed as shown in Eq. 5-79 to Eq. 5-82. These equations are developed to overcome the "division by zero" discussed in section **5.4** and **5.5**, to encounter the problem when the contact node approaches element edge into the "critical area" and leads to the divergence of unbalanced force. Furthermore, owing to the reduction of "critical area" enhanced by these equations, "passing through" could be executed smoothly for the contact node to shift to the next noncontact element with stable convergence result. The effectiveness of these equations is demonstrated in details in each numerical example in the following section.

5.8 Numerical example

5.8.1 Frictionless contact analysis of a cantilever beam

The main objective of this analysis is to investigate the range of the "critical area," by comparing the application of the Timoshenko beam in the element force equation in Eq. 5-79 to Eq. 5-82, to the equations derived in section **5.4** and **5.5** (Eq. 5-71 and Eq. 5-72), and to the previous equations developed by Tsutsui et al. [2]. As shown in Fig. 5.9, the distances between the contact point and the two edges are l_i and l_j, respectively.

In this case, if $l_i \rightarrow 0$ or $l_j \rightarrow 0$ in Eq. 5-71, the matrices become singular. Therefore, if l_i or l_j is close to zero, the unbalanced force would hardly converge. This implies that there is a particular space close to the element edge in which the approach of the contact node is prohibited from achieving convergence result. This is referred as the "critical area".

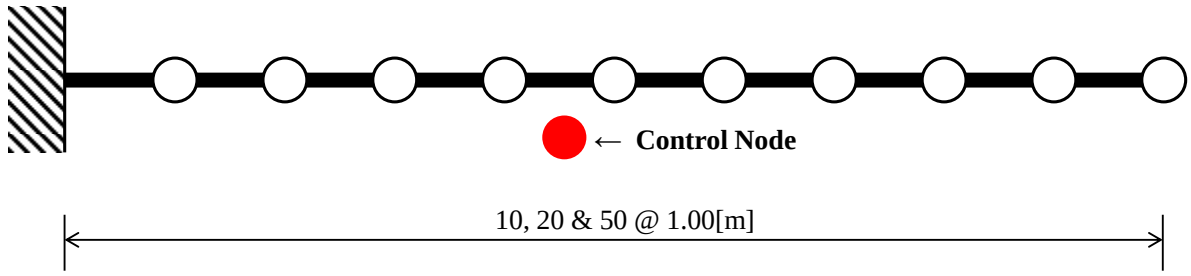

Figure 5.15: Cantilever beam model

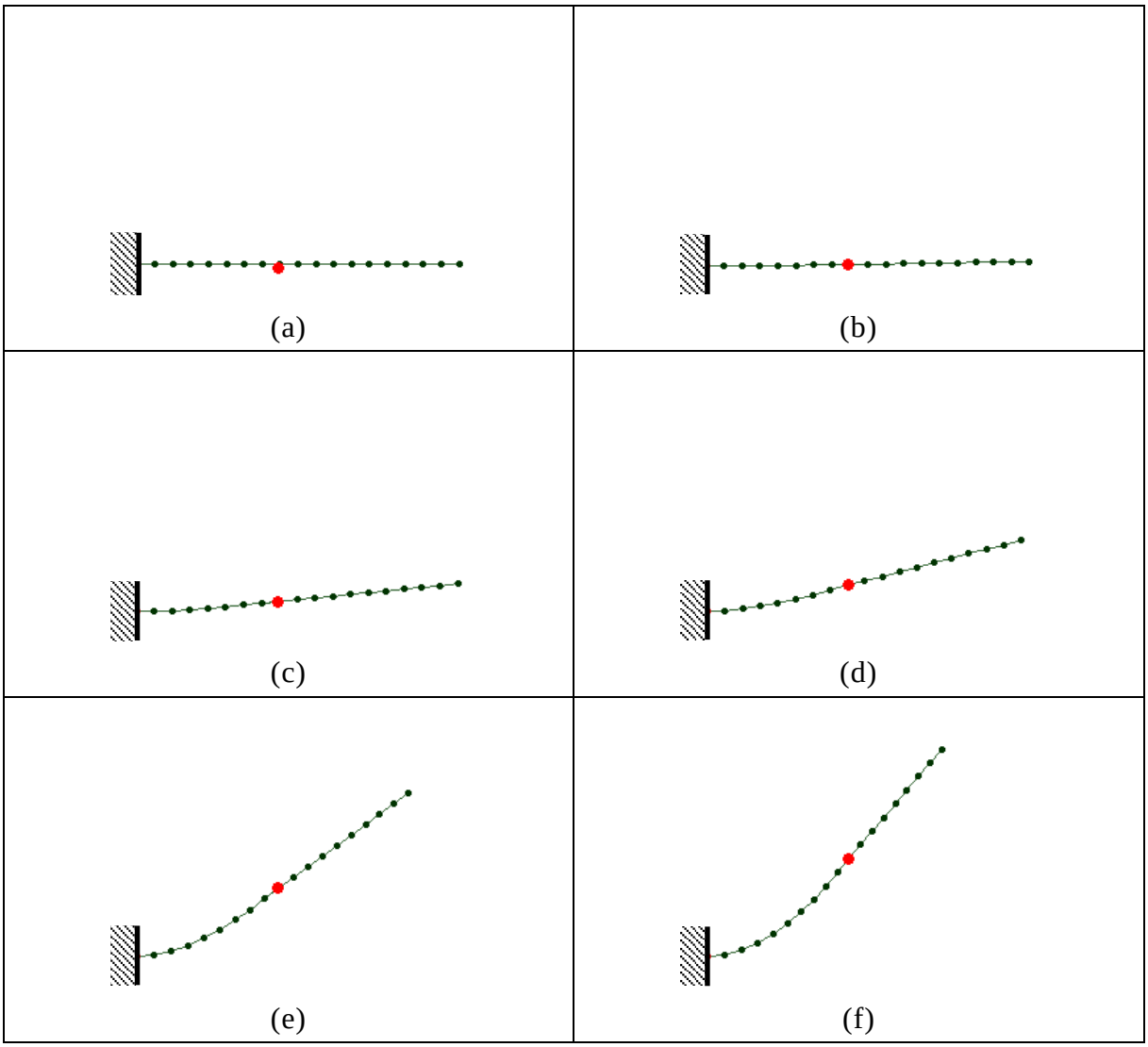

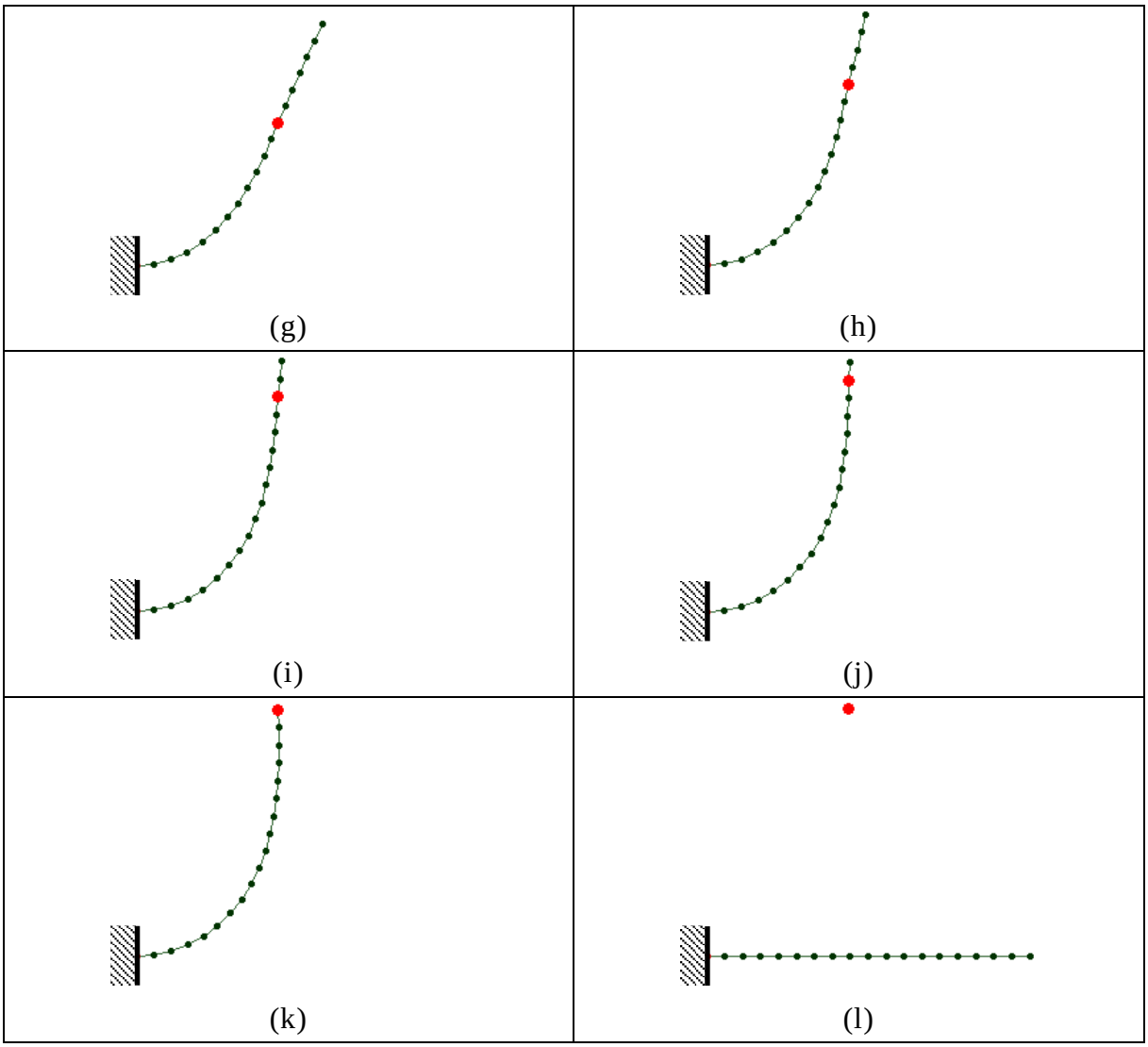

Figure 5.16(a) – (l): Beam deformation diagrams

As shown in Fig. 5.15, a cantilever beam configuration is used in this analysis, and the beam consists of 18 elements and 19 nodes. A compulsory displacement in the lateral upward direction is applied to the control node, which is independent and unconnected to any element in the primary position. The material parameters are $E = 2.1 \times 10^{11}$[N/m^2], $A = 0.005$[m^2], $I = 0.001$[m^4], $G = 7.5 \times 10^{10}$[N/m^2], and $\upsilon = 0.3$.

Fig. 5.16 (a) to (l) represents the beam deformation due to the displacement of the control node and Fig. 5.18 shows the deformation behavior throughout the compulsory displacement, whereas Fig. 5.17 shows the relationship between the ratio l_i/l of a contact element and the displacement of the control node after contact. In this analysis, the control node was set at six primary positions, namely 4.05[m], 4.1[m], 4.2[m], 4.3[m], 4.35[m], and 4.4[m] in the horizontal direction. The results of the analysis showed that the "critical area" of the Euler–Bernoulli beam in Eq. 5-71 and Eq. 5-72 ranged between

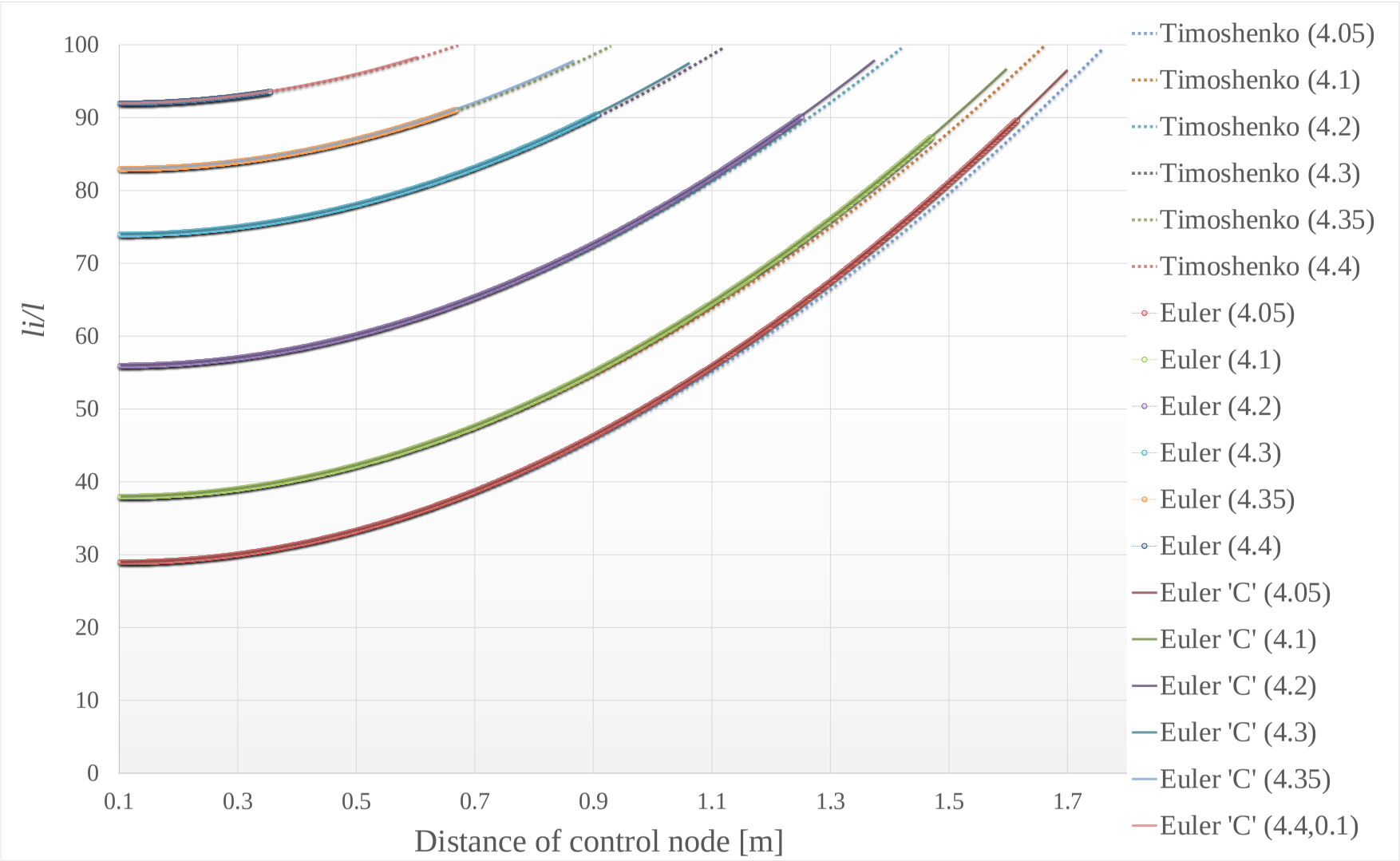

Figure 5.17: Comparison of “critical area” by three different element force equations

7.749% and 12.952%, whereas that of the cantilever coordinate system of Tsutsui et al. [2] ranged between 2.164% and 3.865%. An idealization of the cantilever coordinate system by comparison of the two results can be used to reduce the range of the "critical area". However, using the Timoshenko beam, the "critical area" can be significantly reduced from 0.067% to 0.501%. The reduction of the "critical area" makes it easier for the contact node to smoothly "passing through" the element edge to the next element, producing a strict equilibrium solution.

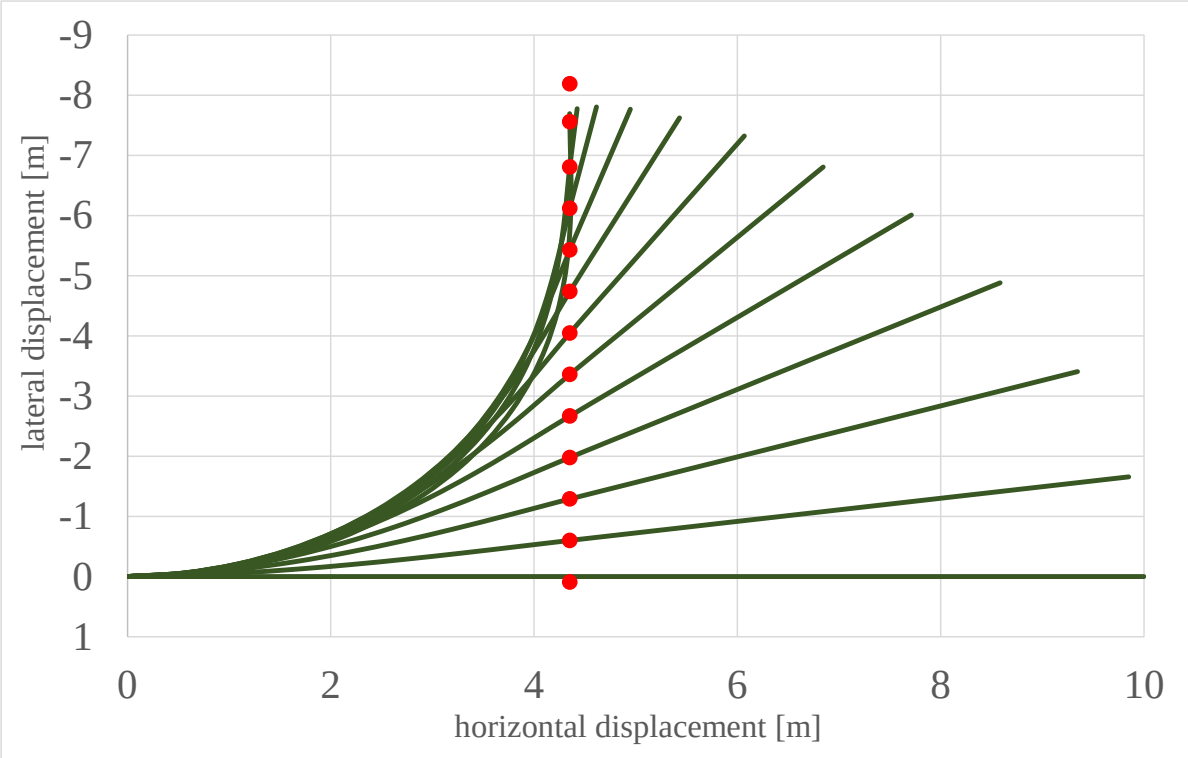

Figure 5.18: Deformation behavior of the cantilever beam

5.8.2 Accuracy comparison of FEM to TSM

In this analysis, a comparison is made between the FEM by Konyukhov and Schweizrhof [4] with the TSM for contact simulation. A cantilever beam with solid elements and 50 divisions was used for the FEM study, whereas simple linear elements were used for TSM. To demonstrate the accuracy of TSM, 10, 20, and 50 divisions of the beam are used in this analysis. The control node is displaced in the upper left direction by the vector [1, 0.6366] as shown in Fig. 5.20, and the material parameters are $E = 2.1 \times 10^4$[N/m^2], $b \times h = 0.02$[m]×0.02[m], $L = 1.00$[m], $G = 7.5 \times 10^{10}$[N/m^2], and $\upsilon = 0.3$. Fig. 5.19 shows the beam deformation for both methods.

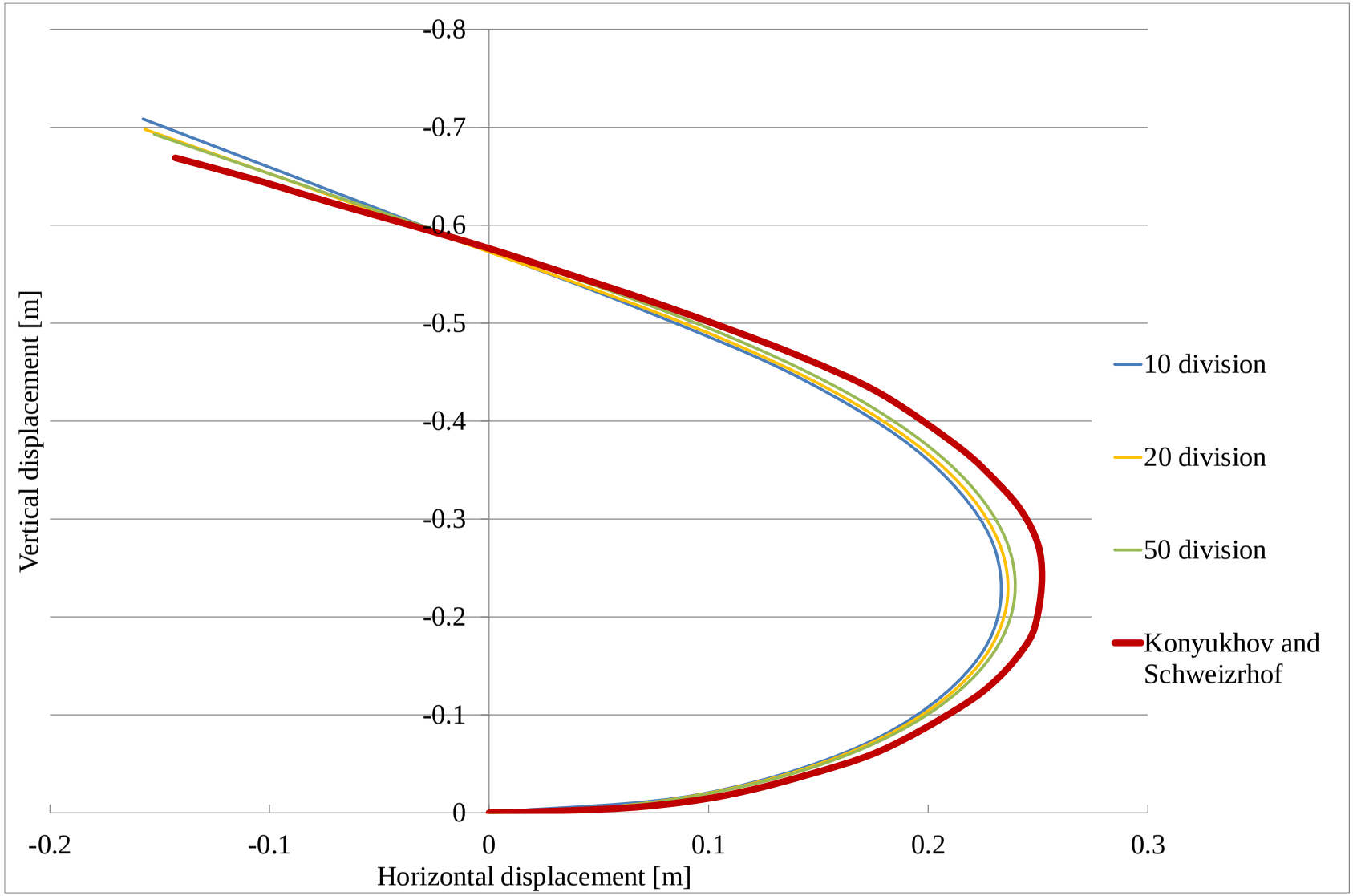

Figure 5.19: The comparison of beam deformation between TSM and FEM

The figure reveals that the beam deformations for TSM and FEM are not significantly different. The TSM solution for the larger 10 and 20 divisions is similar to that of FEM using densely partitioned solid elements. Furthermore, a simple definition of the contact element is sufficient to simulate the TSM contact analysis, while also avoiding the complex settings of the nonlinearity between the strain and the displacement.

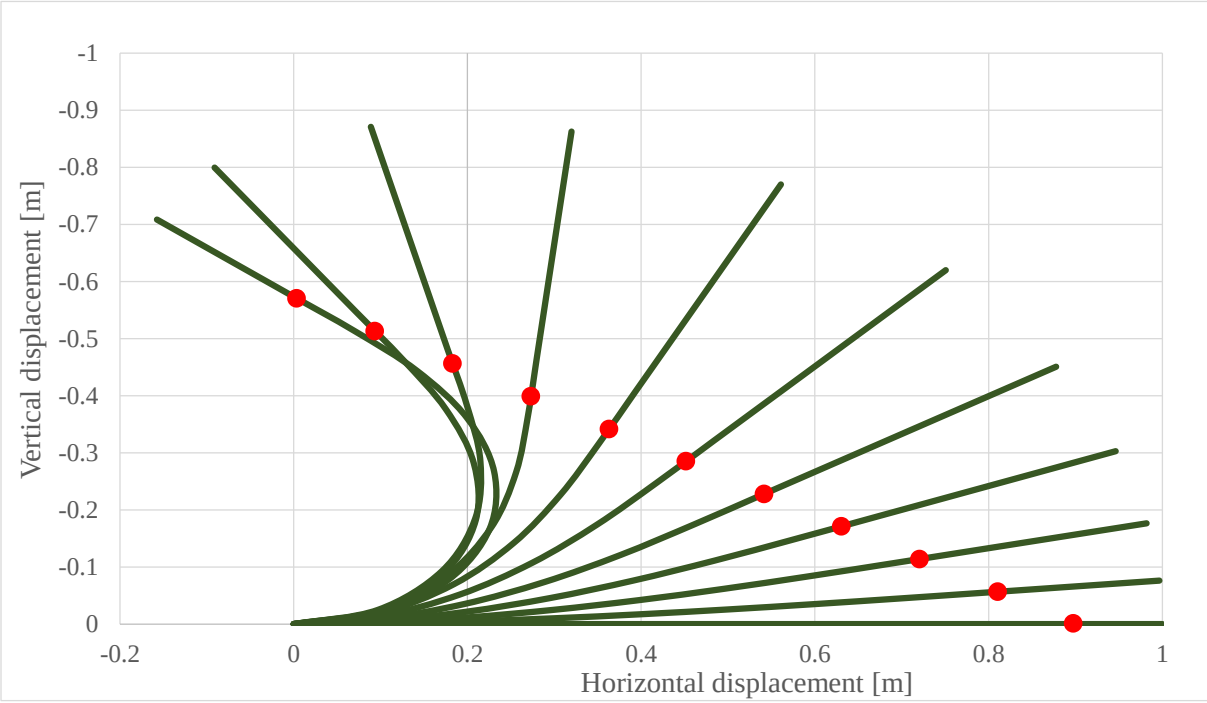

Figure 5.20: Cantilever beam deformation due to contact node compulsory displacement

5.8.3 Contact of two cantilever beams

Two independent cantilever beams are used in this analysis, and the control node is displaced laterally and downward until it exceeds those of the two beams. The objective of this analysis is to perform multiple contacts using the Timoshenko beam, taking into consideration the "critical area", the "passing through" phenomenon, and the deformation behavior of both structures. Both beams have 10 equal divisions, and the material parameters in this case are $E = 2.0 \times 10^{7}$[N/m^2], $A = 3.0 \times 10^{-4}$[m^2], $I = 2.2 \times 10^{-8}$[m^4], $G = 7.142 \times 10^{6}$[N/m^2], and $\upsilon = 0.3$.

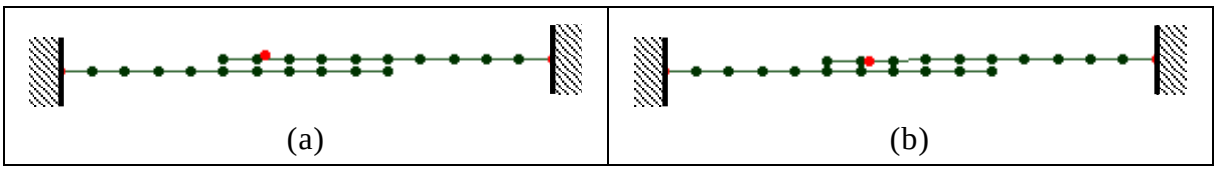

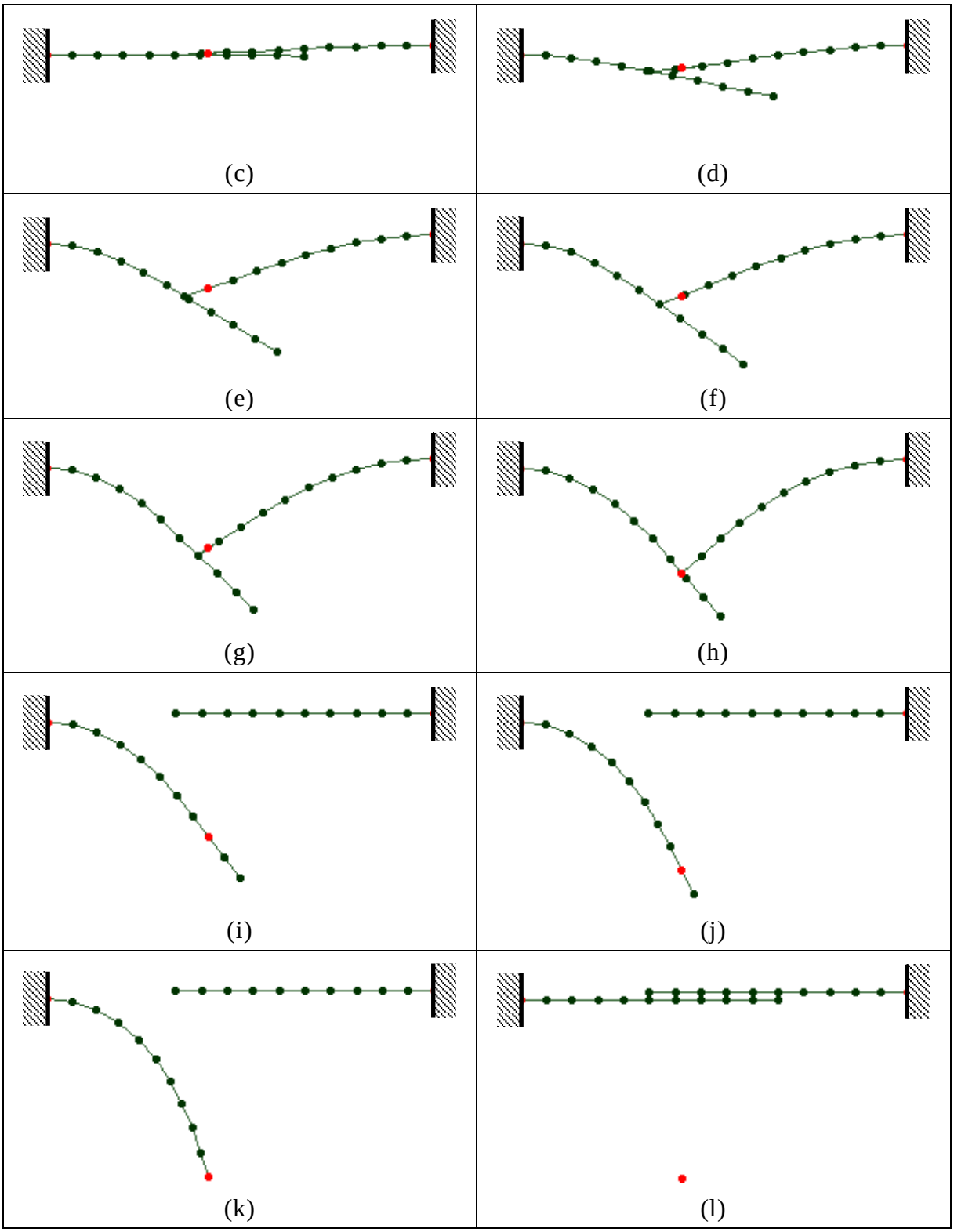

Figure 5.21: Control node displacement quantity and beam deformation diagrams

Contact is about to occur when the displacement of the control node is at stage (a). At stage (c), multiple contacts initially occur between the control node and an element of the upper beam, and between the tip of the upper beam and an element of the lower

beam. The control node is displaced until stage (h), at which time the control node is about to shift from the upper beam and make contact with an element of the lower beam. The analysis is continued until the control node displacement is at stage (k), when the node is about to exceed the lower beam. By applying the Timoshenko beam, the significant reduction of the "critical area" discussed in section **5.6** and **5.7** enables the contact nodes to smoothly and simultaneously "passing through" every element edge.

5.9 Discussion

The contact problem has been known as one of major topics which have difficult nonlinearity to solve. The difficulties that have been prescribed previously were the problem with the calculation stability, discontinuity of element boundary, "finite-sliding" etc. In this study, the author has tried to solve a simple, yet efficient case of contact problem by TSM to encounter all the problems that have been prescribed. Also, the application of TSM for this strong nonlinear analysis has been proven to be efficient when the converged solutions were successfully obtained in all contact analysis and this has been shown throughout this chapter.

In this chapter, two types of contact cases were examined. Firstly, the contact between elements by the axial force elements and followed by node–element contact by the plane frame beams. For the contact between elements, the axial force elements which do not resist to compressional forces were introduced, which simulates the approximation of cables. Here, when the element contacts each other, a contact point where the elements intersect are generated as the "sliding node" which slides on an element without friction by the definition of "isotonic". The occurrence of contact is judged by vector triple product of both edges of each of the elements. Then, the contact force is always monitored, and if the inverse of sign is observed, the sliding node is removed. Using TSM as the theory for geometrically nonlinear analysis, the unbalanced force was successfully converged in very small number of iteration steps.

Also, the case of multiple contact between elements was also considered, where a complex contact phenomena was shown in subsection **5.3.2**. Although with the simultaneous involvement of multiple contact nodes, the calculation was performed smoothly and the unbalanced force was successfully converged in every incremental step.

Furthermore, the simulation of the node–element contact case using the plane frame beam elements was also introduced in this chapter. Here, two types of beam theory were

derived; which are based on Euler–Bernoulli beam theory and Timoshenko beam theory. On applying these elements to the node–element contact, a major problem was that the unbalanced forces were hardly to be converged when the contact node approaches to the element edge. In this study, this area around the element edge is called as the “critical area”.

As the distance between the contact node and the element edge decreases, it shares the similar characteristics to the deep beam elements which are simulated by Timoshenko beam theory. Here, the shear deformation is considered and the components in the element force equation were substituted into ones regarding to Timoshenko beam theory for the contact problem. By the application of the shear deformation into the element force equation, the aim is to eliminate the occurrence of “division by zero” in the stiffness matrix, while producing a stable convergence result throughout the analysis.

As the result for all node–element contact cases, stable convergence results have been successfully achieved at every element edges and “passing through” of the contact node to the next non-contact element was also performed smoothly. Here, by the consideration of the shear deformation, the author has solved the problems regarding the calculation stability, the element discontinuity and “finite-sliding” that have been the obstacles in other studies.

In addition, in subsection **5.8.2**, a comparison of node–element contact between FEM and TSM was executed. In the analysis, the author has compared the behavior of a cantilever beam model with the solution of FEM. Consequently, even if in case of coarse mesh division, the proposed contact element has achieved enough accuracy corresponding to the result by FEM with dense mesh division.

Finally, a multiple contact case of a plane frame beam was introduced in **5.8.3**, to examine the computational stability when the “critical area” and the “passing through” occur simultaneously. All of the results shown in this chapter have proved the superiority of TSM in handling so much complex and strong geometrically nonlinear analysis with contact problem.

References

[1] **M. Murayama, Z. M. Nizam, H. Obiya, K. Ijima, N. Kawasaki,** (2013): Large deformational analysis for net structure with sliding nodes. *Kyushu Association for Bridge and Structural Engineering Symposium*.

[2] **T. Tsutsui, H. Obiya, K. Ijima,** (2009): An algorithm for contact problem with large deformation of plane frame structures. *Advances in Computational Engineering & Science*.

[3] **Z. M. Nizam, H. Obiya,** (2008): A study on non-friction contact problem with large deformational analyses. *Malaysian Technical Universities Conference on Engineering and Technology*.

[4] **A. Konyukhov, K. Schweizerhof,** (2010): Geometrically exact covariant approach for contact between curves. *Computer Methods in Applied Mechanics and Engineering*, vol. 199, pp. 2510–2531.

List of symbols

Symbol		Description
$\mathbf{D}$	:	Nodal force vector
$\boldsymbol{\alpha}$	:	Cosine vector
$\mathbf{S}$	:	Element edge force vector
$\mathbf{K_{GC}}$	:	Tangent stiffness matrix for contact element
U	:	Force component in u-direction
V	:	Force component in v-direction
W	:	Force component in w-direction
α	:	Cosine vector in u-direction
β	:	Cosine vector in v-direction
γ	:	Cosine vector in w-direction
i	:	The i edge of an element
c	:	Contact point of an element
j	:	The j edge of an element
l	:	Element length
u	:	Nodal coordinate in u-direction
v	:	Nodal coordinate in v-direction
w	:	Nodal coordinate in w-direction
N	:	Axial force
M_i	:	Edge moment on i edge
M_j	:	Edge moment on j edge
Y_c	:	Contact force
k_G	:	The matrix element of tangent geometric stiffness matrix
Q	:	Shear force
θi	:	Deflection angle on i edge
θj	:	Deflection angle on j edge
δy_c	:	Deflection at contact point due to axial force and edge moments
l_i	:	Length between i edge to the contact point c
l_j	:	Length between j edge to the contact point c
x	:	Horizontal component in global coordinate system
y	:	Vertical component in global coordinate system
δy_y	:	Deflection at contact point due to contact force
θ_{iy}	:	Deflection angle on i edge due to contact force

List of symbols

Symbol		Description
θ_{jy}	:	Deflection angle on j edge due to contact force
δy_m	:	Deflection at contact point by the principle of superposition
θ_{im}	:	Deflection angle of i edge by the principle of superposition
θ_{jm}	:	Deflection angle of j edge by the principle of superposition
q_s	:	Shear deformation coefficient
γ_i	:	Shear strain
k_b	:	Bending stiffness coefficient by Timoshenko beam theory
A_e	:	Effective cross sectional area

Chapter 6
Conclusion

6.1 The superiority of TSM

In this study, the author has applied tangent stiffness method (TSM) for all of the geometrically nonlinear analyses with extremely large deformational cases. The results obtained in this study are guaranteed to match the "perfect equilibrium" as well as being precise, as the concept of TSM is based on the equilibrium of forces at all nodes. Therefore, if the basic law of physic and Newton's first law are obeyed, a simple and efficient algorithm can always be produced by TSM. Another specialty of TSM is that it treats the element stiffness and the tangent geometric stiffness separately, where the formulization of equations could be easily done without any approximation for unexpected cases.

The derivation of TSM is precisely shown in chapter 2, and followed by a comparison with the finite element method (FEM) in chapter 3, where the superiority of TSM was exhibited. Here, from comparison of the results, it is evidently clear that TSM is far more efficient when the convergence behavior of both methods differed significantly. The difference is caused by the treatment of strain and nodal displacement in the global coordinate system by FEM. The author concluded that the treatment should be made within the local coordinate system, as the results differed between both methods as shown by the numerical analysis. Furthermore, the strictness of the compatibility equation and the tangent stiffness equation also have to be considered in order to achieve reliable result, without the approximation by the shape function, which has been the practice in the TSM.

6.2 An efficient approach for form-finding analysis

By applying TSM to perform form-finding analysis for tensegrity structure, various numbers of equilibrium shapes have been obtained. In this study, the author had implemented the measure-potential element and the truss element for the tensegrity configuration. The form-finding procedure using the measure-potential element with virtual stiffness was compared to the method introduced by force density method (FDM). Also, the definition of measure-potential element is simple and clear, and the equilibrium shape can be achieved by using an ordinary any nonlinear stiffness analysis.

In addition, the author investigated the relation between the incidence rate and the total potential energy for the tensegrity structure. Here, it could be concluded that the target solution (the most preferable morphology) did not have exactly the lowest potential energy, and the highest incidence rate. A correlative relation between those two parameters could not be distinctly determined, and the prediction of emerging morphology from the initial condition is considered to be extremely difficult.

In the following example of form-finding process, the author also executed path finding of equilibrium path in the load–displacement curve. The author has applied a simple yet efficient load or displacement control in order to pursue all possible paths. In this study, all possible main and bifurcation paths have been obtained and were shown in chapter 4. Path finding procedure can be switched into a bifurcation path by substituting an appropriate amount of eigenvector of the tangent stiffness matrix at the bifurcation point.The shapes of the paths are different depending on the kinematic field,

i.e. whether considering gravitational influence or not. In this study, it is clear that when the gravitational influence is taken into account, various independent paths were achieved. In addition, the equilibrium shapes on the bifurcation path showed the sides topple phenomena and loss the degree of symmetricity.

Meanwhile, if the gravitational influence is neglected, the total paths and self-equilibrium shapes are significantly less than when the gravitational effect was considered. All the individual shapes could be classified by the total number of negative eigenvalue, which is equivalent to the concept of the group theory. By applying TSM in form-finding for tensegrity structure in this study, all equilibrium shapes and paths have been successfully extracted, and this showed the superiority and merit of TSM for form-finding process of the tensegrity; which is one of the softest structures with extremely strong nonlinearity.

6.3 The improvement for strong geometrically nonlinear contact problem

As the deformations of tensegrity tower have been observed, the random and large deformational behavior may cause contact phenomena, either the contact between elements or node–element. In the chapter that follows, the author has introduced contact analysis as a preliminary assumption of contact for tensegrity. In chapter 5, the author has presented a three dimensional contact between elements by a non-compressible axial force element. By the application of the non-compressible axial force element, it could simulate the approximation of cable element, which is considered to be applicable to the tensional members of tensegrity structure. While performing the contact algorithm by TSM, sliding nodes are applied at the point where the elements intersect, in order to relate the mechanical properties of the contacted elements and exhibits the phenomena of contact between elements. Also, the multiple contact case has been performed to examine the precision of the formulized equations, and as the analysis result has proved, the unbalanced force was successfully converged throughout the analysis.

The author also introduced the node–element contact analysis for a plane frame beam. Here the Timoshenko short beam theory was applied in order to counter the difficulties that have been prescribed in other earlier studies, by mainly focusing on the calculation instability when performing node-element contact analysis. Also in this study, the author has formulized a simple yet efficient contact cases by TSM to counter

all of the problems with high precision. Especially for the node–element contact, the main problem normally is with regards to the convergability of unbalanced forces when the contact node approaches the element edge. The author defined this phenomenon as the “critical area”. Here, shear deformation by Timoshenko short beam theory is considered and the component was substituted into the element force equation for the contact case. The aim is to eliminate the occurrence of “division by zero” in the stiffness matrix, while producing a stable convergence result throughout the analysis.

As the results showed, stable convergence results have been obtained throughout the analysis and the range of “critical area” has been reduced to almost 100%. By this, it could be concluded that the problems regarding the discontinuity of element edge has been solved in this study. Using the same Timoshenko beam for node–element contact analysis, a comparison was made with an analysis result that was performed by FEM. In the analysis, the author has compared a cantilever beam deformation diagram with the result obtained by FEM, and by coarsely and densely dividing the mesh of the beam. As a result, either using coarse meshing or dense meshing, a relatively similar results have been achieved by TSM, as compared to the densely meshed beam by FEM. The analysis also showed that in TSM, even with less element meshing or fewer nodes, the result is consistent, which is probably not achievable by using other geometrically nonlinear analysis methods.

6.4 Conclusion

Compared to the past decades, the evolution of numerical analysis is proportionate to the rapid growth of science, engineering, information technology and multimedia. The development of computers made it easier and simpler to simulate complex phenomenon in engineering. Currently, the numerical simulation gives us so much information, prediction or new knowledge in various research fields of all around the globe. When developing the computational algorithm for the simulation, the commercial demand may require the aspects of “practicality” and “low cost”, but the “reliance of solution” should be the top priority from the view point of ethics as engineers.

Here, as introduced in every chapter of this study, TSM has both of the “accurate” and “practical” abilities. As mentioned previously, TSM is an expansion version of the displacement method. The displacement method is very easy and primary theory as to be a part of an educational program of engineering for undergraduate level. In other

word, it is simple and efficient method to be used for engineering practice.

Moreover, TSM distinguishes the tangent geometric stiffness caused by the element's rigid body displacement and the element stiffness caused by elements' own deformations strictly. Hence, all of the solutions are guaranteed to satisfy the "perfect equilibrium", and this is the main philosophy of TSM. Therefore, TSM has the potential to be applied extensively with strong robustness.

This study demonstrates the superiority of TSM by considering two aspects of "form-finding" and "contact problems" through tensegrity which is one of the typical structural systems with strong geometrical nonlinearity. To conclude this study, the author has suggested a practical and efficient method that can be referred for future research, either for form-finding, path finding, folding behavior or contact problem for any kind of geometrically nonlinear case, with the aid of TSM. The knowledge obtained in this study can be a core hint to make it evident the essentials of the geometrical nonlinearly.

Acknowledgement

First and foremost, the author would like to express his humble gratitude to Almighty Allah s.w.t for His unconditional love, and guiding me to complete this dissertation. Also, peace and blessing upon prophet Muhammad, His servant and messenger. This dissertation would not have been possible without the guidance and the aid of several individuals who contributed and extended their valuable assistance in the preparation and completion off this study.

The author would like to take this opportunity to express his utmost appreciation to Professor Obiya Hiroyuki of the Saga University for his continuous guidance, enthusiasm, support, sincerity and encouragement throughout the journey of the completion of this study. Also, my sincere gratitude to Professor Ijima Katsushi, Professor Ishibashi Kouji, Professor Ito Yukihiro and Professor Emeritus Goto Shigeo for their support as well as providing me valuable comments and suggestions while serving as members of the examination committee. The same goes to all of my colleagues and staff in the Department of Science and Advanced Technology, Graduate School of Science and Technology, Saga University, Japan.

Last but not least, I also would like to express my sincere thanks to my dearly beloved parents, Professor Dr. Zakaria bin Ismail and Mdm. Aminah bte Yusoff; my siblings Noor Azlin, Noor Azwani, Noor Azmin and Muhammad Nazmi for having faith in me and supporting me all this while. The same goes to their spouses, my kin and my best friends, my highest regard goes to all of you for the supports that have been given to me. May Allah s.w.t bless us all always.

"Great people talk about ideas, average people talk about things, and small people talk about other people."

–Elanor Roosevelt–

Z. M. Nizam @ author

Saga, Japan. March 2014